ANCR-1118

NASA CR-121191

PHASE II TOPICAL REPORT

FLOWING GAS, NON-NUCLEAR EXPERIMENTS ON THE GAS CORE REACTOR

J. F. Kunze
C. G. Cooper
P. J. Macbeth

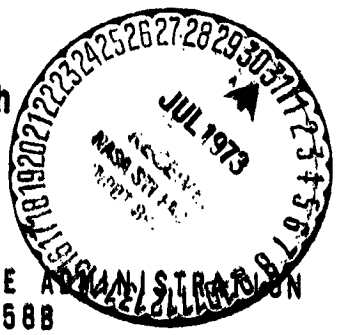

Prepared for
NATIONAL AERONAUTICS AND SPACE ADMINISTRATION
Contract C-545588

H. A. Putre, NASA-LEWIS
Technical Project Manager

Date Published - June 1973

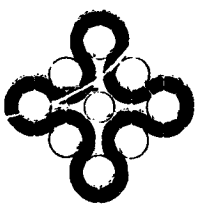

Aerojet Nuclear Company
NATIONAL REACTOR TESTING STATION
Idaho Falls, Idaho - 83401

1. Report No.	2. Government Accession No.	3. Recipient's Catalog No.
NASA CR-121191		

4. Title and Subtitle	5. Report Date
PHASE II TOPICAL REPORT FLOWING GAS, NON-NUCLEAR EXPERIMENTS ON THE GAS CORE REACTOR	June 1973
	6. Performing Organization Code
7. Author(s)	8. Performing Organization Report No.
J. F. Kunze, C. G. Cooper and P. J. Macbeth	ANCR-1118
9. Performing Organization Name and Address	10. Work Unit No.
Aerojet Nuclear Company Idaho Falls, Idaho 83401	11. Contract or Grant No. C-54558B
12. Sponsoring Agency Name and Address	13. Type of Report and Period Covered Contractor Report
National Aeronautics and Space Administration Washington, D.C. 20546	14. Sponsoring Agency Code

15. Supplementary Notes

Technical Project Manager, R. E. Hyland, Advanced Concepts Branch, NASA Lewis Research Center, Cleveland, Ohio 44135

16. Abstract

This report covers the second phase of work on flow tests conducted on models of the gas core (cavity) reactor. Variations in cavity wall and injection configurations were aimed at establishing flow patterns that give a maximum of the nuclear criticality eigenvalue. Correlation with the nuclear effect was made using multigroup diffusion theory normalized by previous benchmark critical experiments. Air was used to simulate the hydrogen propellant in the flow tests, and smoked air or argon or freon to simulate the central nuclear fuel gas. Tests were run both in the down-firing and upfiring directions. Results showed that acceptable flow patterns with high volume fraction for the simulated nuclear fuel gas and high flow rate ratios of propellant to fuel can be obtained. Using a "point" injector for the fuel, good flow patterns are obtained by directing the outer gas at high velocity along the cavity wall, using louvered injection schemes. Recirculation patterns were needed to stabilize the heavy central gas when different gases are used.

17. Key Words (Suggested by Author(s))	18. Distribution Statement
Gas Core Reactor Flow Patterns Nuclear Criticality	Unclassified - Unlimited

19. Security Classif. (of this report)	20. Security Classif. (of this page)	21. No. of Pages	22. Price*
Unclassified	Unclassified		$5.45

* For sale by the National Technical Information Service, Springfield, Virginia 22151

ACKNOWLEDGEMENTS

The authors wish to express appreciation to D. H. Suckling, H. G. Miller, R. R. Jones, and J. H. Lofthouse for the significant help and support rendered to various phases of this experimentation.

TABLE OF CONTENTS

		Page
1.0	SUMMARY	1
2.0	INTRODUCTION	2
3.0	TEST APPARATUS	4
4.0	TEST PROCEDURES	14
5.0	TEST RESULTS AND DISCUSSION	16
	5.1 Injection Nozzle Effects	16
	5.2 Scaling Studies	27
	5.3 Buoyancy Effects	27
	5.4 Velocity Measurements	46
	5.5 Sweep-Out Rates	46
	5.6 Upfiring Tests	53
	5.7 Dust Injection Tests	53
	5.8 Criticality Calculations and Selected Results	70
6.0	CONCLUSIONS AND RECOMMENDATIONS	73
	REFERENCES	75

FIGURES

2.1	Open cycle gas core concept	3
3.1	Basic test apparatus, showing the large blower for providing outer flow, the smoke mixing box and smoke injector for inner flows, the test box plenum, and the 18 in. spherical test cavity	6
3.2	Basic apparatus showing improved larger test box plenum, 18 in. spherical cavity, and 3 in. spherical injector.	7
3.3	36 in. "spherical" test cavity with 3 in. spherical injector.	8
3.4(a)	Vertical cross section of small, 18-in. diameter "spherical" cavity.	9
3.4(b)	Vertical cross section of large, 36-in. diameter "spherical" cavity.	10

TABLE OF CONTENTS

(Continued)

		Page
	FIGURES (Cont'd)	
3.5	Typical 18 in. two-dimensional test cavity configuration . . .	11
3.6	Typical 36 in. two-dimensional cavity configuration.	12
3.7	Cross section of 36 in. two-dimensional test cavity used for typical test series.	13
5.1	Injectors used for two-dimensional smoke tests	18
5.2	Typical injector smoke dispersing plug designs	19
5.3	3 in. and 6 in. spherical injectors.	20
5.4	3 in. and 6 in. spherical injector details	21
5.5	Typical cavity recirculation patterns.	23
5.6	18 in. spherical test cases showing recirculation effects arising from varying 3 in. injector position	24
5.7	36 in. spherical test cases showing recirculation effects arising from varying 6 in. injector position	25
5.8	Effect of preferential direction of injection.	26
5.9	Scaling series with two-dimensional cavities	28
5.10	Scaling series with two-dimensional cavities	29
5.11	Scaling series with spherical cavities	30
5.12	Scaling series with spherical cavities	31
5.13	Cavity volume fraction vs injector buoyancy number	41
5.14	Cavity volume fraction vs recirculation buoyancy number. . . .	42
5.15	Cavity volume fraction vs combination buoyancy number.	43
5.16	Cavity volume fraction vs area buoyancy number	44

TABLE OF CONTENTS

(Continued)

Page

FIGURES (Cont'd)

5.17	Cavity volume fraction vs residence buoyancy number	45
5.18	Typical velocity profile map of 36 in. two-dimensional test cavity.	47
5.19	Typical velocity profile map of 36 in. two-dimensional test cavity.	48
5.20	Typical velocity profile map of 36 in. two-dimensional test cavity.	49
5.21	Typical velocity profile map of 36 in. two-dimensional test cavity.	50
5.22	Typical velocity profile map of 36 in. two-dimensional test cavity.	51
5.23	Typical velocity profile map of 36 in. two-dimensional test cavity	52
5.24	Cavity smoke density vs decay time.	54
5.25	Cavity sweepout rate vs initial center gas flow rate.	55
5.26	Cavity sweepout rate vs outer gas flow rate	56
5.27	Comparison of upward exhausting cavity case to downward exhausting cavity	57
5.28	Comparison of upward exhausting cavity case to downward exhausting cavity	58
5.29	Up-firing cavity cases showing good containment of air, argon, and freon	59
5.30	Dust injection series showing effect of scattering dust both upward and downward	60
5.31	Isodensity contour map for typical dust (talcum powder) injection test.	61
5.32	Computer solution model I	62

TABLE OF CONTENTS

(Continued)

Page

FIGURES (Cont'd)

5.33 Computer Solution Model IX 63

5.34 Computer Solution Model X. 64

5.35 MONA Computer Solution - Keff vs Radius Ratio. 67

5.36 MONA Computer Solutions - Keff vs Reff at Constant Radius Ratio. 68

5.37 MONA Computer Solutions - Keff vs Volume Fraction at Constant Radius Ratio 69

5.38 Comparison of Computer Solutions - SCAMP and MONA vs DISNEL Keff vs Reff 72

TABLES

5.1 18 in. - 2D Cavity - All Solid Louvers - Body 51% Open, 3/16 in. Holes. 33

5.2 36 in. - 2D Cavity - All Solid Louvers - Body 47% Open 5/16 in. Holes. 36

5.3 35% Volume Fraction Model Specifications 65

5.4 Material Specifications. 66

1.0 SUMMARY

The results of Phase II flow experiments on the open cycle gas core concept are discussed in this report. The first phase[1] achieved flow configurations which gave high volume fractions for the inner gas, which simulated the fuel gas. Typically using air and air as the two gases, both simulating a propellant flowing around the outside and the fuel suspended in the center, volume fractions up to 35% in spherical configurations were obtained. The second phase of this work concentrated on improving the conditions when gases of different density were employed, the central gas being the heavier. Again, both two-dimensional and three-dimensional tests were run. In the two-dimensional cases, the round-shaped cavity was bounded by two flat walls on the viewing ends.

Since the largest tests were conducted on 3 ft diameter cavities, scaling up will be required to determine what the effects would be in the actual gas core rocket reactor which will have a cavity diameter of between 8 and 12 ft. The question of scaling from small models to larger sizes was investigated, using 18 in. and 36 in. diameter cavities. The results indicate that neither the Reynolds nor the modified Froude number are satisfactory scaling indicies. The most nearly equivalent flow patterns for different sizes of cavities generally resulted when a compromise was achieved between attempts to obtain a matching Froude number in one case, and a matching Reynold's number in another case.

Several difficult and unusual aspects of conditions in the flowing gas cavity were investigated. For instance, a dust injection test series was run. Such tests would simulate startup conditions in a cold reactor. Also, upside down arrangements, with the exhaust nozzle facing up were tested. This puts the inertial forces in the opposite direction from those in an accelerating space rocket. However, the upside down cases could be used in magnetohydrodynamic applications. In essence, containment of the heavy central gas was excellent in these upside down tests, with the principle problem being how to keep the central gas away from the walls of the cavity.

For the normal downfiring directions, one of the main considerations is the method of dispersing the heavy central gas so that it occupies a large volume of high density within the cavity before it "falls out" the exhaust nozzle. This results from the gravitational effect relative to the light propellant gas flowing around it. One mechanism that was found to be particularly effective was a strong upward recirculation pattern for the outer gas. Such a pattern could be generated by the convergence of the annular gas streams near the outlet nozzle. Such recirculation was most noticeable in the three-dimensional spherical configurations, and was undoubtedly dependent on the shape of the lower part of the cavity. The upward recirculation tended to prevent the heavy center gas from dropping straight to the exit nozzle, and also dispersed the central gas. Since the central gas simulated uranium fuel, this dispersal reduced the self-shielding and enhanced the nuclear reactivity of the system. This dependence of the shape of the lower portion of the cavity on containment that can be obtained with gases of different density is at variance with results reported in Phase I of the study[1]. In those cases, principally two-dimensional studies were performed and mostly on gases of the same density, where the gravitational effect was not of concern.

2.0 INTRODUCTION

The open cycle co-axial flowing gas core concept[2] is shown in Figure 2.1. This concept has been studied experimentally in a number of laboratories. Patterns with high ratios of outer to inner gas flow rates were initially studied in cylindrical-geometry configurations[3,4]. Subsequent experiments concentrated on spherically shaped configurations, which would closely resemble conditions which would be achieved in actual high temperature operating engines and which gave the most clearly reactive configuration[1,5]. Critical experiments to study the reactor physics characteristics of a dilute gas core surrounded with hydrogen and a low absorption moderator (heavy water) have also been reported[6,7]. Since the ideal nuclear geometry is spherical, and since a gaseous fuel is to be used, nuclear considerations bear very heavily on the types of flow patterns which will be acceptable. In particular, the flow patterns must be capable of going critical within an engineering feasible operating pressure, which is generally assumed to be less than 1000 atm. These recent flow tests, conducted at Aerojet Nuclear, have concentrated on obtaining flow configurations which expand the central gas, simulating the fuel, into as large a volume as possible with as high as possible volume fraction. The goals for the conditions under which the system will be operated are: minimum cavity pressures, maximum propellant-to nuclear fuel flow rate ratios, minimum reactor size, and more recently, overall low flow rates to correspond to the low thrust applications which are foreseen for nuclear rockets of the not too distant future.

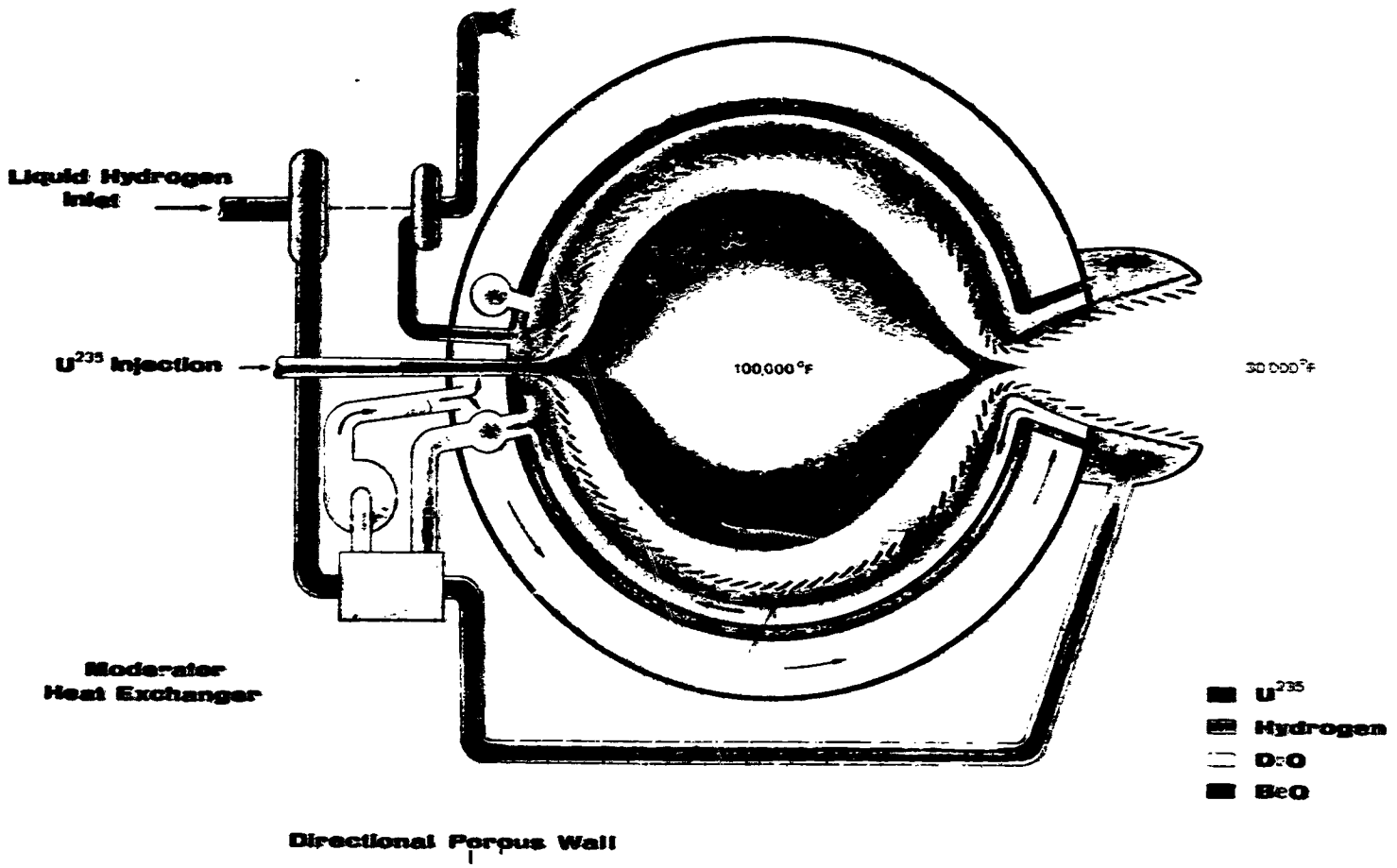

Fig. 2.1 Open Cycle Gas Core Concept

3.0 TEST APPARATUS

The flow test apparatus was designed so that modifications could be made easily to the cavity shape, to its walls, to the louver configurations, to the injectors, and to the exhaust nozzle. The important consideration was ease of disassembly and reassembly. Fine tuning of the flow distributions into the cavity and measurements of the flow parameters were of secondary importance. However, the total flow rates for both the inner and outer gases were measured with high accuracy. The basic apparatus is shown in Figure 3.1, a large blower with a rated capacity of 1500 cfm provided the main outside gas flow. Air was used as the outer gas in all cases, and was fed through a large 8 in. pipe into the large test box. In the figure, the 18 in. diameter spherical cavity can be seen. This was constructed of molded methylacrilate plastic, and is the identical sphere that was described in the Phase I report[1]. The central gas flow was provided from a smoke mixing box, which can be seen on the left hand side of the picture, and thence through a 2 in. pipe into the central gas injector inside the cavity. The mixing box was 30 cubic ft in volume, and hence provided a relatively large accumulator which would give constant smoke density for reasonable periods of time. The output from the smoke box, near its top, was continuously monitored by a photo-electric cell light beam. This was used to establish a uniform smoke density for all tests for the smoke entering the pipe on its way to the test chamber. Orifice flow measuring sections were installed in both the 8 in. and 2 in. pipes. Figure 3.2 shows a larger test cavity box with the same small sphere installed. This large box was more versatile, allowing cavity to be installed either in the downfiring or unfiring configurations,* and provided a more even distribution of flow into the test cavity region. The large 36 in. diameter plastic sphere is shown in Figure 3.3. The dimensions of this sphere were an exact factor of two scale up from those of the small 18 in. sphere. However, there were a few minor differences between the two spheres. As can be noticed, the large sphere did not have a circular cross section but was octagonal. This was done so as to facilitate construction of such a large device. Molding of large 3 ft diameter rings was difficult, and facilities for performing the molding were generally unavailable. Furthermore, several extra louvers were added at the bottom of the large sphere. These were blocked off for the tests which studied scale up conditions. For comparison, engineering drawings of the 18 in. and 36 in. spheres are shown in Figures 3.4a and 3.4b.

For the so-called "two-dimensional" tests, the cavity shape was flat in the direction perpendicular to the viewing direction. This arrangement facilitated viewing and interpretation of the tests and made the construction of a number of different cavity shapes relatively simple. The flat end walls did perturb the flow patterns somewhat. However, this end perturbation extended only a few inches from the viewing wall surface, and at least qualitatively did

---

* The basic configurations tested incorporated downward firing (downward exhausting) cavities, thus using gravity to simulate the effect of forward acceleration on a rocket engine in space. Upward firing can be utilized in practice for a stationary power plant MHD application, or possibly for simulating rocket with a thrust reverser unit.

not compromise the interpretation of the test results. Close-up photographs of the two configurations used in the two-dimensional testing are shown in Figure 3.5 (the 18 in. cavity) and Figure 3.6 (the 36 in. cavity). Again, each configuration is an exact scale model of the other. Each contains an outer cavity wall with perforations, and on this wall were attached 24 perforated louvers for directing the flow in an tangential direction along the cavity wall. Figure 3.7 shows cross-sectional details of the 36 in. test cavity for a typical test series. As was discovered in Phase I of this testing (Reference 1, Section 5.4), the transpiration cooling holes in the louvers should be kept to the minimum necessary to provide adequate cooling. When this is done, the transpiration flow is small and has a negligible effect on the flow patterns. Therefore, for many of the tests the transpiration cooling holes in the louvers were blocked. (For the three-dimensional transparent spheres, there were no transpiration cooling holes, only louvers to direct the flow.)

Since flow rates were provided by a blower, and since pressure capabilities of the apparatus were minimal, choke flow conditions could not be tolerated. The nozzle areas were at least 1 square inch. Phase I testing (Reference 1, Section 5.3) had shown that the exhaust nozzle diameter had little or no effect on the flow patterns established inside the cavity.

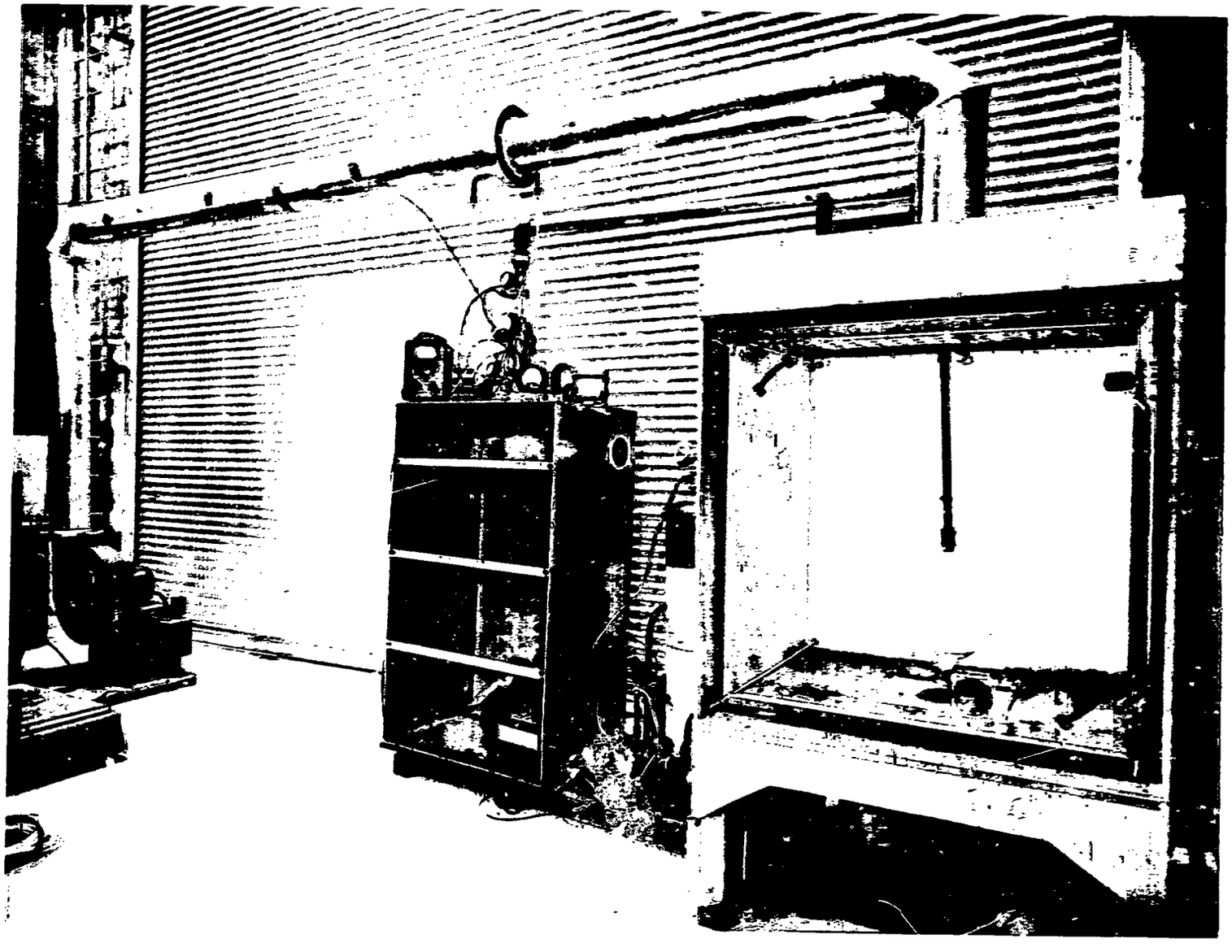

Fig. 3.1 Basic test apparatus, showing the large blower for providing outer flow, the smoke mixing box and smoke injector for inner flows, the test box plenum, and the 18 in. spherical test cavity.

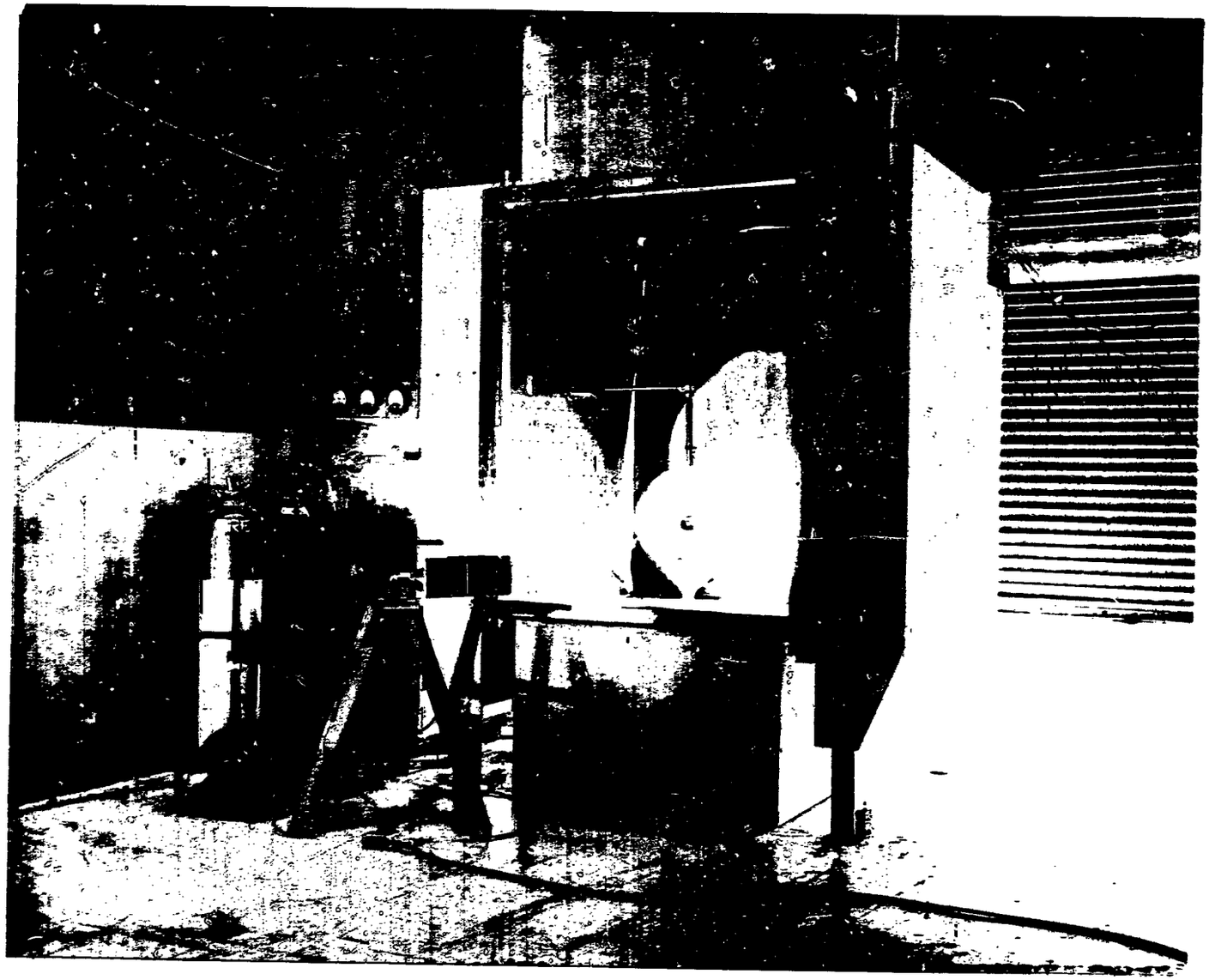

Fig. 3.2 Basic apparatus showing improved larger test box plenum, 18 in. spherical cavity, and 3 in. spherical injector.

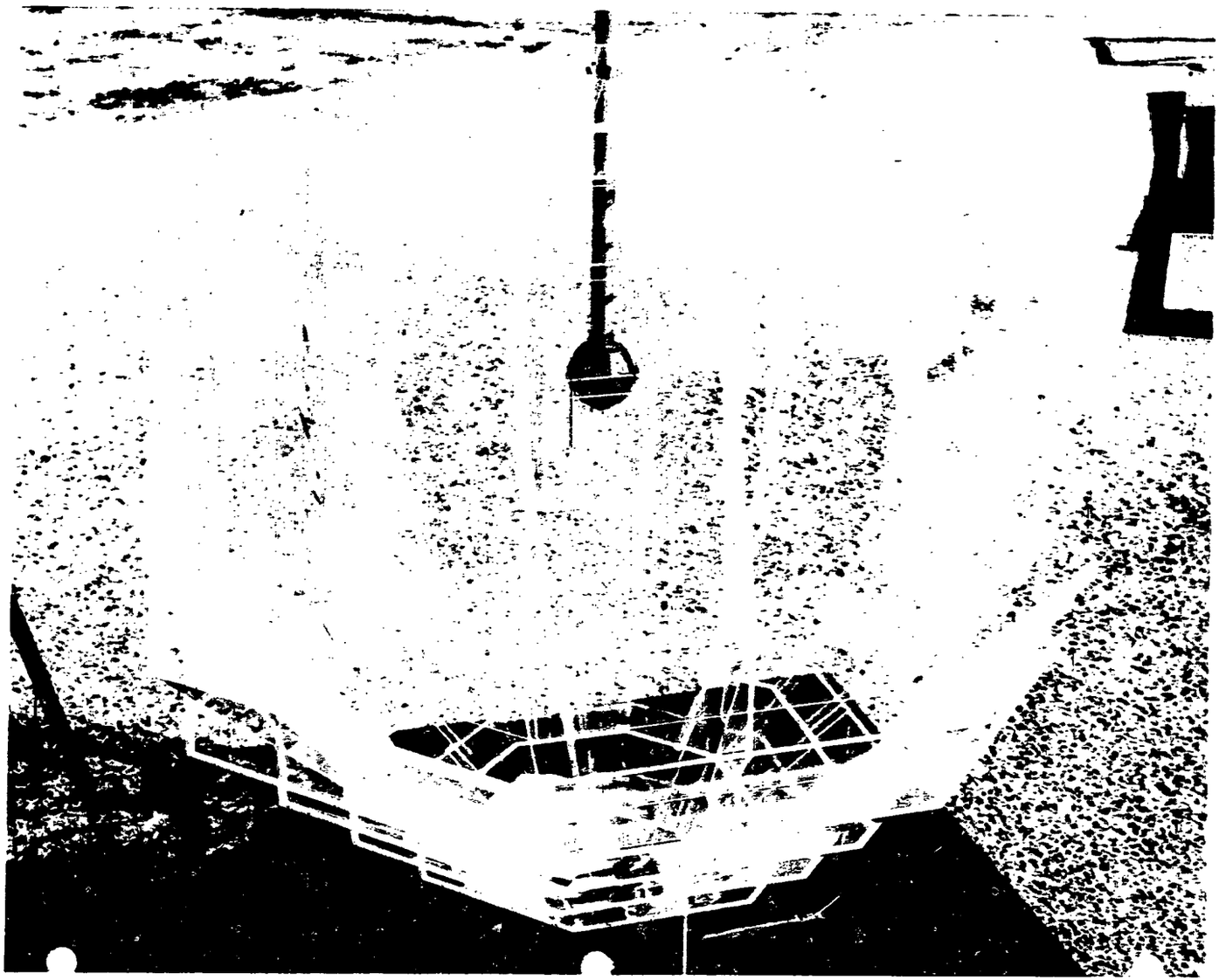

Fig. 3.3 36 in. "spherical" test cavity with 3 in. spherical injector.

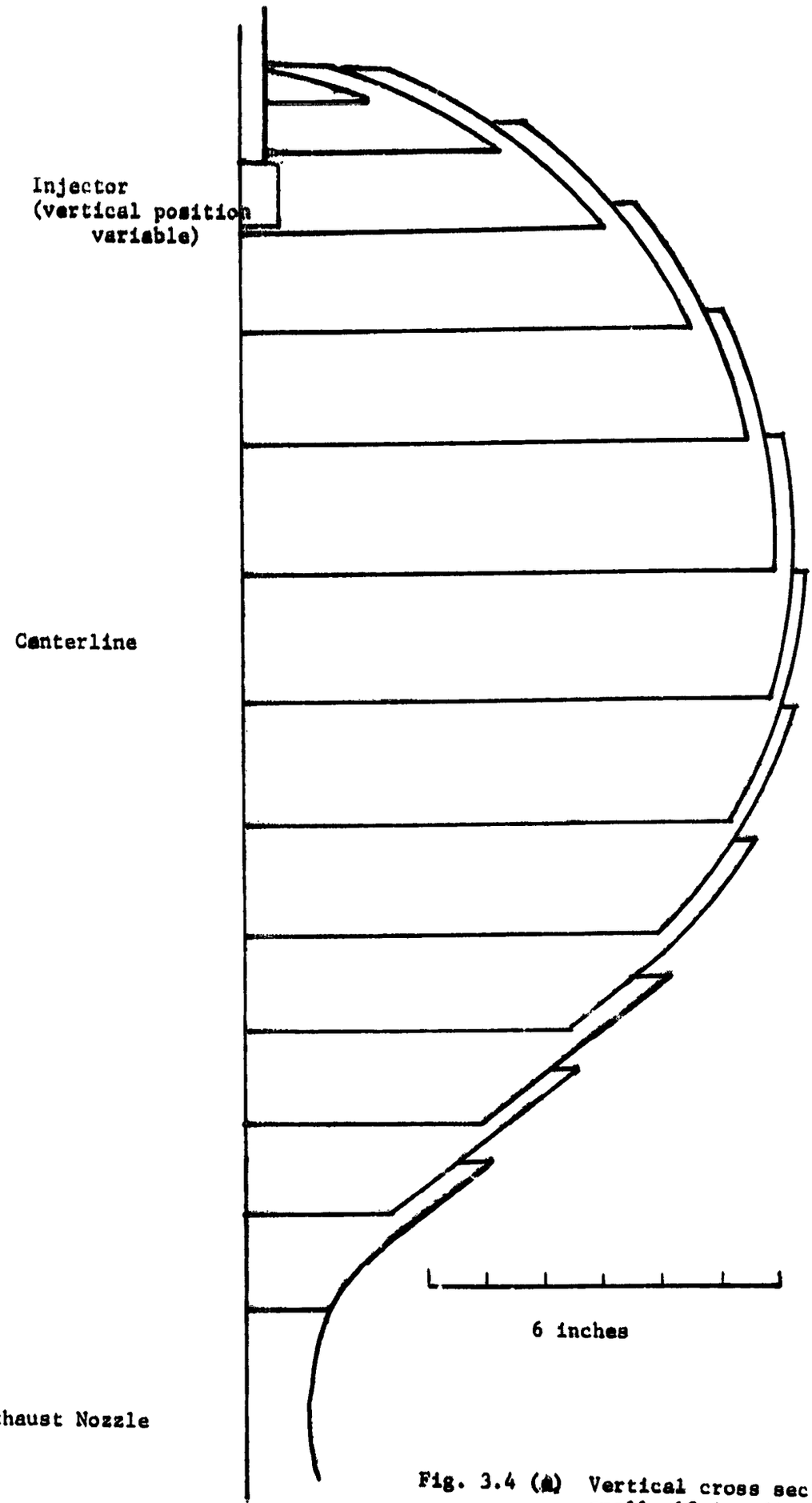

Fig. 3.4 (a) Vertical cross section of small, 18-in. diameter "spherical" cavity.

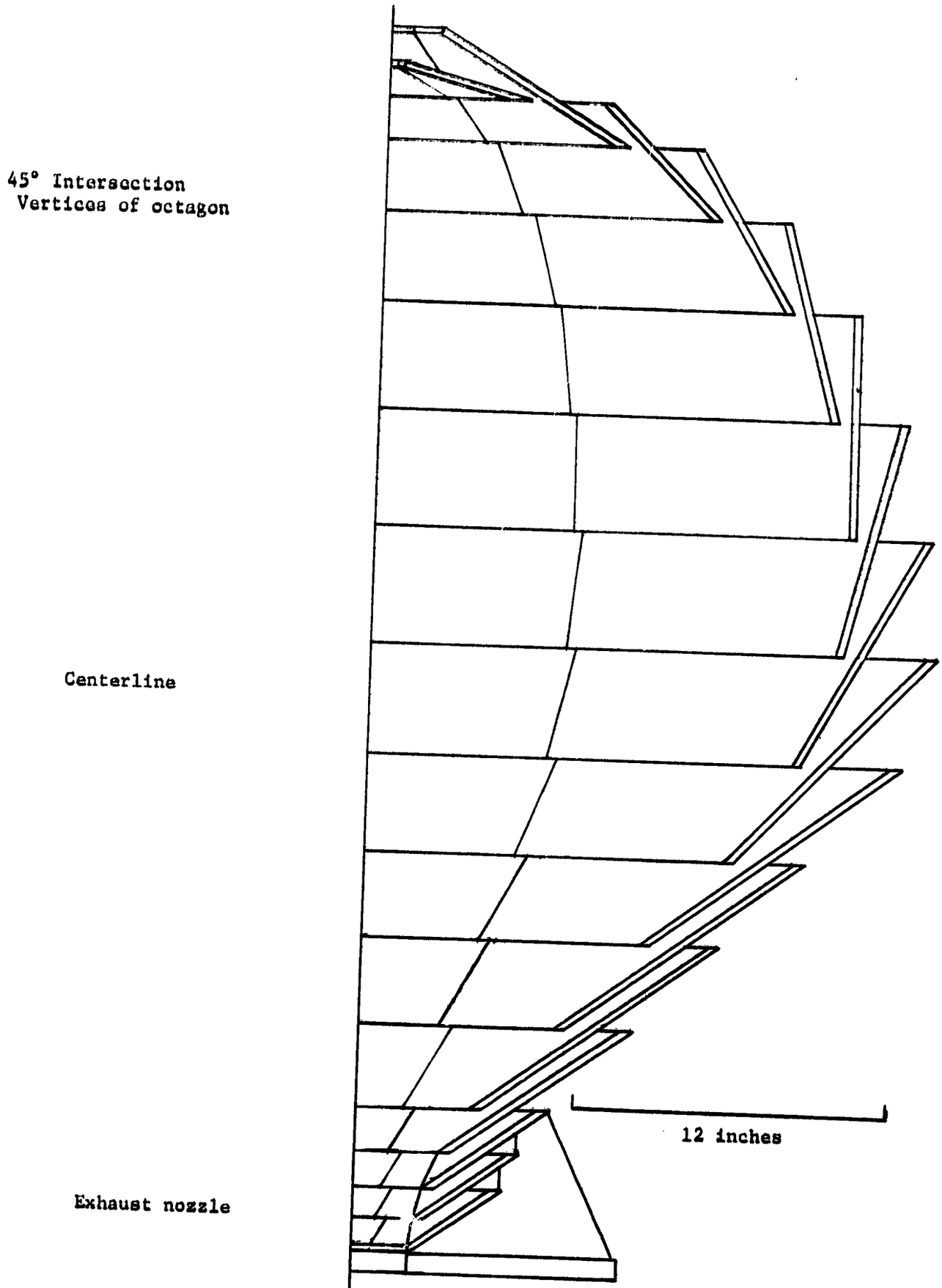

Fig. 3.4 (b) Vertical cross section of large, 36-in. diameter "spherical" cavity.

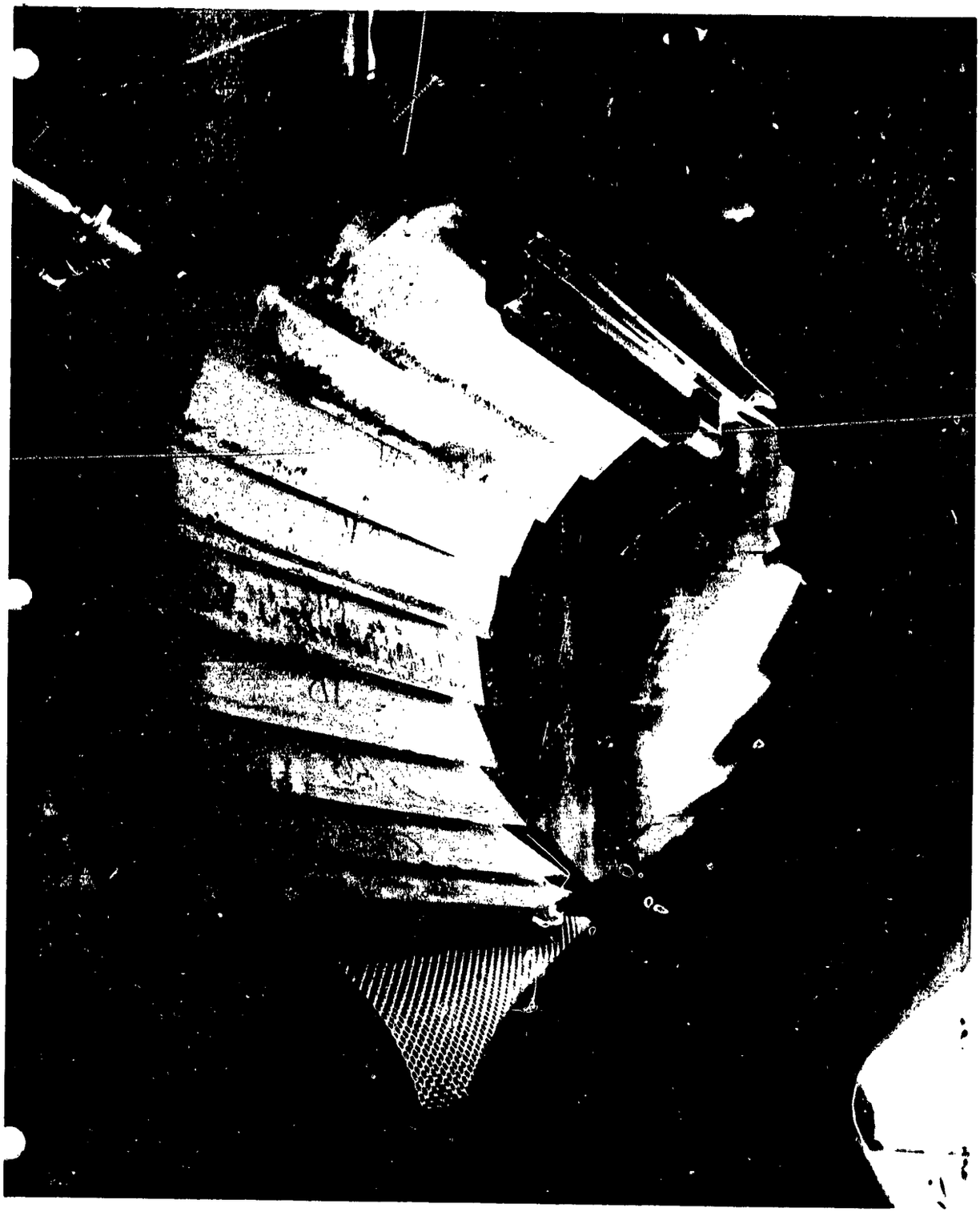

Fig. 3.5 Typical 18 in. two-dimensional test cavity configuration

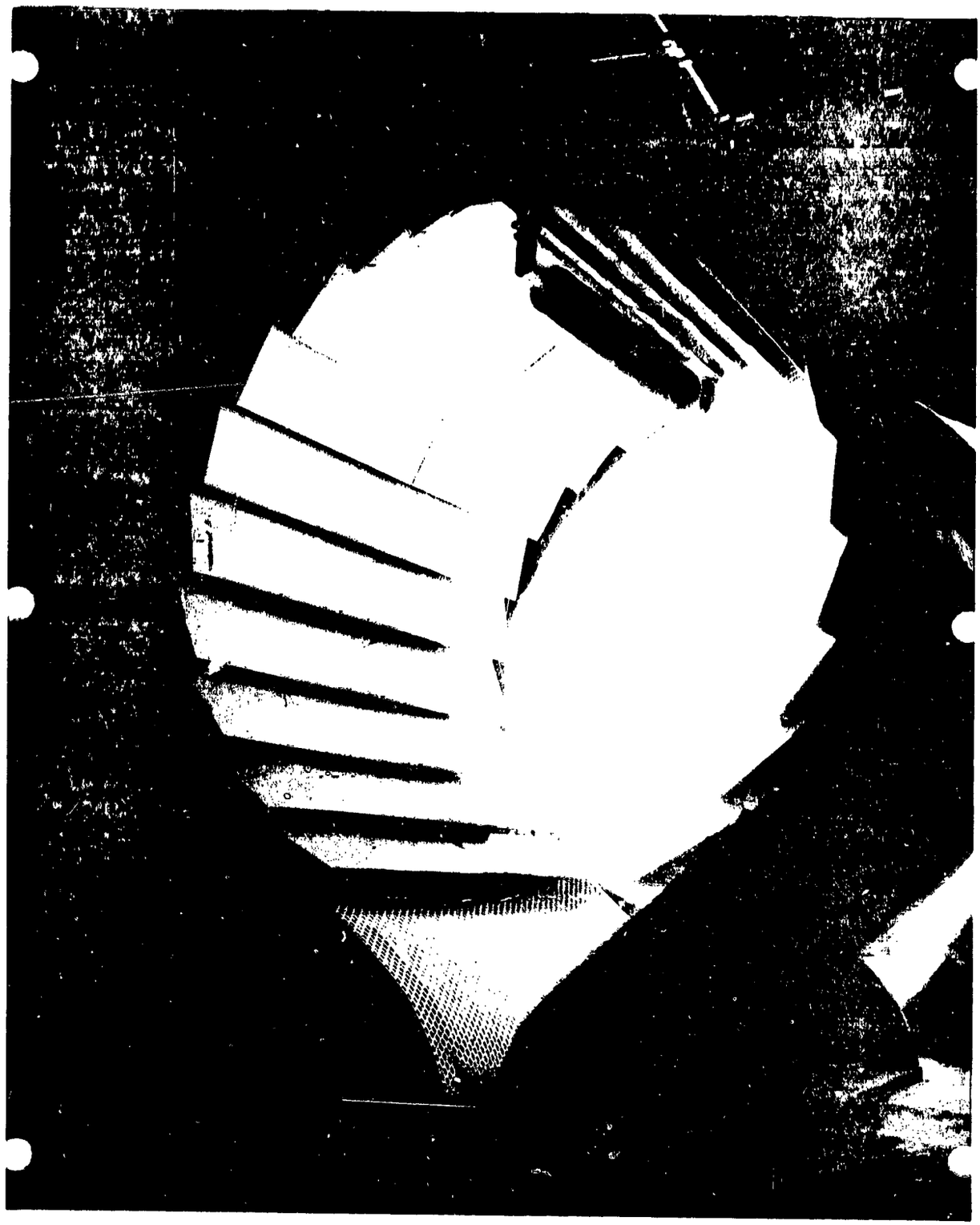

Fig. 3.6 Typical 36 in. two-dimensional cavity configuration

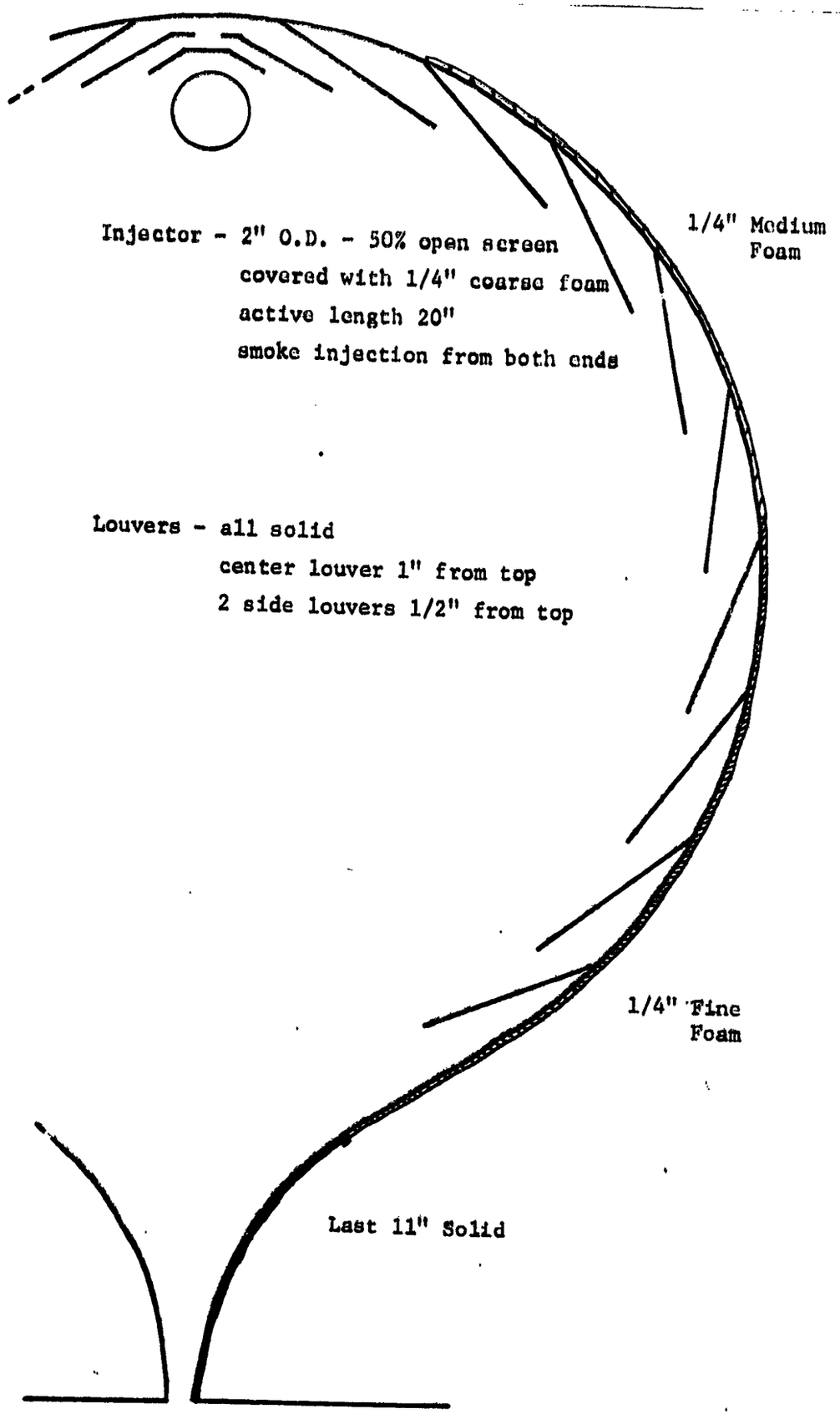

Fig. 3.7 Cross section of 36 in. two-dimensional test cavity used for typical test series.

4.0 TEST PROCEDURES

The procedures for operating these tests capitalized on the flexibility and ease of experimental changes. The front face of either test box could be easily removed to make alterations on the cavity arrangement or to the inlet injector. After the front was replaced on the box and sealed, constant flow was then established for both the outer and inner gas circuits. The flow rates were monitored visually on differential pressure meters. A standard series of even numbered flow rates for the outside gas were used for most of the test. These ranged from 50 cfm to 600 cfm on the 18 in. cavities to 100 to 1100 cfm on the 36 in. cavities. The inner gas flow rates were established so as to give an even numbered ratio with the outside gas. For the initial experiments, these flow rate ratios were even in terms of volume flow rates. But for the latter phases of the experiments, even numbers were chosen for the mass flow rate ratios. Flows were regulated by means of valves at each gas source, i.e., the blower for the outer gas and the pressure regulator for the inner gas. The only adjustments provided beyond this point were at the walls of the cavity, where Scott foam or plastic sheet was used to partially or fully restrict air flow through certain portions of the cavity wall. The basic data for each test were the two flow rates and the photographs that were taken of the visible flow patterns.

Among the types of supplementary data obtained were flow velocity measurements within the cavity. These have been conducted to date only on the two-dimensional configurations, because of the difficulty of obtaining access to the interior of the three-dimensional cavities. These velocity measurements were made with hot wire anemometers. In general, the gas velocities were independent of the inner gas flow rate. However, in the case of very heavy gases for the interior gas, the gravitational effect perturbed the main flow patterns near the centerline of the cavity. In such cases, flow measurements were taken with the hot wire anemometer with but a single gas flowing, since gas mixtures will perturb the output of the anemometer. However, to determine if the heavy central gas did indeed have an effect on the flow patterns, smoke traces were inserted along the centerline and in other sensitive regions of the cavity to determine the exact direction of the flow in these areas. (The anemometer itself would not determine the direction of the flow; it was only capable of determining the line of the maximum velocity or gradient.) Other, and perhaps more important, supplemental information was obtained by scanning the photographs with a densitometer in order to determine smoke densities, and hence densities of the central gas, throughout the cavity. To obtain satisfactory pictures for the densitometer scanning, time exposures were taken. These averaged-out the time dependent fluctuations in the smoke density. These time exposure photographs were exposed such that the linear portion of the log density exposure curve of the film was utilized. Selection of the proper exposure times are discussed in Reference 1, Section 4.0.

The time exposure photographs were scanned on a Joyce automatic scanning densitometer. Traces were obtained radially across the cavity at a number of different longitudinal locations. The resultant traces were normalized for smoke densities varying between 0 and 100%. The 100% value was established as the density at the outlet of the injection nozzle. For the two-dimensional cavity tests, the effective density through the cavity could easily be interpreted directly from the smoke density traces, and the isodensity lines could be directly plotted accordingly.

In the case of the three-dimensional cavity, with chord lengths varying across the scan, density interpretations could not be directly made. The density had to be unfolded from the observed density traces. The unfolding scheme is equivalent to solving for the coefficients in a matrix of simultaneous equations. The method used and computer program for the unfolding scheme are shown in Appendix C of Reference-1. Furthermore, background corrections were made in the data reduction program so as to correct for the varying attenuation of the walls of the Plexiglas sphere and of variations in lighting conditions. Thus, the three-dimensional tests required a rather involved process to obtain the radial smoke density function. For the two-dimensional tests the process was quite simple, since chord-viewing-length and background effects were essentially constant. However, the end wall effects distorted the two-dimensional results and made these density measurements only semi-quantitative. Further simplifications were made in many cases in the two-dimensional density scans so as to obtain a larger quantity of data of a semi-quantitative nature. On many of the configurations, a single vertical and a single horizontal trace was made, from which estimates of the integrated volume fraction were obtained. Comparison of selected samples of such simplified scan cases with complete detailed scans showed that the errors were only a few percent at the most.

The relative accuracy of the densitometer scans is quite good, far better than 1% of reproducibility. The estimated accuracy on the integration of the density contours is estimated to be about ±10%. The principle uncertainty in the densitometer results, however, is establishing a base line condition of 100% smoke density. Since this could only be determined by a measurement directly at the surface of the injection nozzle, the assumption was made that smoke density at this location was indeed 100%. Gas samples were withdrawn at this location with the configuration running on air and argon mixtures without smoke. The results of these gas samples indicate that the inlet density at the surface of the injection nozzle is nearly 100%. The actual analyses results indicated 87% density, but a portion of this difference from 100% is attributed to the sampling technique, which sucked the volume of the gas to be sampled in rapidly. The net effect of all uncertainties is such that it is estimated the volume fraction results are accurate to within 20% of the quoted number, with the quoted value more apt to be too large than too small.

5.0 TEST RESULTS AND DISCUSSION

This major section of the report deals separately with the various sub-phases of the testing program. Each of the major aspects of the variables that affect the flow configuration are dealt with in the subsections. No attempt has been made to arrange these results into a specific order; they are listed in the following order for convenience only.

5.1 Injection Nozzle Effects

Phase I of these studies[1] clearly showed that the injection nozzle for the center gas or, alternatively, the method of injecting the center gas, is the key to obtaining acceptable flow patterns and densities for the inner gas. It should not be assumed that there will be but a single injection method, or even a single injector in the final rocket engine design. While such does make for simplicity of design of the actual reactor, further studies will be necessary before the final configuration can be selected.

It is assumed that in such a rocket, either pellets of metal or a thin wire of uranium metal will be injected rapidly into the cavity from the top. Upon reaching the very hot gas in the interior of the cavity, the metal will literally explode to a gas. However, some mechanism must be present to disperse this newly formed gas into all regions of the cavity where it is most effective in creating the nuclear chained reaction. Thus, the non-nuclear flow testing checked injection designs which introduce the center gas into the cavity with very low velocities. This essentially takes little or no credit for any explosive radial velocity which will result when the metal comes in contact with the hot gas. By positioning the injector properly, so as to place it in a velocity stream set up by the fast flowing outer gas, is one method of achieving the desired dispersal. However, too much entrainment of the center gas into the inside gas stream will result in the center gas being quickly swept around the walls of the cavity and out the exhaust nozzle. The second consideration involves setting up flow patterns of a non-turbulent nature in the central regions of the cavity, flow patterns which will tend to buoy up the heavier center gas. Without such buoyancy forces, a heavy center gas tends to fall under the influence of gravity directly to the exhaust nozzle, resisting whatever other dispersal forces might be present.

5.1.1 "Two-Dimensional" Injector Designs

The "two-dimensional" configurations represent an unusual problem in injector design. The two-dimensional basic configuration was intended to merely be a minor deviation from a truly spherical arrangement. However, the long viewing cord length between the two viewing plates should represent throughout its length a uniform flow pattern. This is not possible unless the injection nozzle also is a length nominally equivalent to that between the two viewing surfaces. The need for a long injector, plus the desire for minimum, and virtually zero, injection velocity are generally incompatible. In order to distribute the flow uniformally along the length of the injector, a pressure drop is needed. A pressure drop on the other hand will result in finite injection velocities. Conversely, if no pressure drop is employed, the gas tends to move straight down the pipe until it reaches an obstruction (such as the end of the pipe), at which time the gas will come through the injection nozzle openings into the cavity. Figure 5.1 shows the general type of flow to be expected under these circumstances. If flow is introduced from both ends

of the injector, flow patterns similar to that shown in part B of Figure 5.1 tend to result.

Some improvement in the above patterns can be obtained by fashioning baffles or plugs for distributing the flow as desired inside the injector nozzles. Some typical plug designs are shown in Figure 5.2. These generally achieved the type of uniformity in injection pattern desired. Their one disadvantage was that when designed to work on one type of injection gas, the nozzle did not function as desired on a different density gas.

The above described difficulties in achieving uniform injection over the entire length of the injection nozzle, plus the compromises already inherent in the two-dimensional configurations, dictates that the two-dimensional results should be interpreted only in a qualitative manner. The two-dimensional configuration is much easier to interpret and to understand in flow patterns, visual operation is much easier, and eddies in turbulent flow can be more easily identified than is the case with the spherical models. A further advantage is relative ease in which cavity wall and its louvers can be varied. It is for these reasons that the two-dimensional configurations were employed, and developed into a basic arrangement which gave the most satisfactory flow results.

5.1.2 Spherical Injector Designs

Originally, the small, short cylinders, approximately 1-1/2 to 2 inches long and 1 inch in diameter, were used as the injection nozzles in the spherical configurations. However, these also had similar disadvantages to the pipe configurations used in the two-dimensional cavities. The flow tended to come out of only the bottom part of the pipe. Again, the insertion of especially made plugs or baffles was able to obtain a more uniform distribution of flow over the small area of the injection nozzle. However, a more suitable pattern for injection nozzle arrangement would be a spherical injector containing perforations. Such injectors are shown in Figure 5.3. The 3 in. diameter injector was used in the 18 in. cavity while the 6 in. diameter injector was used in the 36 in. cavity. Figure 5.4 shows each of these spherical injectors disassembled. The inner perforated cylinder formed the pressure wall which helped create relatively uniform dispersal over the spherical surface. The second or outside wall then allowed the gas to issue forth into the cavity with a very low injection velocity. The outside walls of the spherical injectors were 50% open area consisting of nominally 0.125 in. diameter holes. These injectors generally worked quite satisfactorily when air was the injection medium, giving uniform dispersal over the entire spherical surface. However, for the heavier than air gases, the tendency still existed for the gas to preferentially issue from the lower portion of the sphere. Since a uranium pellet or thin uranium wire being injected into the cavity would also have a preferentially velocity towards the nozzle from both its initial velocity and from the accelerating effect, these effects with the injector are believed to be realistic.

5.1.3 Effect of Injector Position

The injector position in the cavity will determine how much of the inlet gas can be pulled out by velocity shear forces originating from the fast moving outer gas flowing along the walls. The original results of such investigations are given in Section 5.1 of Reference 1. In brief, these tests showed that an optimum position for the injection nozzle can be found

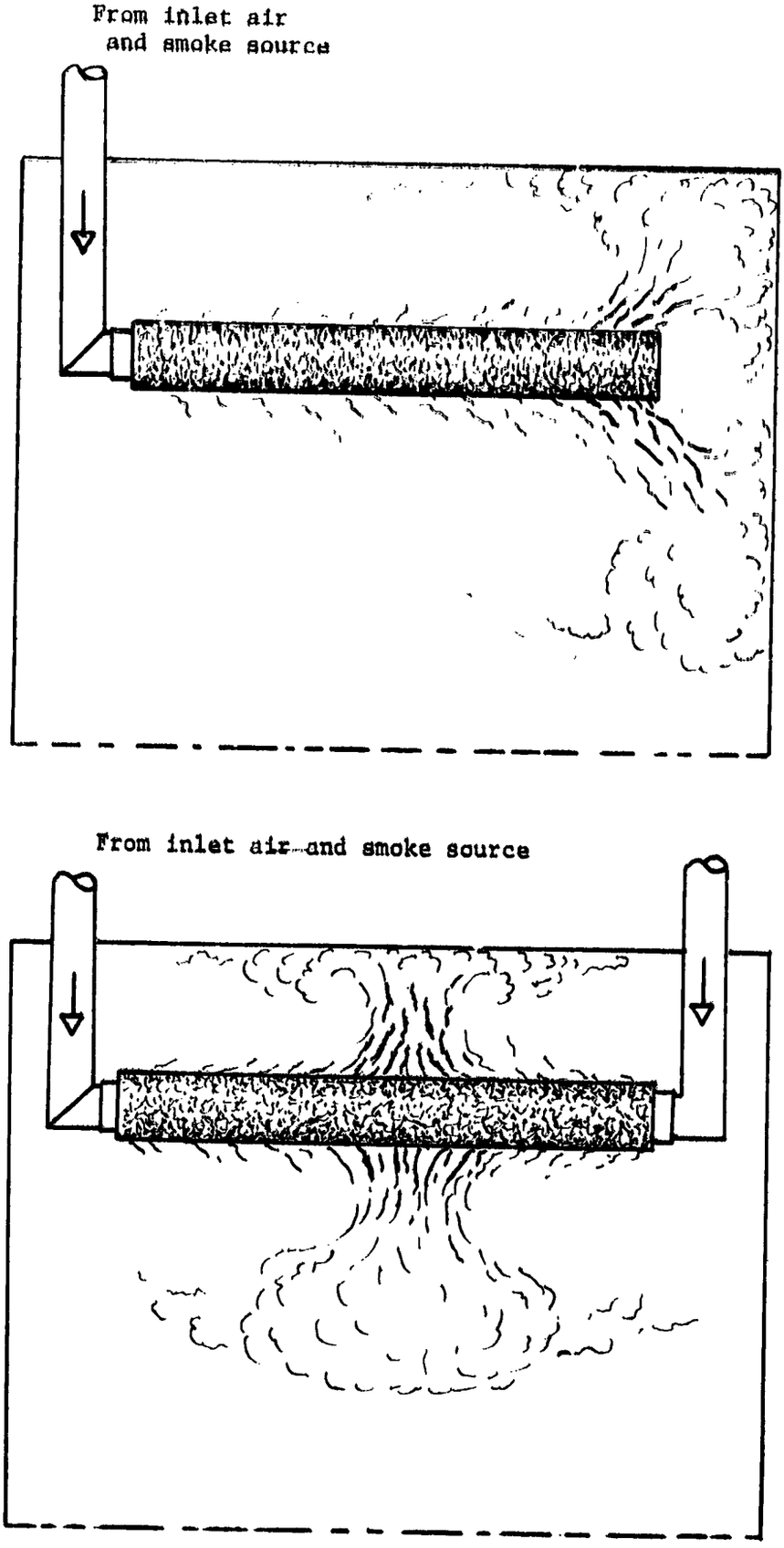

Top picture shows effect when smoke was let into injector through single pipe, and bottom picture shows effect of double inlets into the injector. Injector consisted of a perforated metal cylinder covered with a layer of Scott foam. The end of the single inlet injector was a solid disk. (Note, rectangular box outline has no significance.)

Fig. 5.1 Injectors used for Two-Dimensional Smoke Tests

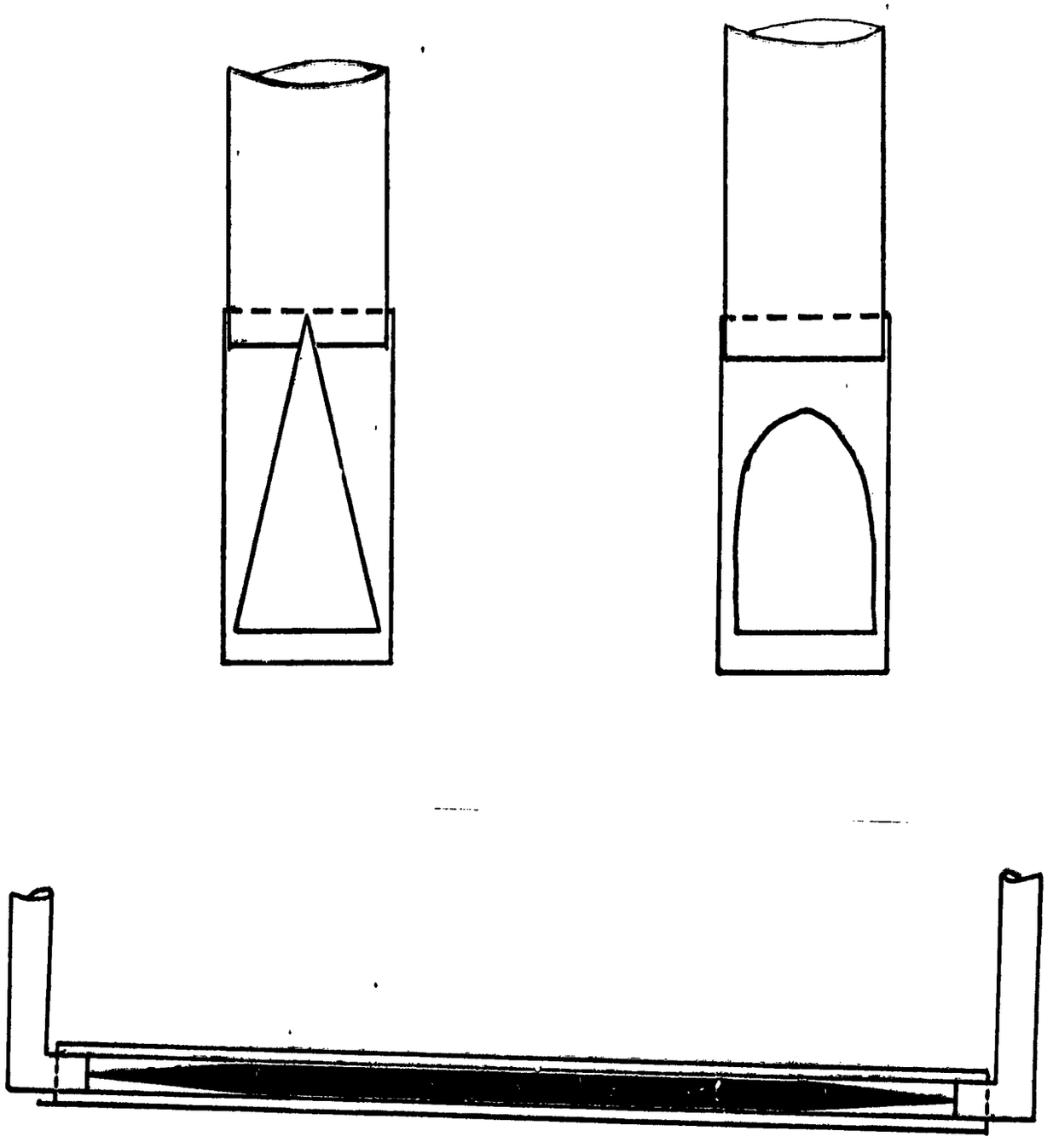

Fig. 5.2 Typical injector smoke dispersing plug designs

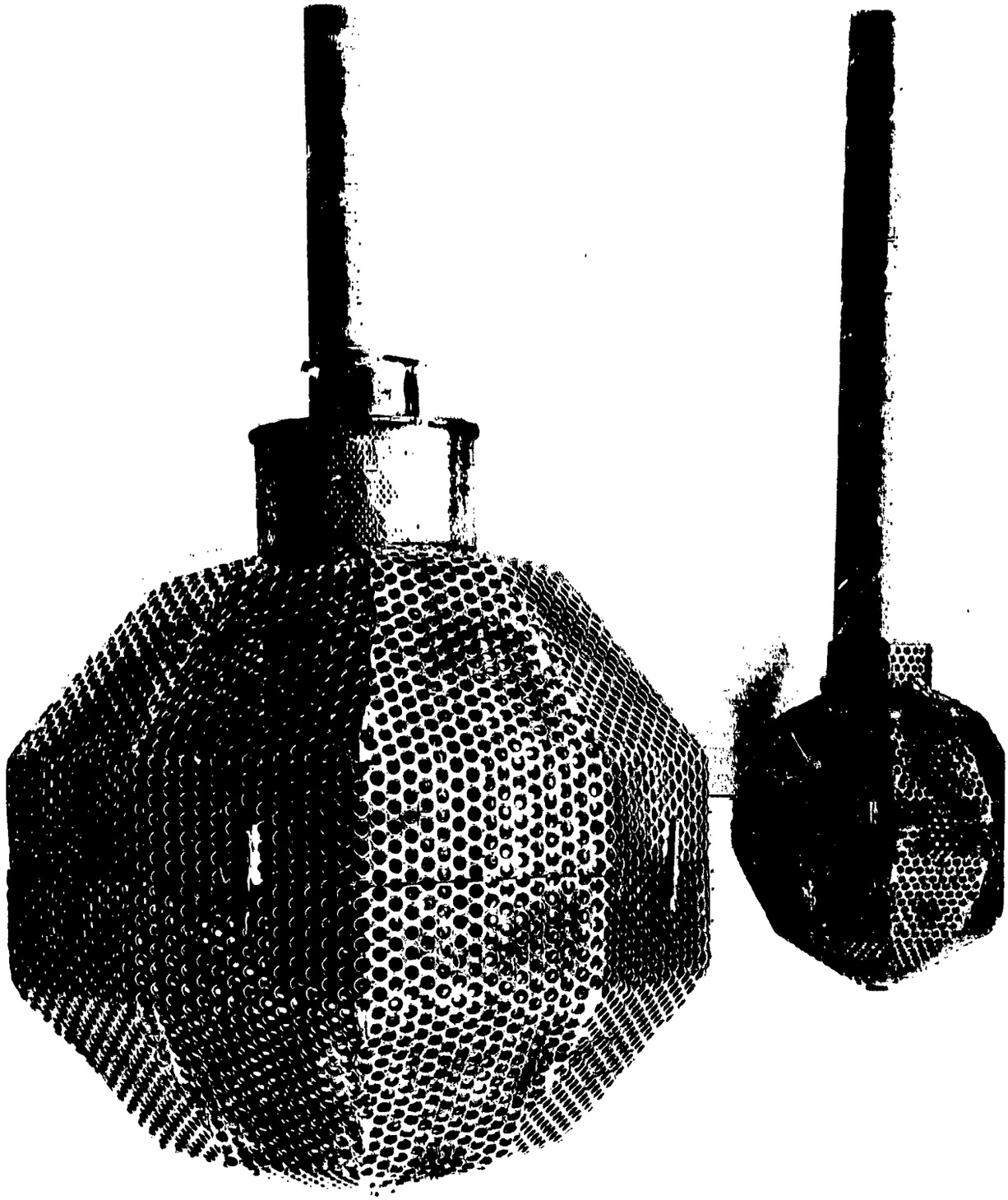

Fig. 5.3 3 in. and 6 in. Spherical injectors

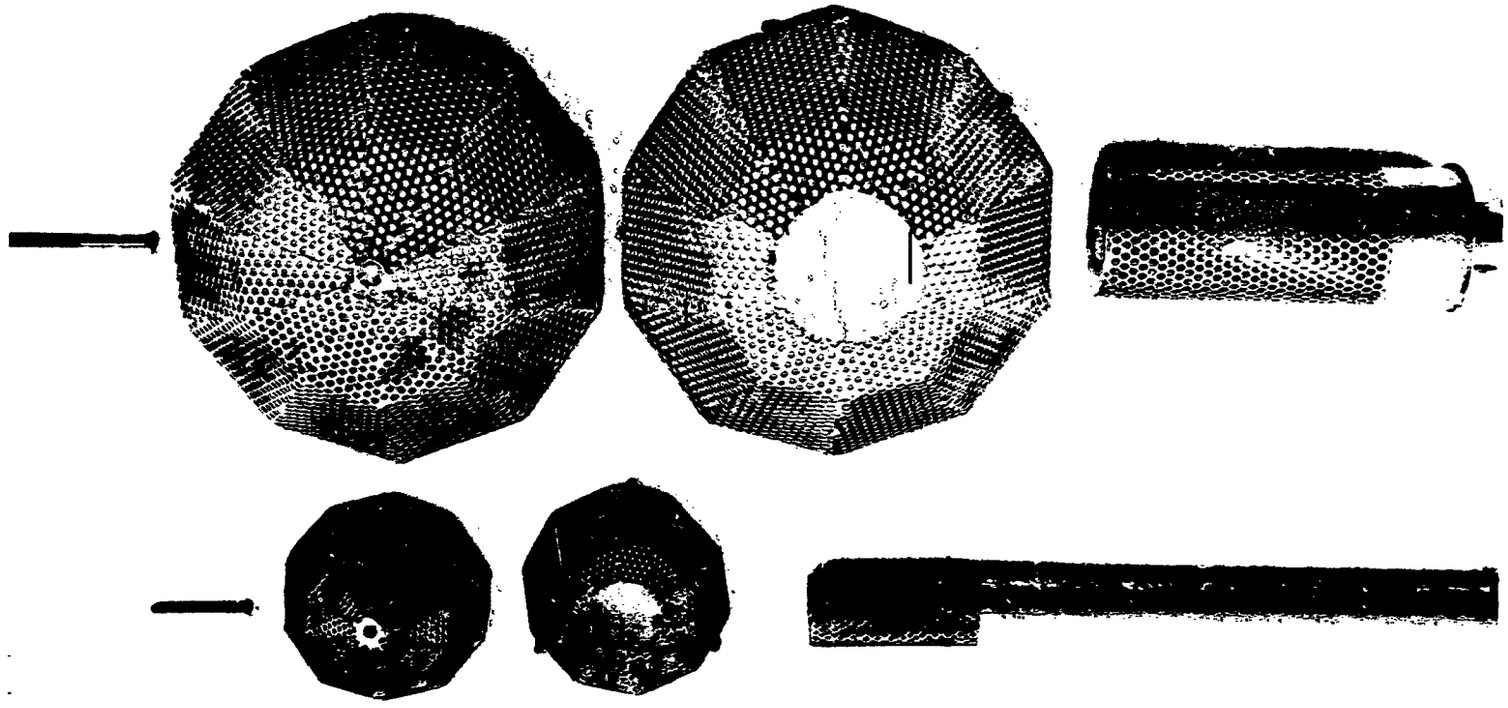

Fig. 5.4 3 in. and 6 in. Spherical injector details

which gives maximum volume fraction of the central gas in the cavity. When heavier-gas-than-air gases are involved for the central gas, it becomes difficult to provide sufficient dispersal forces without also entraining so much of the central gas in the outside gas stream that volume fraction suffers significantly.

With tests in the spherical arrangement involving heavier than air gases for the center gas, an unexpected buoyancy force resulted from the recirculation patterns produced in the interior of the sphere. These recirculation patterns are shown in Figure 5.5. The effect of these recirculation patterns on the central gas is shown in Figures 5.6 and 5.7, for the 18-inch and 36-inch spheres, respectively. The upward recirculation with air as the center gas is quite evident, and even with argon there is evidence of significant buoyancy, enough to even cause the argon to circulate upwards. As can be seen, the position of the injection nozzle is not nearly as critical with this spherical arrangement as it was in the cylinder core arrangement. The latter did not have nearly as strong as recirculation pattern and hence needed to rely more heavily on the velocity shear effects.

The net effect of such recirculation patterns is not only additional buoyancy but additional mixing of the inner and outer gases. However, mixing of hydrogen with the uranium gas is not necessarily a deleterious effect, unless it reduces the overall amount of uranium in the cavity. What is important is to attain the highest possible mass of the central gas distributed in as large as possible radius inside the cavity, in the constraints of the desired low flow rates of outer tubular gas.

5.1.4 Effect of Preferential Direction of Center Gas Injection

Though it has generally been assumed that injection of the center gas will occur from the top of the cavity, this need not necessarily be the case. In fact, since the pellets or fine wire will be injected with a rather high velocity, directing this velocity toward the exhaust nozzle may be considered an inappropriate design. Therefore, some brief studies were done on injection of the center gas from other positions along the cavity wall. In particular, upward injection from a mechanism located near the exhaust end of the nozzle was examined. Figure 5.8 shows comparisons between preferential upward and preferential downward injection.

As can be seen, upward injection offers an additional control mechanism to overcome gravitational or acceleration forces which tend to move the heavy gas out of the cavity. Such flexibility would not exist in the real operating gas core rocket. There, no mechanisms could be positioned inside the cavity, at least near the exhaust nozzle end. However, it might be conceivable that the injection velocity of the pellets or of the fine wire could be varied significantly enough so that the effective injector position (i.e., the point at which the pellet vaporizes) could be made to vary at different longitudinal positions inside the cavity.

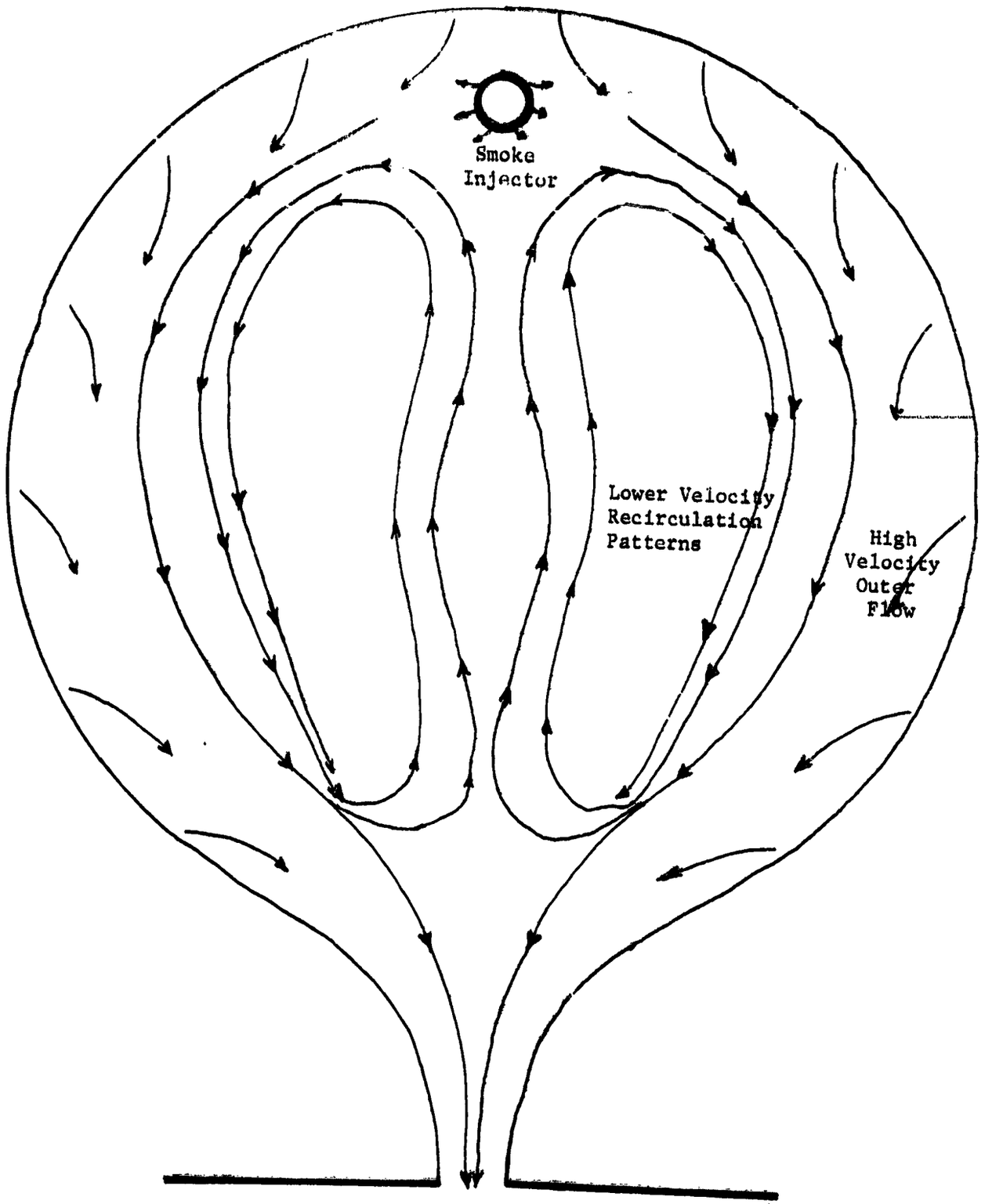

Fig. 5.5 Typical cavity recirculation patterns

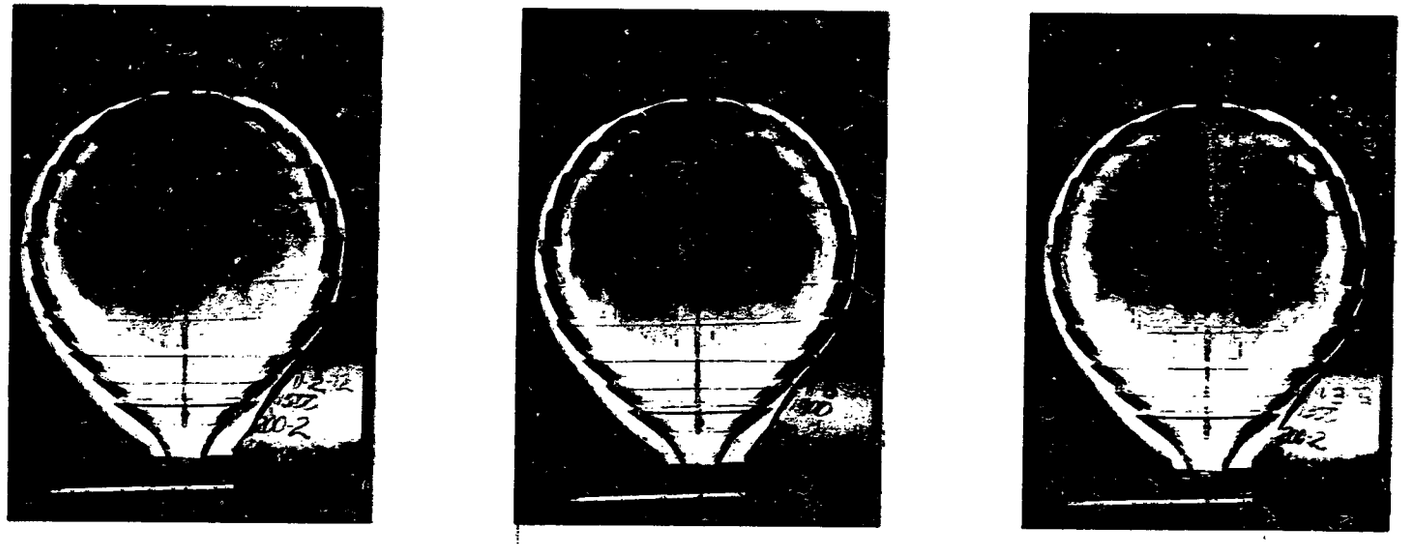

18 in. 3-D, Air, injector (3 in. sphere) at 2 in., 5 in., and 10 in. down

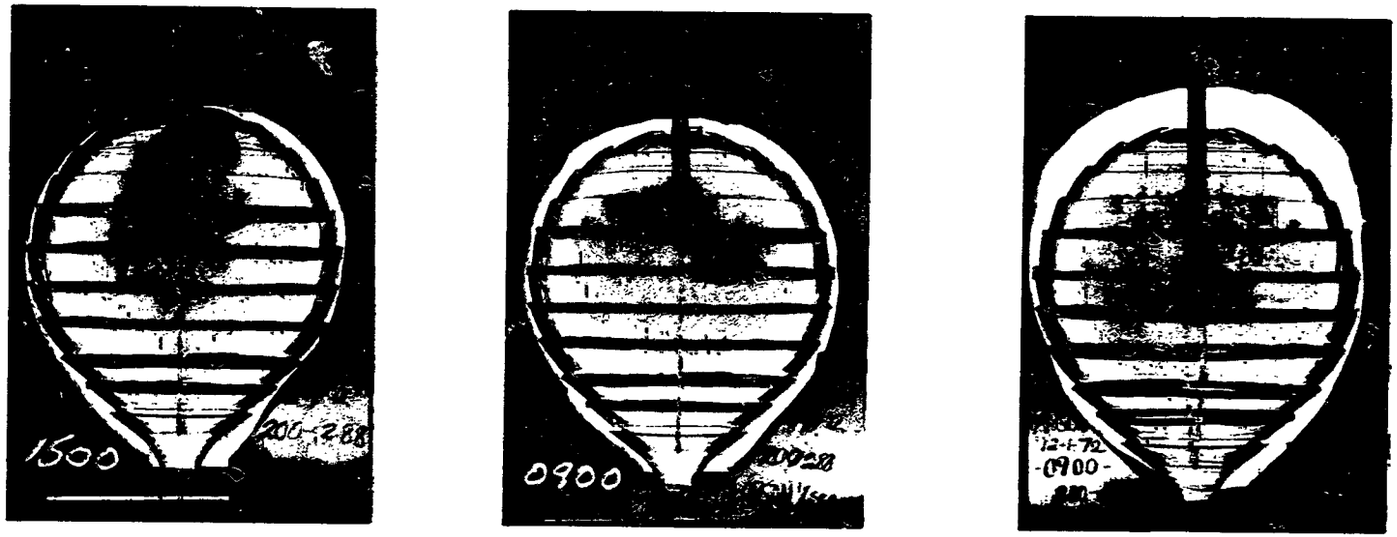

18 in. 3-D, argon, injector at 2 in., 5 in., and 10 in. down

(Some louvers blocked with Scott foam)

Fig. 5.6 18 in. spherical test cases showing recirculation effects arising from varying 3 in. injector position

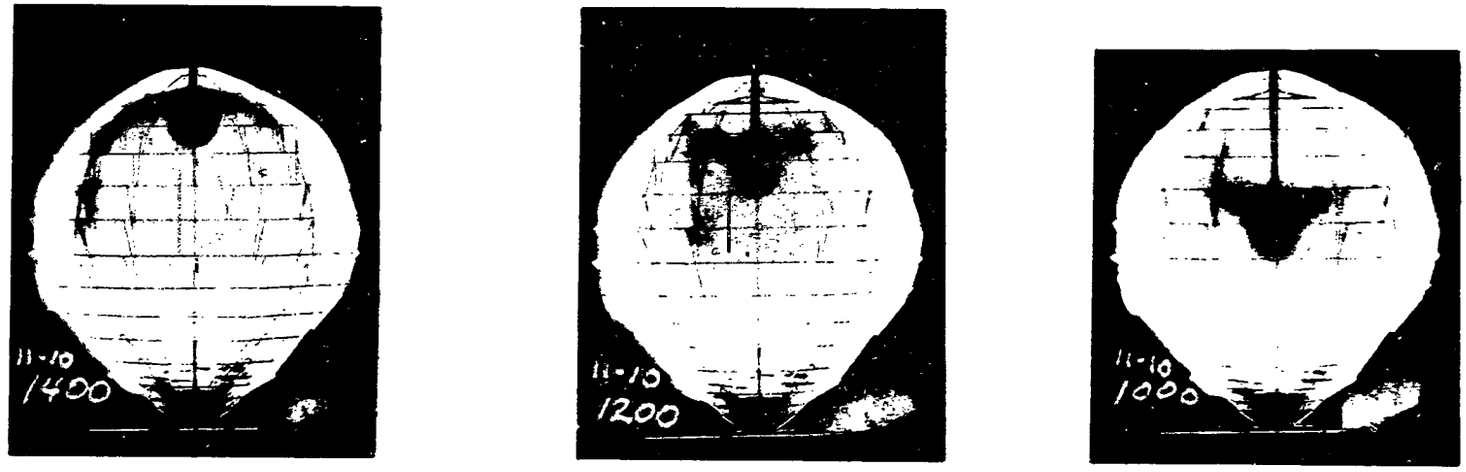

36 in. 3-D, Air, injector (6 in. sphere) at 4-1/2 in., 10 in., and 20 in. down

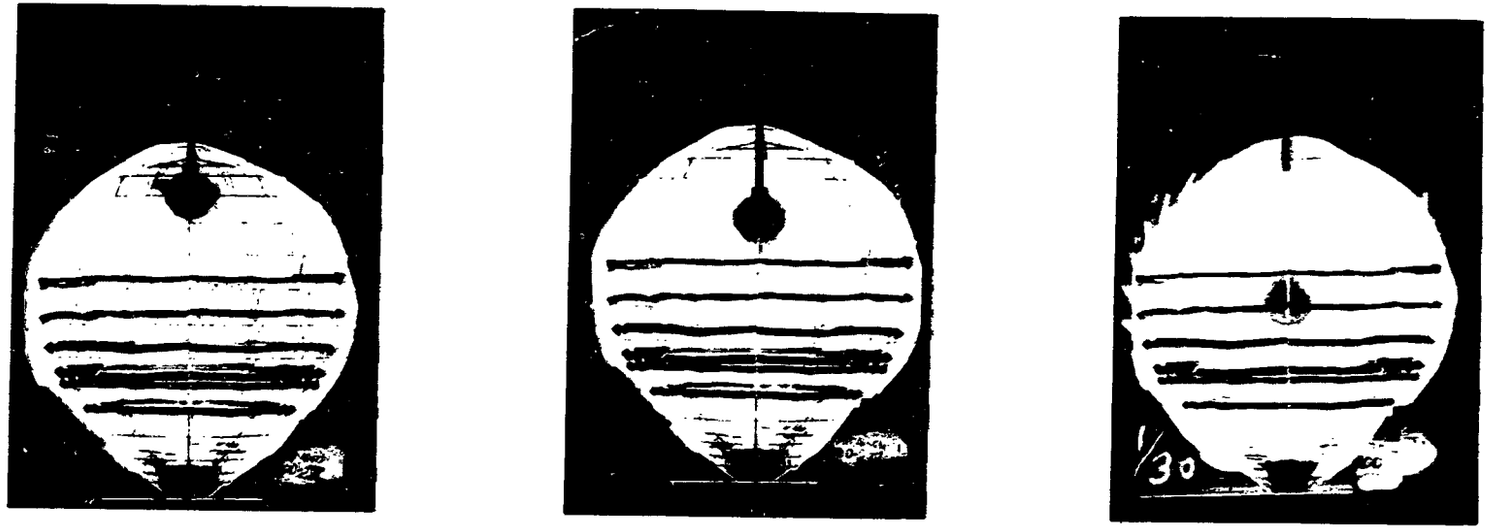

36 in., 3-D, argon, injector at 4-1/2 in., 10 in., and 20 in., down
(Some louvers blocked with Scott foam)

Fig. 5.7 36 in. spherical test cases showing recirculation effects arising from varying 6 in. injector position

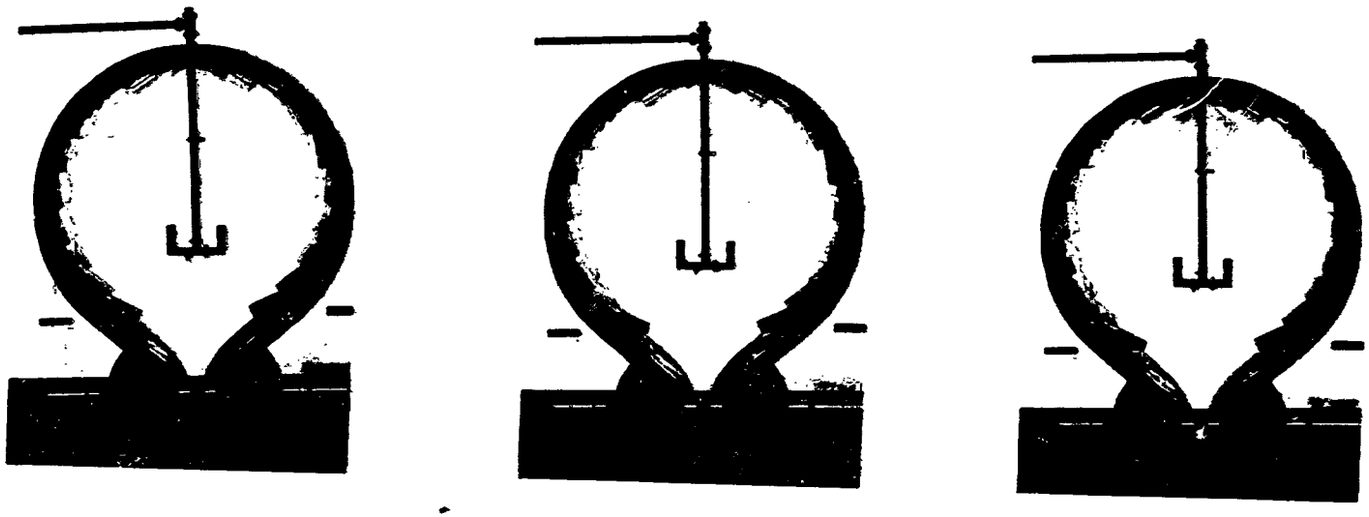

Upward injection of air through two diffused nozzles at 1, 2, and 4 cfm total. 400 cfm outside air

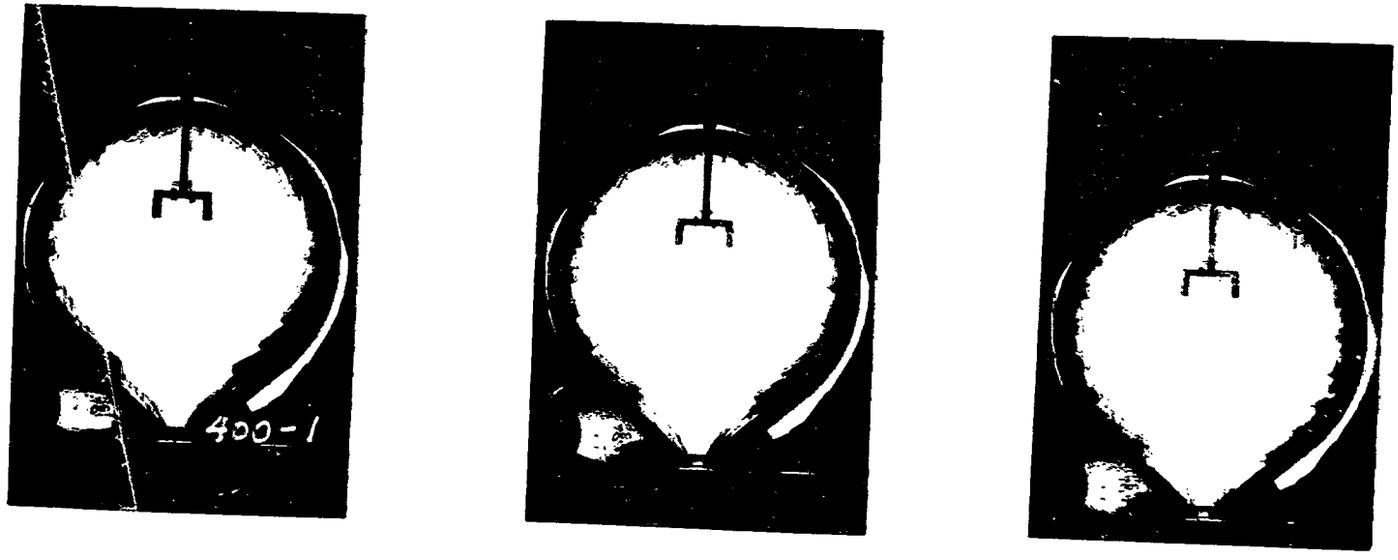

Downward injection of smoke (Same flow conditions)

Fig. 5.8 Effect of preferential direction of injection

5.2 Scaling Studies

A problem of primary importance in developing analysis techniques for gas core reactor technology is that of scaling from small test configurations to large reactor cavities. In an effort to determine the applicable scaling laws for a flowing gas cavity, tests were conducted on the two-dimensional and spherical cavities in both the 18 in. and 36 in. sizes. In these tests, the 2-D cavities were of essentially identical geometry even including the injector dimensions. The 36 in. spherical cavity was a factor of two scale-up from the 18 in. case, except that the large sphere was octagonal, instead of having a circular cross section as for the small one. (The difference between an octagon and circle on the experimental results should be insignificant.)

Figures 5.9 to 5.12 show examples of some of the scale-up comparisons, for both argon and air as the inner gas. (The outer gas was air in all cases.) As is well known, the equation of motion in fluid flow is dimensionless for constant values of the modified Froude and Reynold's numbers. But as is equally well known, it is usually impossible to maintain dynamic similarity if the size is changed, unless the fluid physical characteristics can be manipulated also. Therefore, the figures cited each show a comparison example in which the Reynold's number in one case, and the modified Froude number in another, is approximately constant.

In determining the scaling for these numbers, it was assumed that the inlet velocities vary inversely with surface area change. Hence, in scaling from the small to large cavities, linear dimensions doubling, the Reynold's number is constant for a factor of two increase in flow. The modified Froude number is constant for a factor of $\sqrt{32} = 5.7$ increase in flow. Note that all of the pictures do not reflect exactly these ratios, since for other considerations a particular sequence of test conditions was employed.

As can be seen, neither the Reynold's nor modified Froude numbers appear to be satisfactory scaling indices. However, the results generally indicate an apparent dynamic similarity somewhere between the matching modified Froude and Reynold's number conditions, but favoring somewhat the Reynold's number. It does appear that the scaling up from 1-1/2 ft diameter to 3 ft diameter cavities occurs in a logical manner and that similar extrapolations to 8 or 10 ft diameter cavities can be made, but with care.

5.3 Buoyancy Effects

An important common fluid hydraulic parameter in rocket engine applications is the Froude number. This dimensionless number is empirically derived to show the effect of gravity (or engine acceleration in outer space) on the fuel-propellant in the engine chamber. In the gas core reactor rocket engine, the regular Froude number has to be modified to account for the difference between the fuel and propellant densities. Petre[8] suggested that the modified Froude number, called the buoyancy number, be given by

$$B = \sqrt{\frac{gD}{v^2}\,\frac{\Delta\rho}{\rho_F}}$$

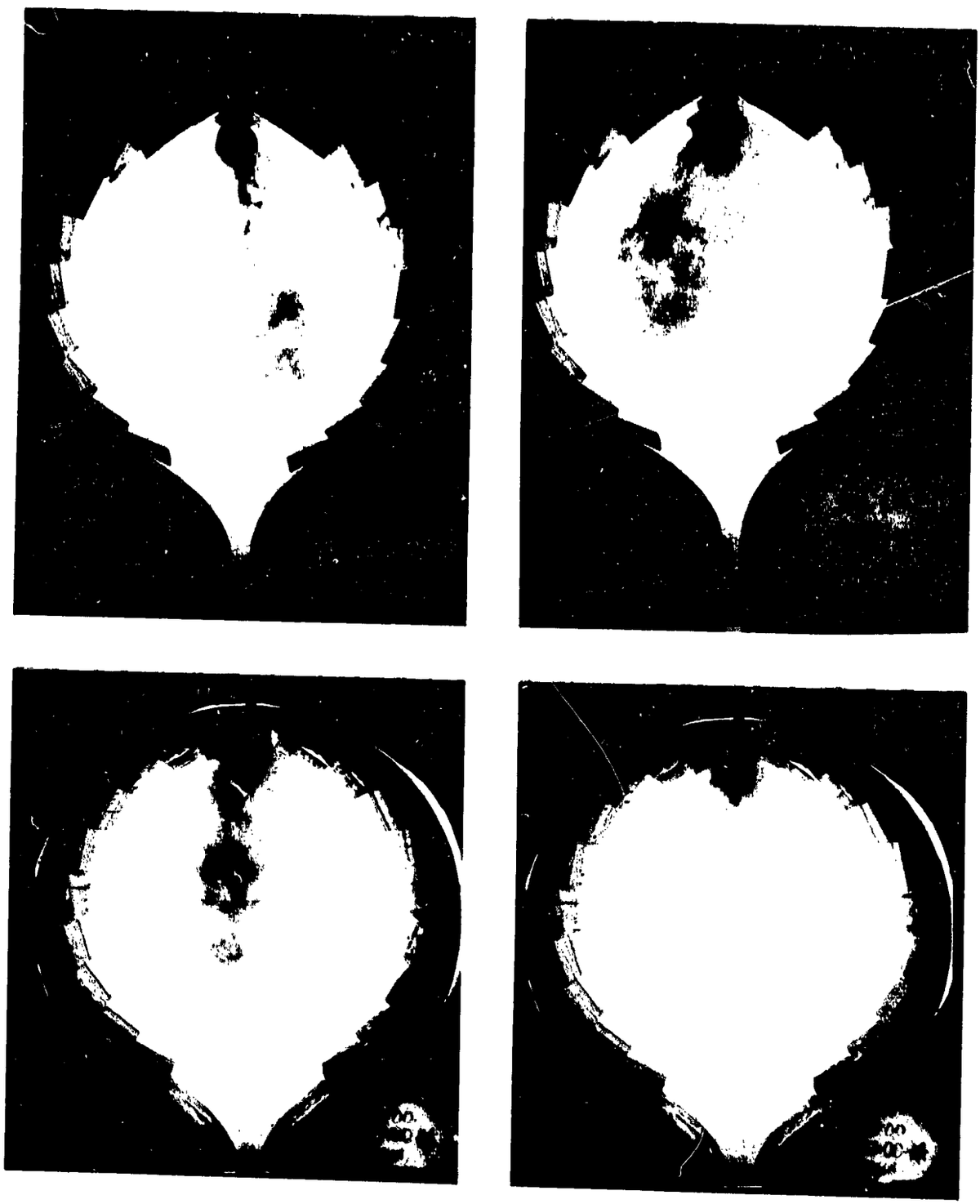

Upper pictures, 18 in. cavity, 100 cfm/0.72 cfm and 200/1.44
Lower pictures, 36 in., cavity, 720 cfm/2.88 cfm and 400/2.88

Fig. 5.9 Scaling series with two-dimensional cavities

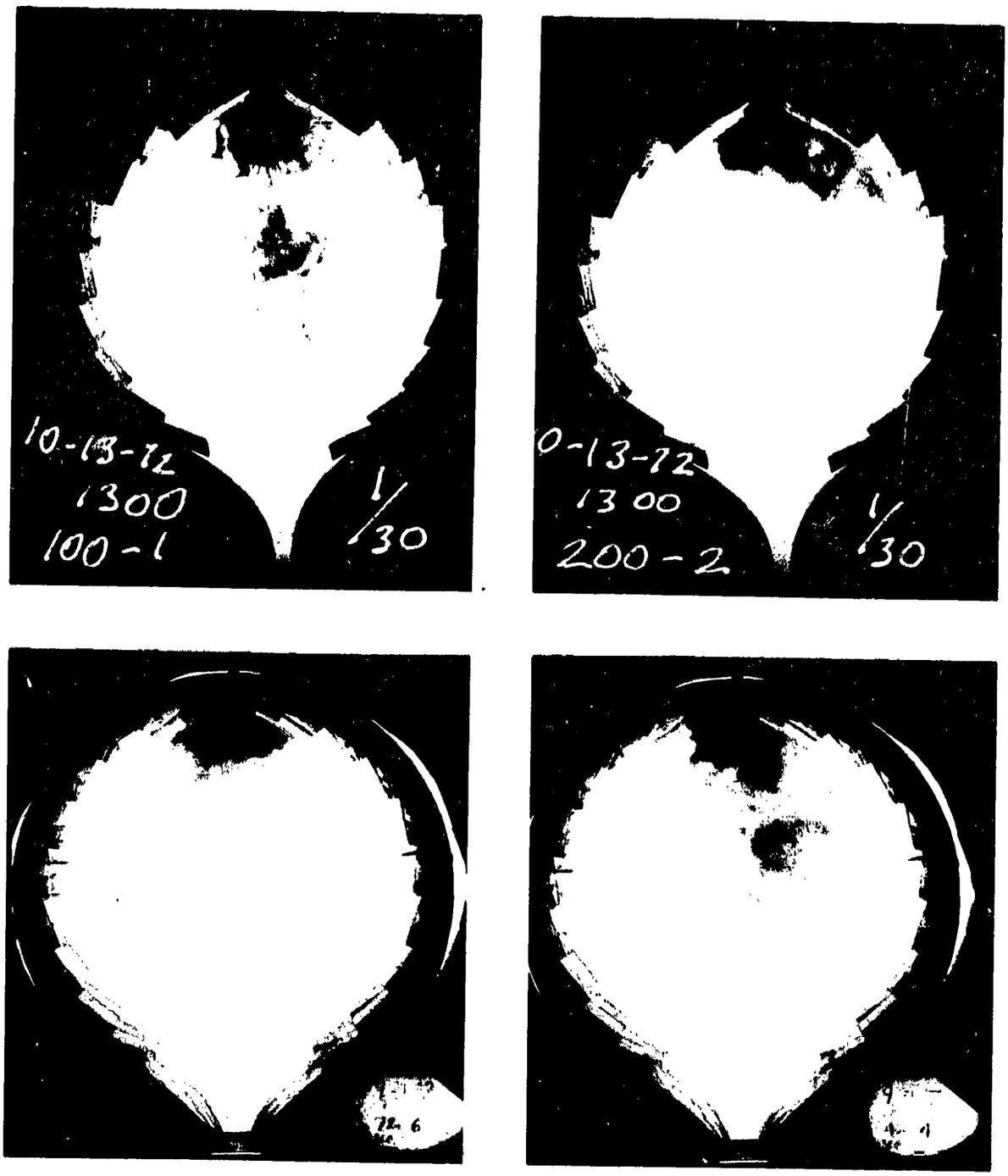

Upper pictures, 18 in., cavity, 100 cfm/1 cfm and 200/2
Lower pictures, 36 in., cavity, 720 cfm/6 cfm and 400/4

Fig. 5.10 Scaling series with two-dimensional cavities

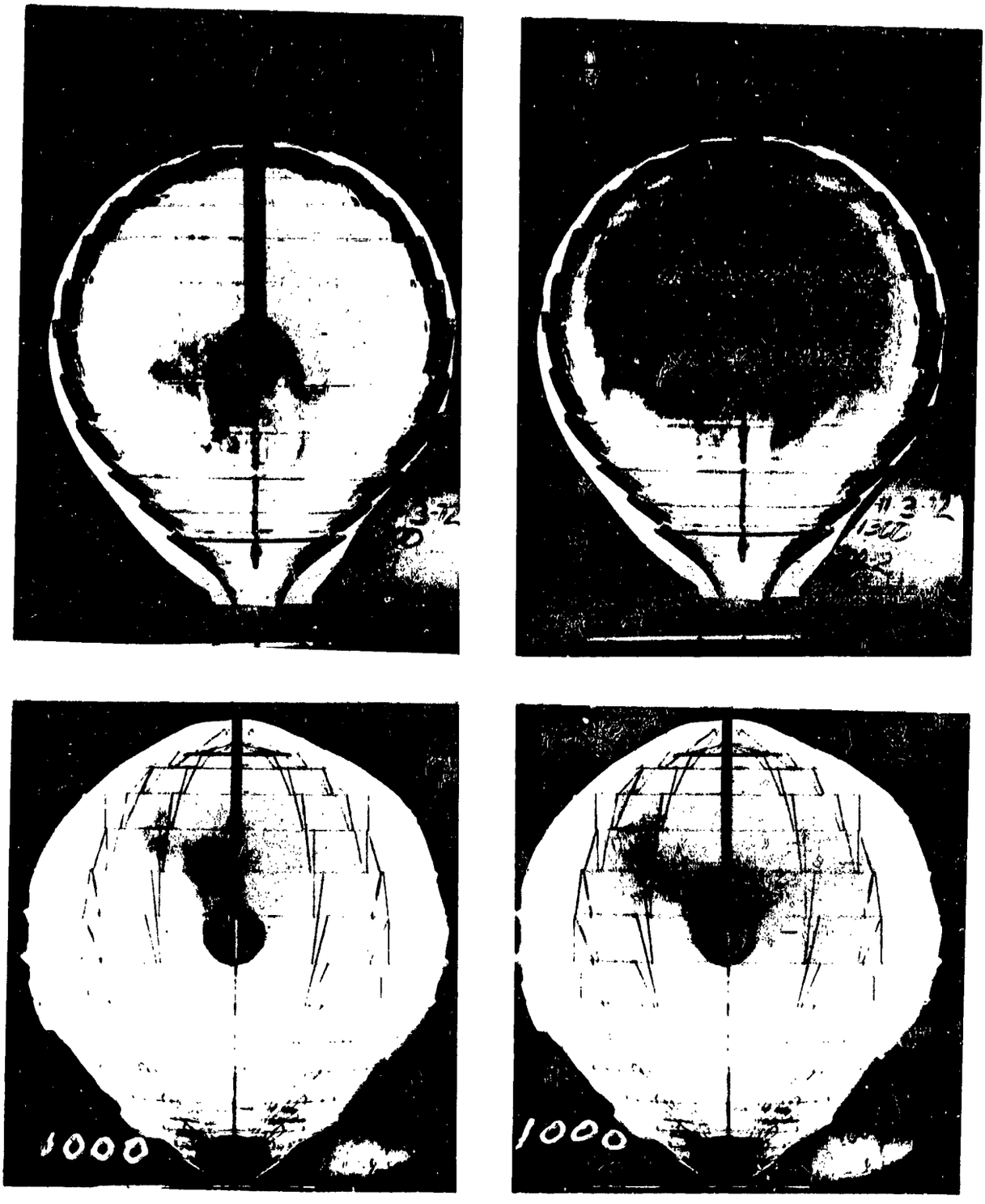

Upper pictures, 18 in., cavity, 100 cfm/1 cfm and 200/2
Lower pictures, 36 in. cavity, 600 cfm/6 and 400/4

Fig. 5.11 Scaling series with spherical cavities

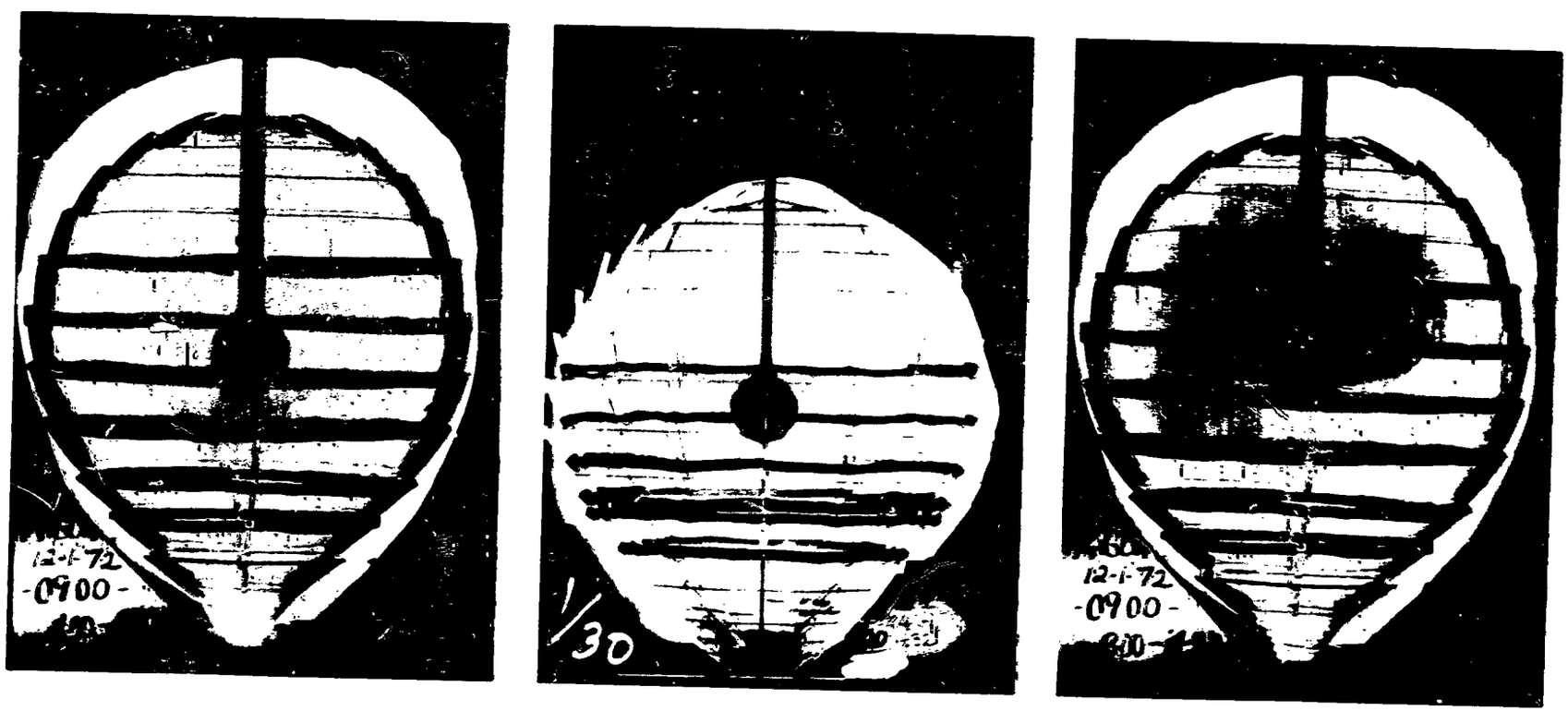

Middle picture, 36 in., cavity at 600 cfm/4.32 cfm
Left picture, 18 in. cavity at 100 cfm/0.72 cfm
Right picture, 18 in. cavity at 300 cfm/4.32 cfm

Fig. 5.12 Scaling series with spherical cavities

which is the square root of the inverse of the usual Froude number, times a factor for the relative density effect. Experimentation has shown that as the relative densities increase, fuel containment decreases, making the buoyancy number proportional to the mass ratio of the inner and outer gases, and inversely proportional to the fuel containment.

The buoyancy numbers were calculated for a large series of 2-D test cases for both the 18 and 36 in. cavities. The D in the formula was taken in all cases to be the nominal distance from the injector to the exit nozzle, a reasonably representative measure of the distance a fuel particle travels within the cavity. The velocity term in the formula is squared, which fact, coupled with poor correlation hoped for between buoyancy and fuel containment, led to the choice of "combined" buoyancy numbers, using the product of two differently determined velocities for the velocity squared term. These calculations are summarized in Tables 5.1 and 5.2.

Initially it was assumed that the velocity to be used in determining buoyancy should be the injection velocity of the inner gas. The measure of fuel containment to which the buoyancy numbers should correspond is taken to be the cavity volume fraction, the ratio of volume of the cavity that would be filled with fuel, if all the fuel were collected into a region of 100% density, to the total cavity volume. Figure 5.13 shows this initial buoyancy number, called the Injector Buoyancy number, vs the fuel volume fraction. While a general trend can be seen, better correlation was hoped for, so additional buoyancy numbers were postulated.

Figure 5.14 shows the Recirculation Buoyancy number, which uses 1/10 of the outer gas flow velocity for the velocity squared term. This scheme assumes that an arbitrary fraction of the outer gas recirculates within the cavity, buoying up the inner gas. Correlation is poor in this case also.

Figure 5.15 depicts the results of the Combination Buoyancy numbers, derived by combining the injection velocity times the recirculation velocity for the velocity squared term. Again, no distinct correlation between buoyancy and volume fraction was observed.

Since no definite correlations were found with the previously mentioned methods for arriving at a buoyancy number, an Area Buoyancy number was defined by choosing the velocity to be used by assuming that the volume of the inner gas injected per unit time crosses the midplane turbulence area of the cavity, giving a velocity for the fuel. These numbers are displayed in Figure 5.16. Again, a general trend may be seen, but no inflection point between good and poor volume fractions.

The last buoyancy number shown, the Residence Buoyancy number, Figure 5.17, used a velocity derived from the distance from the injector to the exit nozzle divided by an average fuel particle residence time. The residence time was determined by dividing the volume occupied by fuel by the volume flow rate, to give a representative time that a fuel particle recirculates in the cavity. Here, as in the preceding cases, it can be seen that, in general, as buoyancy number increases, volume fraction decreases, but no optimum buoyancy numbers could be identified.

Table 5.1

18 in. - 2D Cavity - All Solid Louvers - Body 51% open, 3/16 in. holes

1 in. diameter injector 51% open 3/16 in. hole covered with 1/4 in. coarse foam 10 in. long

1/4 in. foam from louver 2 to midplane, 1/2 in. foam from there to bottom - last 5 in. of body solid

1	2	3		4	5	6	7	8	9	10	11	12	13	14
Run				CFM Outer Air	Inner Gas		Mass Flow Ratio	Inner Injection Velocity		Outer Eff. Velocity at Midplane(4)	1/10 Outer Velocity	Inner Effective Velocity Through Midplane(5)	Residence Time (Effective)(6)	Inner Effective Velocity From Residence Time(7)
Date	Time	Frame No. (1)			Type	CFM		Length(2)	Velocity(3)					
10-13-72	1330	1A	(26A)	50	Air	1	50	10	0.076	1.41	0.141	0.0113	31.94	D.0535
		2A	(25A)			2	25	10	0.153			0.0227	16.30	D.1048
		3A	(19A)	100		1	100	10	0.076	2.81	0.291	0.0113	28.06	D.0609
		4A	(20A)			2	50	10	0.153			0.0227	16.64	D.1027
		5A	(22A)			4	25	10	0.306			0.0454	11.66	D.1465
		6A	(23A)			6	17	10	0.458			0.0680	8.55	D.1997
		7A	(16A)	200		1	200	10	0.076	5.62	0.562	0.0113	34.34	D.0497
		8A	(15A)			2	100	10	0.153			0.0227	21.25	D.0804
		9A	(13A)			4	50	10	0.306			0.0454	7.52	D.2243
		10A	(12A)			6	33	10	0.458			0.0680	5.46	D.3130
10-13-72	1400	15A	(2A)	100	Argon	0.72	100	7	0.078	2.81	0.281	0.0082	27.10	D.0630
		14A	(3A)			1.44	50	7	0.157			0.0163	14.48	D.1180
		13A	(5A)			2.88	25	7	0.314			0.0326	9.79	D.1745
		10A	(9A)	200		0.72	200	7	0.078	5.62	0.562	0.0082	36.19	D.0472
		11A	(8A)			1.44	100	7	0.157			0.0163	22.46	D.0761
		12A	(6A)			2.88	50	7	0.314			0.0326	11.60	D.1473
10-13-72	1400	18A	(25A)	100	Freon	0.5	50	3*	0.240	2.81	0.281	0.0057	20.04	D.0852
		17A	(26A)			1.0	25	3	0.255			0.0113	9.76	D.1751
		19A	(23A)	200		0.5	100	4*	0.171	5.62	0.562	0.0057	23.79	D.0718
		20A	(22A)			2.0	25	7	0.218			0.0228	7.22	D.2367

* Indicates that smoke seemed not to come from entire circumference of injector, and adjusted area values were used for computations.

Table 5.1 (Cont'd)

15	16	17	18	19	20	21	22	23
B_1 v_1 = Col. 9	B_2 v_2 = Col. 11	B_3 $v_3^2 = v_1 \times v_2$	B_4 v = Col. 12	B_5 v_5 = Col. 14	Volume Fraction Inner Gas in Cavity	Data Method for Col. 20[8]	Outer Reynold's Number	Inner Reynold's Number
12.27	6.67	9.06	82.74	17.54	23.9	PS	9246	568
6.14		6.39	41.37	8.95	24.4	PS		1144
12.27	3.33	6.42	82.74	15.41	21.0	PS	18428	568
6.14		4.52	41.37	9.14	24.9	PS		1144
3.07		3.20	20.68	6.40	34.9	PS		2288
2.04		2.61	13.79	4.70	38.4	PS		3424
12.27	1.67	4.53	82.74	18.86	25.7	PS	36857	568
6.14		3.20	41.37	11.67	31.8	PS		1144
3.07		2.26	20.68	4.18	22.8	PS		2288
2.04		1.85	13.79	3.00	24.5	PS,PS		3424
44.29	12.37	23.50	426.12	55.18	14.6	PS	10428	691
22.14		16.56	213.06	29.48	15.6	PS		1391
11.07		11.71	106.53	19.94	21.1	PS		2781
44.29	6.18	16.61	426.12	73.70	19.5	PS	36859	691
22.14		11.71	213.06	45.73	24.2	PS		1391
11.07		8.28	106.53	23.62	25.0	PS		2781
23.94	20.42	22.12	1013.34	67.41	7.5	PS	18428	3307
22.50		21.46	506.67	32.80	7.3	PS		3513
33.51	10.21	18.53	1013.34	80.000	8.9	PS	36857	2356
26.33		16.41	253.34	24.27	10.8	PS		3004

Table 5.1 (Cont'd)

(1) Frame number not in parenthesis is for instantaneous shot. Number in parenthesis is time exposure.

(2) Not applicable for sphere

(3) Based on full area (not just open portion) over effective injection length

(4) Based on apparent width of high velocity turbulent layer at the widest plane in the cavity (middle)

(5) Based on remaining area not included in 10 (footnote 4)

(6) Residence Time $T = \frac{\text{mass of "fuel" in cavity}}{\text{fuel flow rate}} = \frac{\text{Vol. cavity x Vol. fraction x } \rho}{\text{ft}^3/\text{sec x } \rho} = \frac{\text{Vol. cavity x Vol. Fraction}}{\text{ft}^3/\text{sec inner gas}}$

(7) $v_5 = \frac{\text{Length of Cavity from Injector to Discharge Nozzle}}{\text{Residence Time}}$

(8) FS ≡ full scan on densitometer, PS ≡ partial (one vertical, one horizontal or equivalent) scan, EST ≡ "eyeball" estimate comparison from similar case.

Table 5.2

36 in. - 2D Cavity - All Solid Louvers - Body 47% Open 5/16 in. holes

2 in. diameter Injector 51%, open 3/16 in. holes covered with 1/4 in. coarse form

1/4 in. foam from louver 2 to midplane, 1/2 in. foam from there down. Last 11 in. of body solid

1	2	3		4	5	6	7	8	9	10	11	12	13	14
Run				CFM Outer Air	Inner Gas		Mass Flow Ratio	Inner Injection Velocity		Outer Eff. Velocity at Midplane(4)	1/10 Outer Velocity	Inner Effective Velocity Through Midplane(5)	Residence Time (Effective)(6)	Inner Effective Velocity From Residence Time(7)
Date	Time	Frame No.(1)			Type	CFM		Length(2)	Velocity(3)					
9-21-72	1300	1A	(1A)	100	Air	1	100	10	0.038	0.78	0.078	0.0027	94.86	0.0360
		4A	(2A)			2	50	10	0.076			0.0055	48.21	0.0709
		5A	(4A)			4	25	10	0.153			0.0109	24.88	0.1343
		8A	(5A)	200		1	200	10	0.038	1.55	0.155	0.0027	73.48	0.0465
		9A	(7A)			2	100	10	0.076			0.0055	48.60	0.0703
		12A	(8A)			4	50	10	0.153			0.0109	29.06	0.1176
		13A	(10A)			6	33	10	0.]]9			0.0164	22.81	0.1498
		16A	(11A)	400		1	400	10	0.038	3.10	0.310	0.0027	49.37	0.0692
		17A	(13A)			2	200	10	0.076			0.0055	39.71	0.1112
		20A	(14A)			4	100	10	0.153			0.0109	20.12	0.1698
		21A	(16A)			6	67	10	0.229			0.0164	12.83	0.2663
		25	(17A)	720		4	180	10	0.152	5.58	0.558	0.0109	9.52	0.3587
		25A	(19A)			6	120	10	0.229			0.0164	11.02	0.3102
9-21-72	1400	2A	(33A)	100	Argon	0.72	100	15	0.018	0.78	0.078	0.0020	31.32	0.1091
		3A	(31A)			1.44	50	10	0.055			0.0039	19.87	0.1710
		6A	(30A)			2.88	25	8	0.138			0.0079	10.26	0.3330
		7A	(28A)			4.32	16	8	0.206			0.0118	9.00	0.3797
9-21-72	1500	2A	(18A)	200		0.72	200	12	0.023	1.55	0.155	0.0020		
		3A	(19A)			1.44	100	10	0.055			0.0039		
		4A	(21A)			2.88	50	8	0.138			0.0079		
		5A	(22A)			4.32	33	8	0.206			0.0118	6.66	0.5131
		9A	(12A)	400		0.72	400	12	0.023	3.10	0.310	0.0020	36.72	0.0931
		8A	(13A)			1.44	200	10	0.055			0.0039	37.96	0.0917
		7A	(15A)			2.88	100	8	0.138			0.0079		
		6A	(16A)			4.32	67	8	0.206			0.0118		

Table 5.2 (Cont'd)

15	16	17	18	19	20	21	22	23
B_1 v_1 = Col. 9	B_2 v_2 = Col. 11	B_3 $v_3^2 = v_1 \times v_2$	B_4 v = Col. 12	B_5 v_5 = Col. 14	Volume Fraction Inner Gas in Cavity	Data Method for Col. 20[8]	Outer Reynold's Number	Inner Reynold's Number
34.71	17.11	24.37	485.55	36.83	24.44	PS	9493	581
17.35		17.23	242.78	18.72	24.8	PS		1162
8.68		12.14	121.39	9.66	25.6	PS		2339
34.71	8.56	17.29	485.55	28.53	18.9	PS	18864	581
17.35		12.22	242.78	18.87	25.0	PS		1162
8.68		8.61	121.39	11.28	29.9	PS		2339
5.78		7.04	80.92	8.86	35.2	PS		3500
34.71	4.28	12.22	485.55	19.17	12.7	PS	37728	581
17.35		8.64	242.78	11.93	15.8	PS		1162
8.68		6.09	121.39	7.81	20.7	PS		2339
5.78		4.98	80.92	4.98	19.8	PS		3500
8.68	2.38	4.54	121.39	3.70	9.8	PS	67910	2339
5.78		3.71	80.92	4.28	17.0	PS		3500
268.17	63.46	131.29	2500.67	45.09	5.8	PS	9493	326
89.39		75.11	1250.33	28.77	7.4	PS		996
35.73		47.42	625.17	14.77	7.6	PS		2499
23.82		38.81	416.78	12.96	10.0	PS		3731
214.46	31.73	82.39	2500.67				18864	417
89.39		53.28	1250.33					996
35.73		33.64	625.17					2499
23.82		27.53	416.78					3731
214.46	15.86	58.26	2500.67	9.59	7.4	PS	37728	417
89.39		37.67	1250.33	52.87	6.8	PS		996
35.73		23.78	625.17	53.64	13.8	PS		2499
23.82		19.47	416.78					3731

Table 5.2 (Cont'd)

1	2	3		4	5	6	7	8	9	10	11	12	13	14
Run				CFM	Inner Gas		Mass	Inner Injection Velocity		Outer Eff. Velocity	1/10	Inner Effective Velocity		Inner Effective Velocity From
Date	Time	Frame No.(1)		Outer Air	Type	CFM	Flow Ratio	Length(2)	Velocity(3)	at Midplane(4)	Outer Velocity	Through Midplane(5)	Residence Time (Effective)(6)	Residence Time(7)
9-21-72	1400	10A	(27A)	720	Argon	1.44	360	10	0.055	5.58	0.558	0.0039	29.43	0.1161
		11A	(25A)			2.88	180	10	0.110			0.0079	25.11	0.1361
		14A	(25)			4.32	120	8	0.206			0.0118	16.83	0.2030
		15A	(22A)			5.76	90	8	0.275			0.0157	11.34	0.3013
		19A	(21A)			7.20	72	8	0.344			0.0197	10.75	0.3180
9-25-72	1300	11	(22)	100	Freon	0.5	50	8*	0.075	0.78	0.078	0.0014	45.87	0.0745
		7	(23)			1.0	25	15*	0.053			0.0027	32.66	0.1046
		10	(25)			2.0	13	8	0.096			0.0055	23.52	0.1453
9-28-72	1500	10	(24A)	200		0.5	100	8*	0.075	1.55	0.155	0.0014	41.21	0.0829
		9	(25A)			1.0	50	15*	0.053			0.0027	11.66	0.2929
		8	(27A)			2.0	25	8	0.096			0.0055	8.36	0.4088
		7	(28A)			2.5	20	6	0.159			0.0068	7.00	0.4882
		3	(34A)	400		0.5	200	8*	0.075	3.10	0.310	0.0014	27.99	0.1221
		4	(33A)			1.0	100	15*	0.053			0.0027	15.94	0.2144
		5	(33A)			2.0	50	8	0.096			0.0055	6.80	0.5022
		6	(31A)			2.5	40	6	0.159			0.0068	8.55	0.3995
9-25-72	1300	6	(26)	720		1.0	180	15*	0.053	5.58	0.558	0.0027	29.16	0.1172
		3	(28)			2.0	90	8	0.096			0.0055	20.60	0.1658
		2	(29)			2.5	72	6	0.159			0.0068	13.68	0.2497

* Indicates that smoke seemed not to come from entire circumference of injector, and adjusted area values were used for computations.

Table 5.2 (Cont'd)

15	16	17	18	19	20	21	22	23
B_1 v_1 = Col. 9	B_2 v_2 = Col. 11	B_3 $v_3^2 = v_1 \times v_2$	B_4 v = Col. 12	B_5 v_5 = Col. 14	Volume Fraction Inner Gas in Cavity	Data Method for Col. 20(8)	Outer Reynold's Number	Inner Reynold's Number
89.39	8.81	28.08	1250.33	42.36	10.9	PS	67910	996
44.69		19.86	625.17	36.15	18.6	PS		1992
23.82		14.51	416.78	24.23	18.7	PS ,FS		3731
17.86		12.56	312.58	16.33	16.8	PS		4981
14.29		11.23	250.07	15.47	19.9	PS		6230
108.32	104.80	106.22	5946.80	109.08	5.9	PS	9493	243
152.32		126.35	2973.40	77.65	8.4	PS		1493
84.96		93.88	1486.70	55.92	12.1	PS		2705
108.32	52.40	75.35	5946.80	97.99	5.3	PS	18864	2113
152.32		89.63	2973.40	27.73	3.0	PS		1493
84.96		66.60	1486.70	19.87	4.3	PS		2705
51.05		51.75	1189.36	16.64	4.5	PS		4479
108.32	26.20	53.28	5946.80	66.56	3.6	PS	37728	2113
152.32		63.38	2973.40	37.98	4.1	PS		1493
84.96		47.09	1486.70	16.18	3.5	PS		2705
51.05		36.59	1189.36	20.34	5.5	PS		4479
152.32	14.56	47.24	2973.40	69.33	7.5	PS	67910	1493
84.96		35.10	1486.70	48.99	10.6	PS		2705
51.05		27.27	1189.36	32.54	8.8	PS		4479

Table 5.2 (Cont'd)

(1) Frame number not in parenthesis is for instantaneous shot. Number in parenthesis is time exposure.

(2) Not applicable for sphere

(3) Based on full area (not just open portion) over effective injection length

(4) Based on apparent width of high velocity turbulent layer at the widest plane in the cavity (middle)

(5) Based on remaining area not included in 10 (footnote 4)

(6) Residence Time $T = \frac{\text{mass of "fuel" in cavity}}{\text{fuel flow rate}} = \frac{\text{Vol. cavity x Vol. fraction x } \rho}{\text{ft}^3/\text{sec x } \rho} = \frac{\text{Vol. cavity x Vol. Fraction}}{\text{ft}^3/\text{sec inner gas}}$

(7) $v_5 = \frac{\text{Length of Cavity from Injector to Discharge Nozzle}}{\text{Residence Time}}$

(8) FS ≡ full scan on densitometer, PS ≡ partial (one vertical, one horizontal or equivalent) scan,
EST ≡ "eyeball" estimate comparison from similar case.

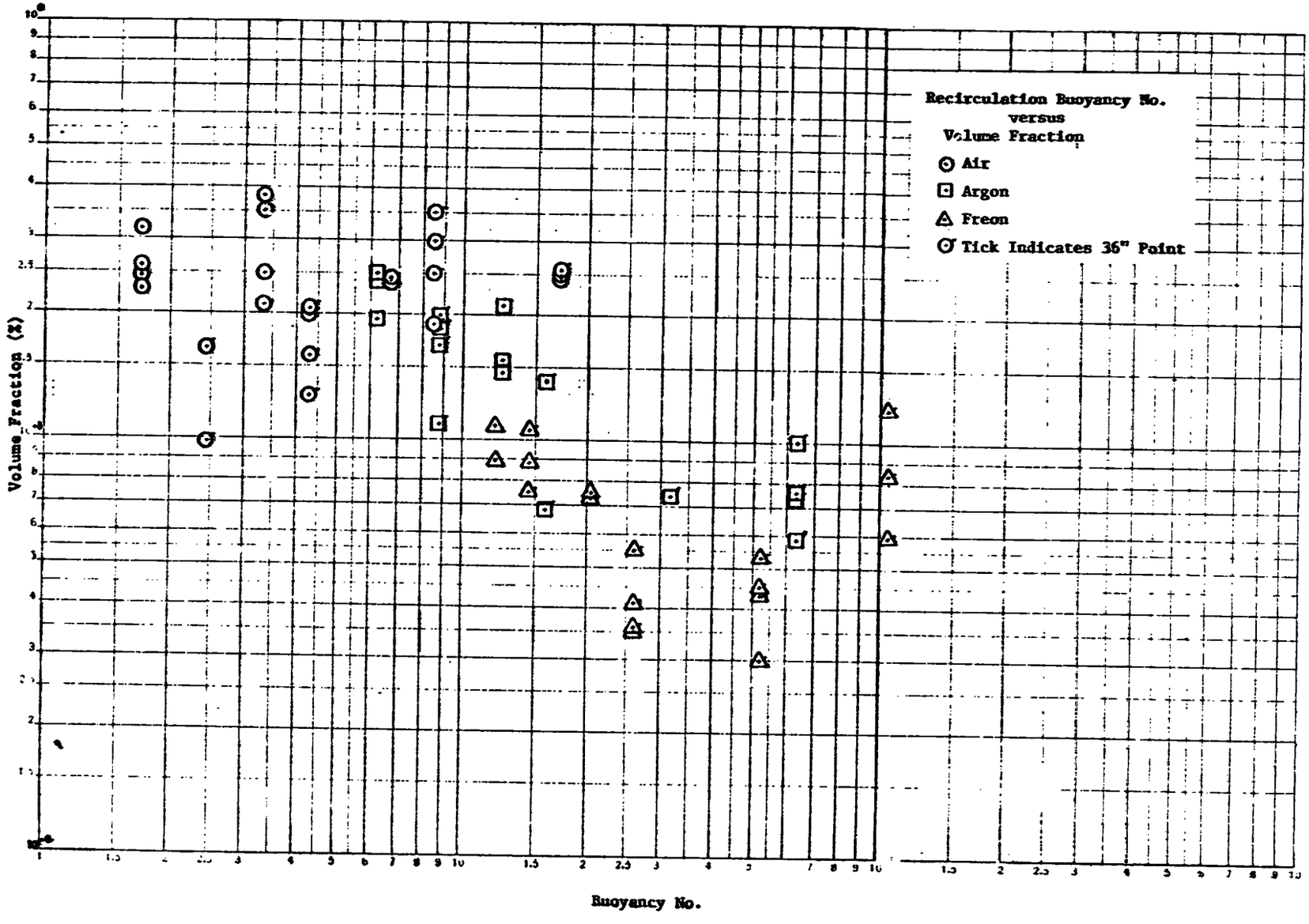

Fig. 5.13 Cavity volume fraction vs injector buoyancy number

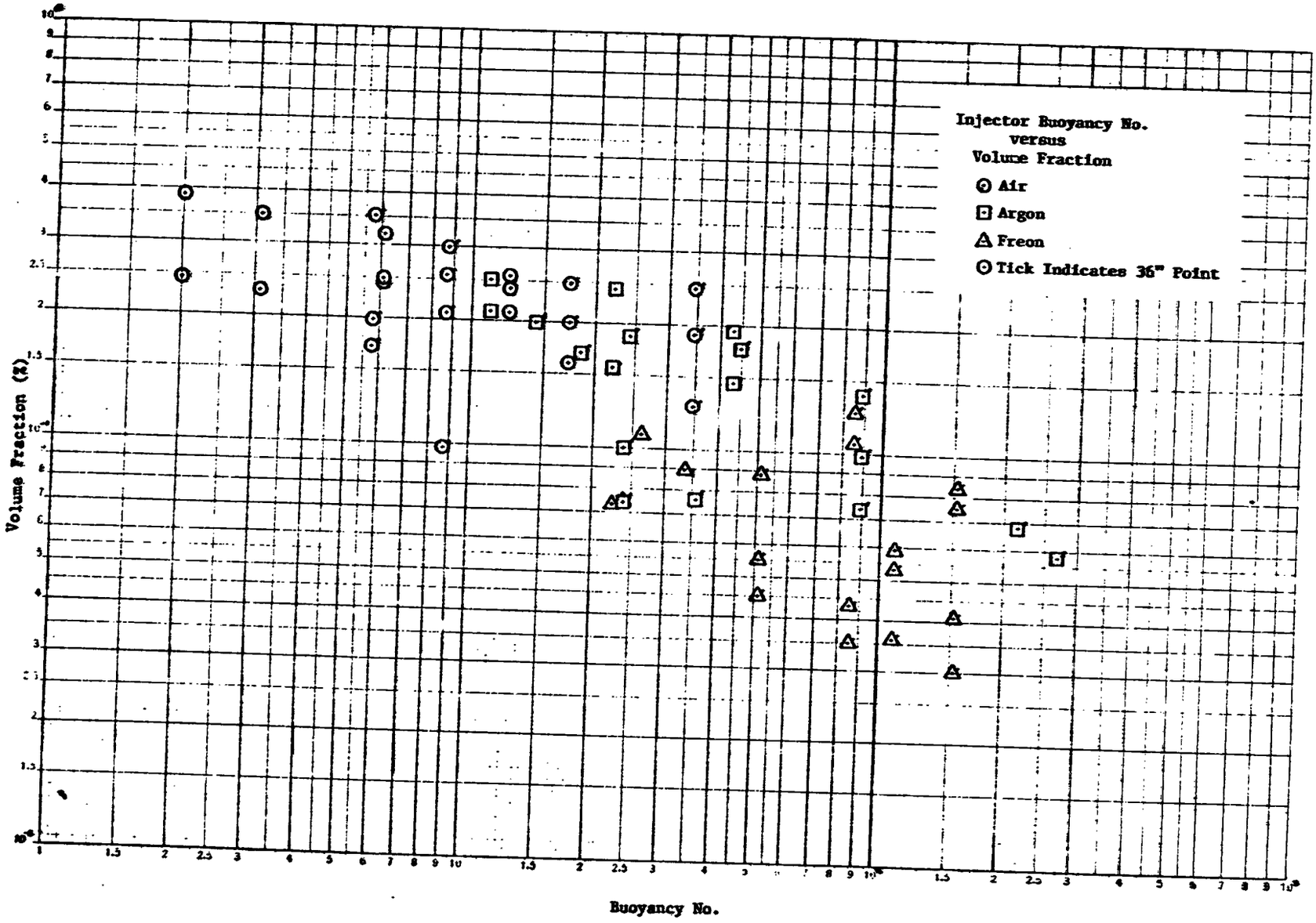

Fig. 5.14 Cavity volume fraction vs recirculation buoyancy number

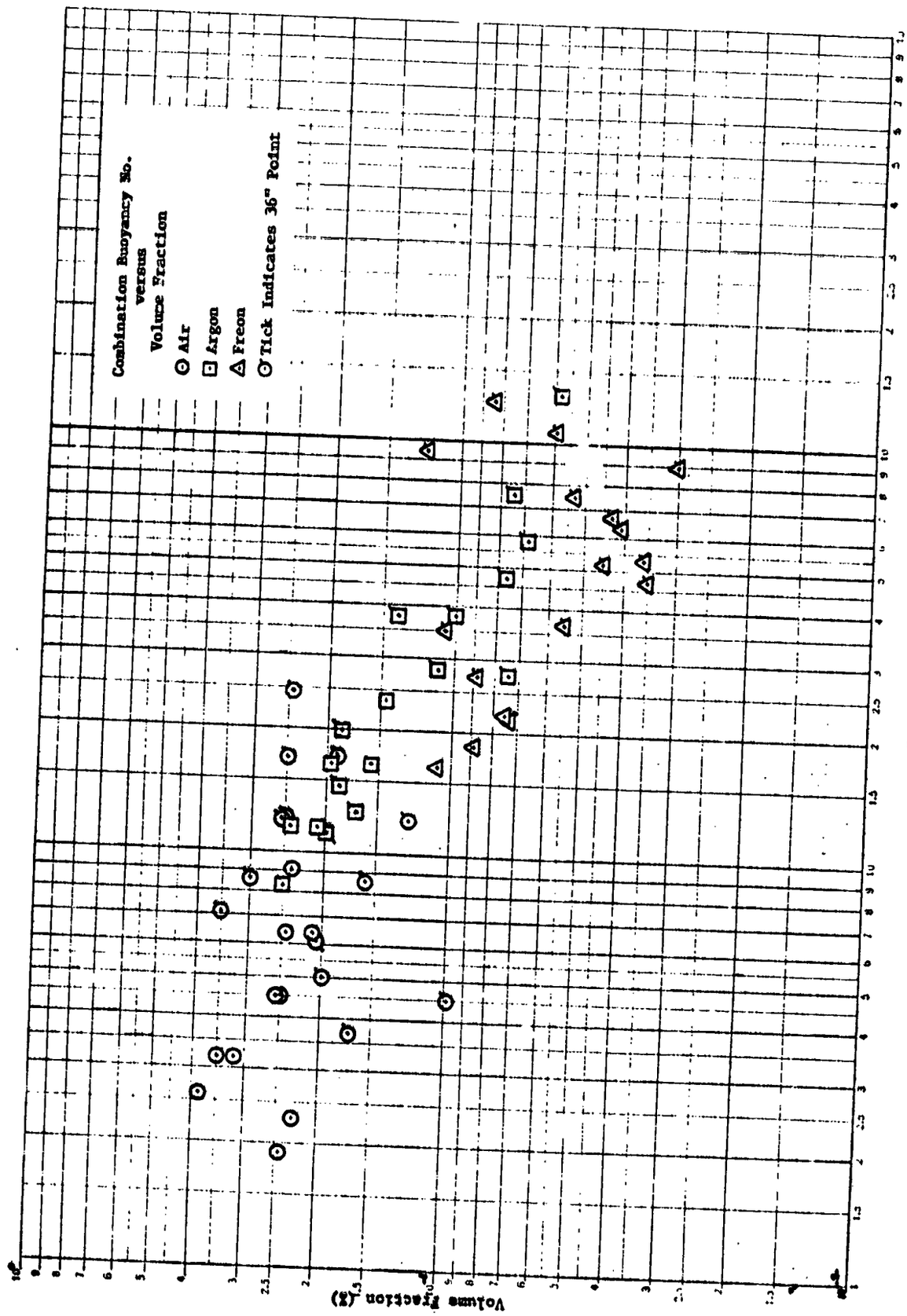

Fig. 5.15 Cavity volume fraction vs combination buoyancy number

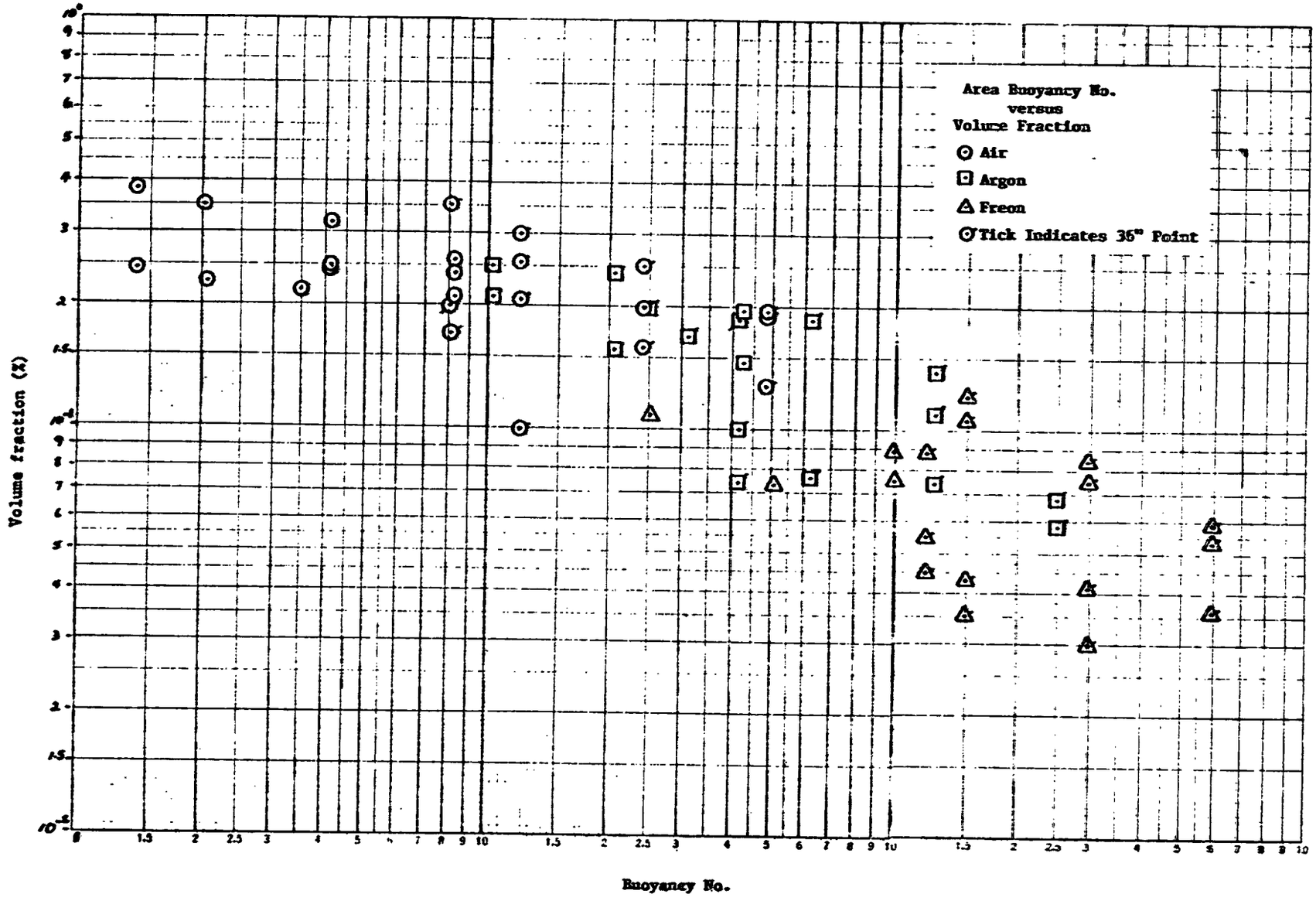

Fig. 5.16 Cavity volume fraction vs area buoyancy number

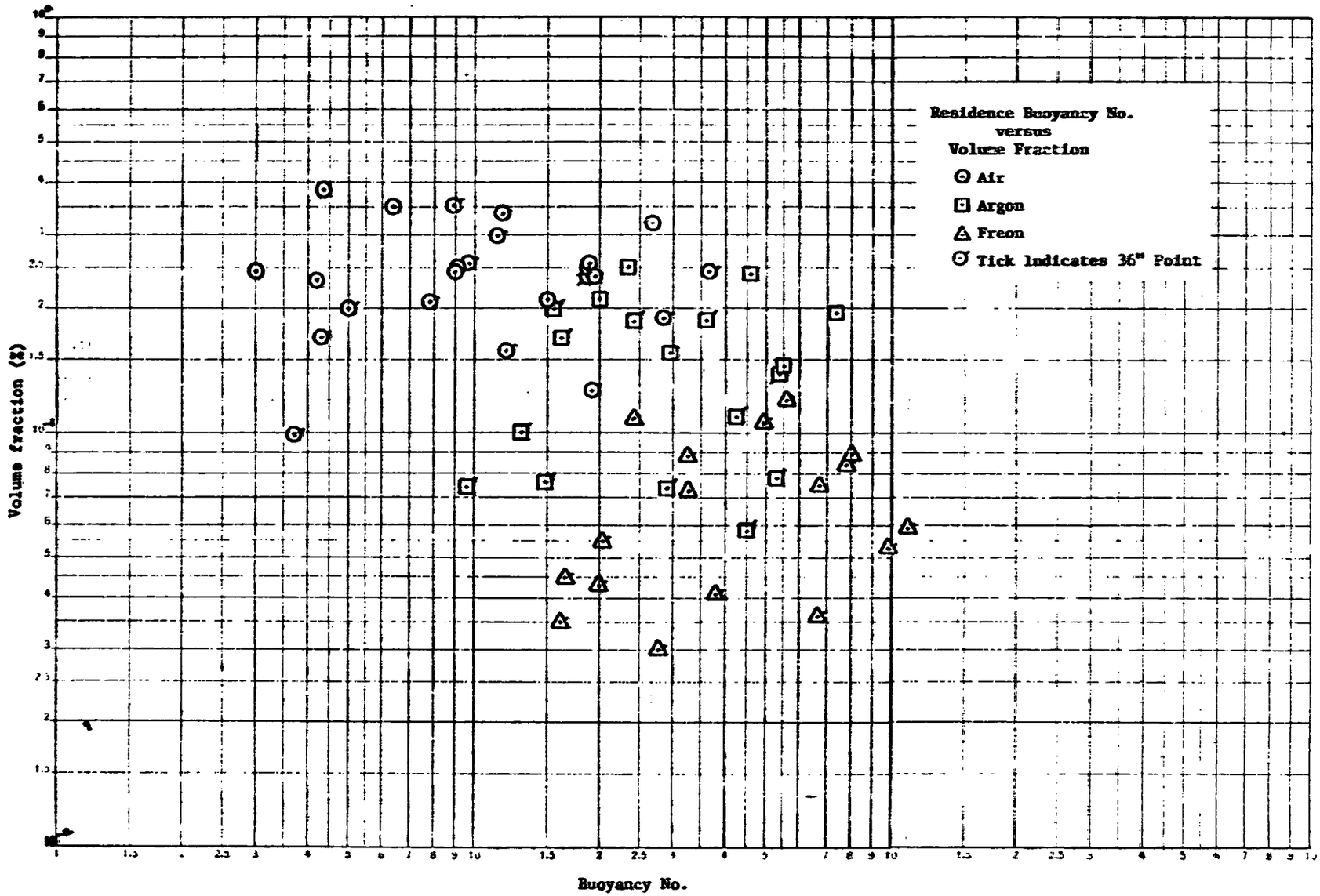

Fig. 5.17 Cavity volume fraction vs residence buoyancy number

Due to the length of time needed for reduction of spherical scan cases to volume fractions, little spherical buoyancy data were amassed. Because of the subjectivity of the volume fraction determinations from the densitometer scan cases used, the data in this section should be taken to be qualitative only.

5.4 Velocity Measurements

Velocity measurements similar to those reported in Phase I of this study were taken in the 3 ft diameter 2-D cavity using a hot wire anemometer. Using outer propellant flows of 200, 400, and 720 cfm, the cavity was mapped for both velocity gradient and direction.* However, even at 720 cfm outer flow conditions, the sign of the gradient would not be easily established inside the inner 2/3 radius of the cavity. In that interior region, velocities were less than 25 ft/min. At these low velocities, the usual direction indicator (fine thread) did not respond. Later attempts using smoke tracers were successful in showing that the recirculation pattern inside the cavity was ostensibly upward, away from the exhaust nozzle, all the way out to 2/3 of the radius.

Since hot wire anemometers are perturbed by different density gases, the results shown are mostly for air as both outer and inner gas. Due to the inaccessibility of the interior of the three-dimensional spheres, no velocity measurements were made for these cavities.

5.5 Sweep-Out Rates

Most of the testing reported thus far has been concerned largely with the parameters of the central gas region under steady-state flow conditions for both gases. If there were no sweep-out of inner gas by the outer gas, a very low fuel injection rate would be needed to replace fuel lost to the system through fissioning and neutron capture. Therefore, very low, or even zero, center gas injection rates were of primary interest in the sweep-out rate tests conducted.

The recirculating center gas region exists, whether there is enough tracer smoke to render it visible or not. The size and character of this central region depends on the cavity and flow parameters for the particular configuration under study. It seems plausible, however, that there should exist a minimum effect gas/injection rate below which the central turbulence region does not significantly change. One way to determine that minimum effect rate is to shutoff the central gas once steady state has been reached and measure the rate at which the smoke is swept from the cavity. This sweep-out rate should be independent of the central gas injection rate at values below the minimum effect rate, and should be a measure of the minimum fuel loss rate for a particular configuration.

---

* Figures 5.18 to 5.23 show the maps obtained from these measurements. The outer fast moving layer can be seen to be of relatively constant thickness, the velocity peaking at around 14 in. radius.

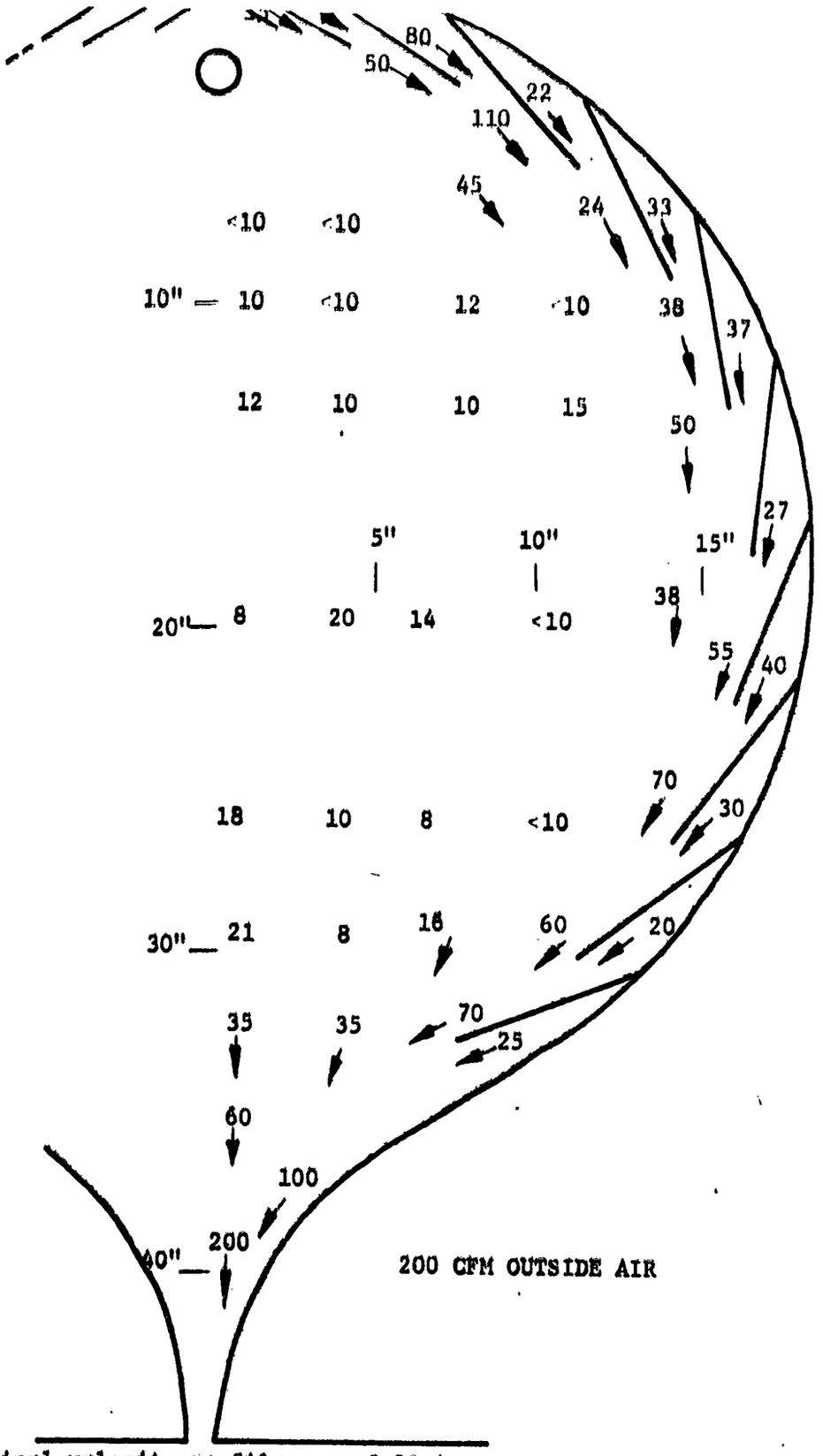

Fig. 5.18 Typical velocity profile map of 36 in. two-dimensional test cavity

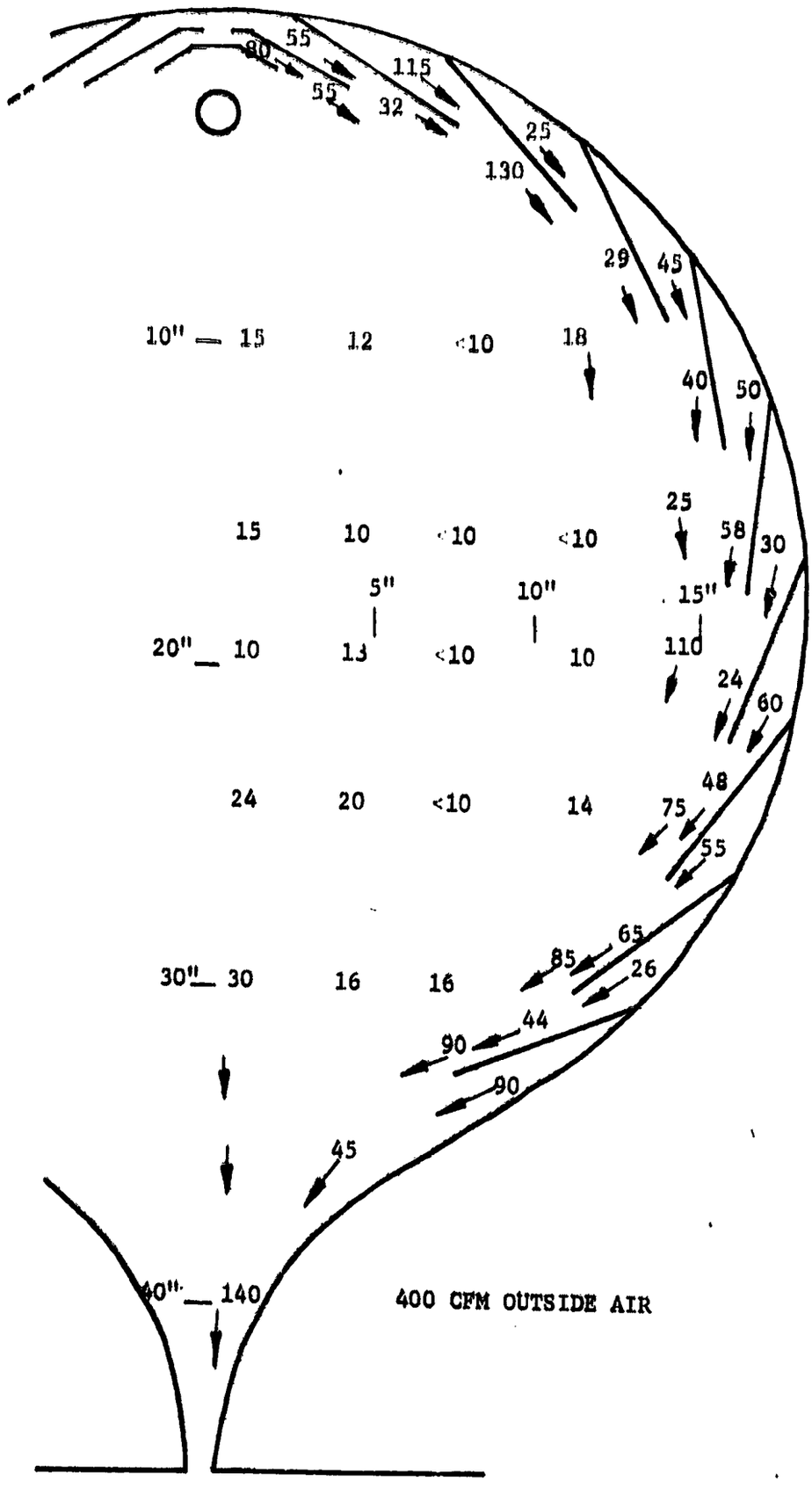

Fig. 5.19 Typical velocity profile map of 36 in. two-dimensional test cavity

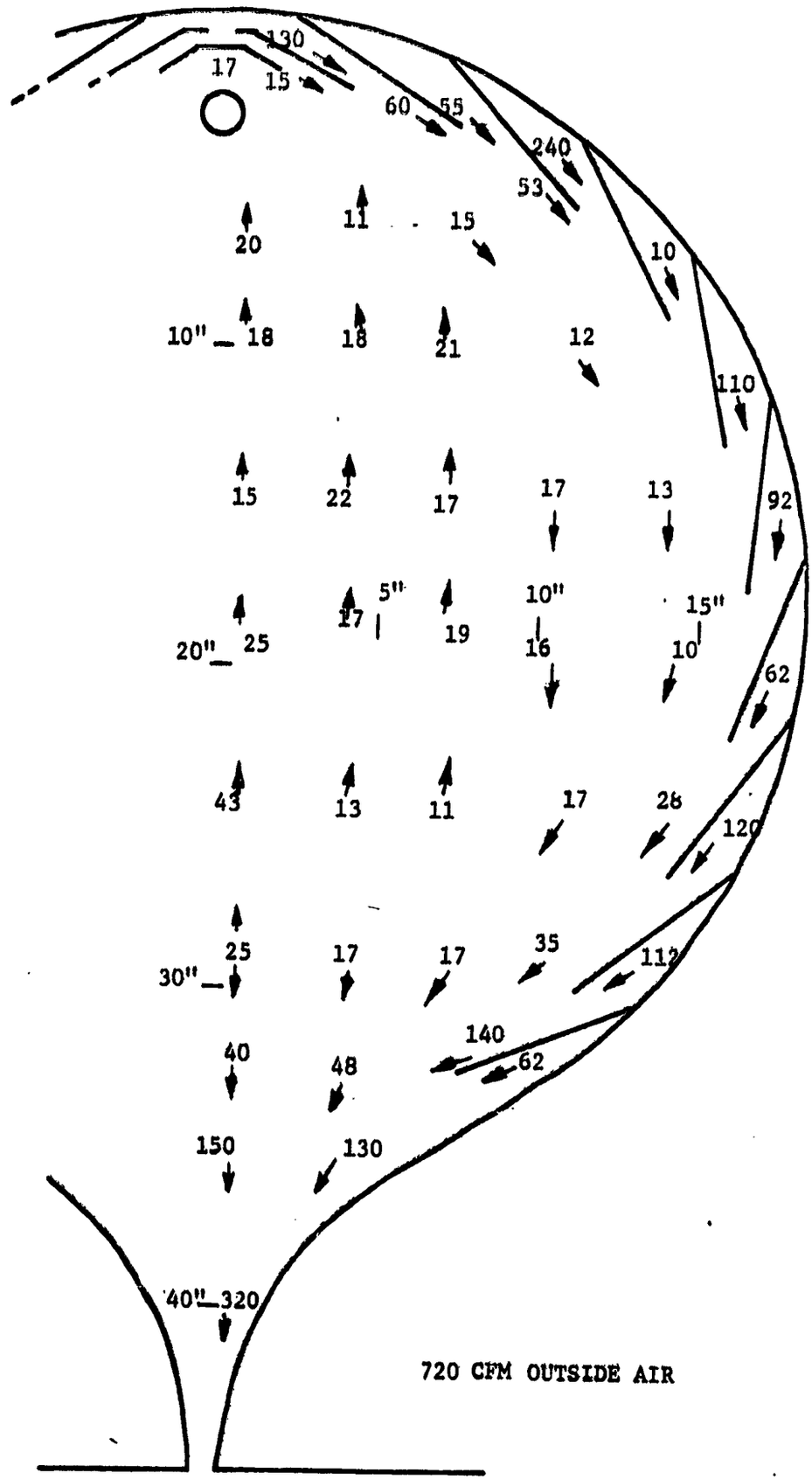

Fig. 5.20 Typical velocity profile map of 36 in. two-dimensional test cavity

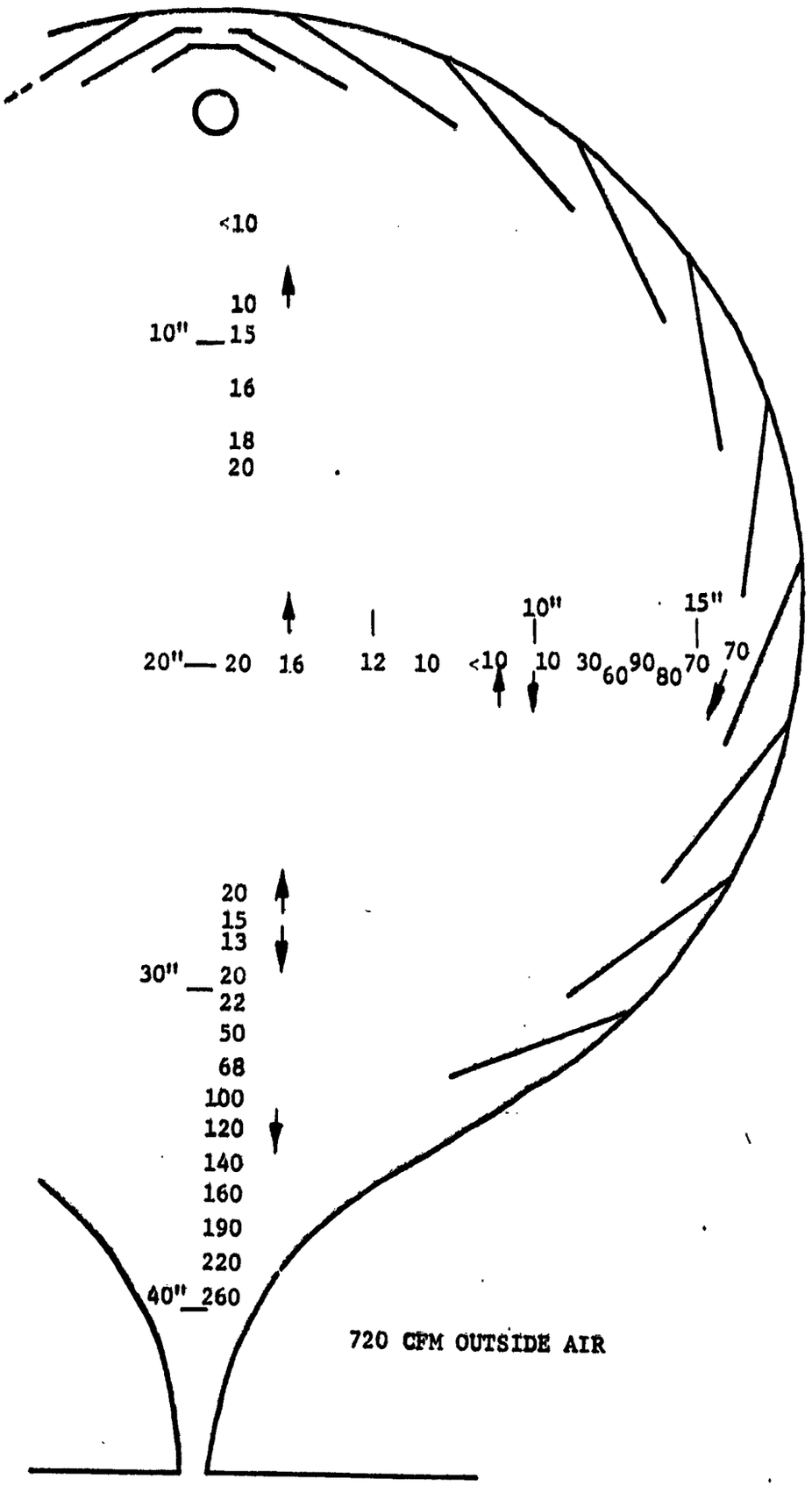

Fig. 5.21 Typical velocity profile map of 36 in. two-dimensional test cavity

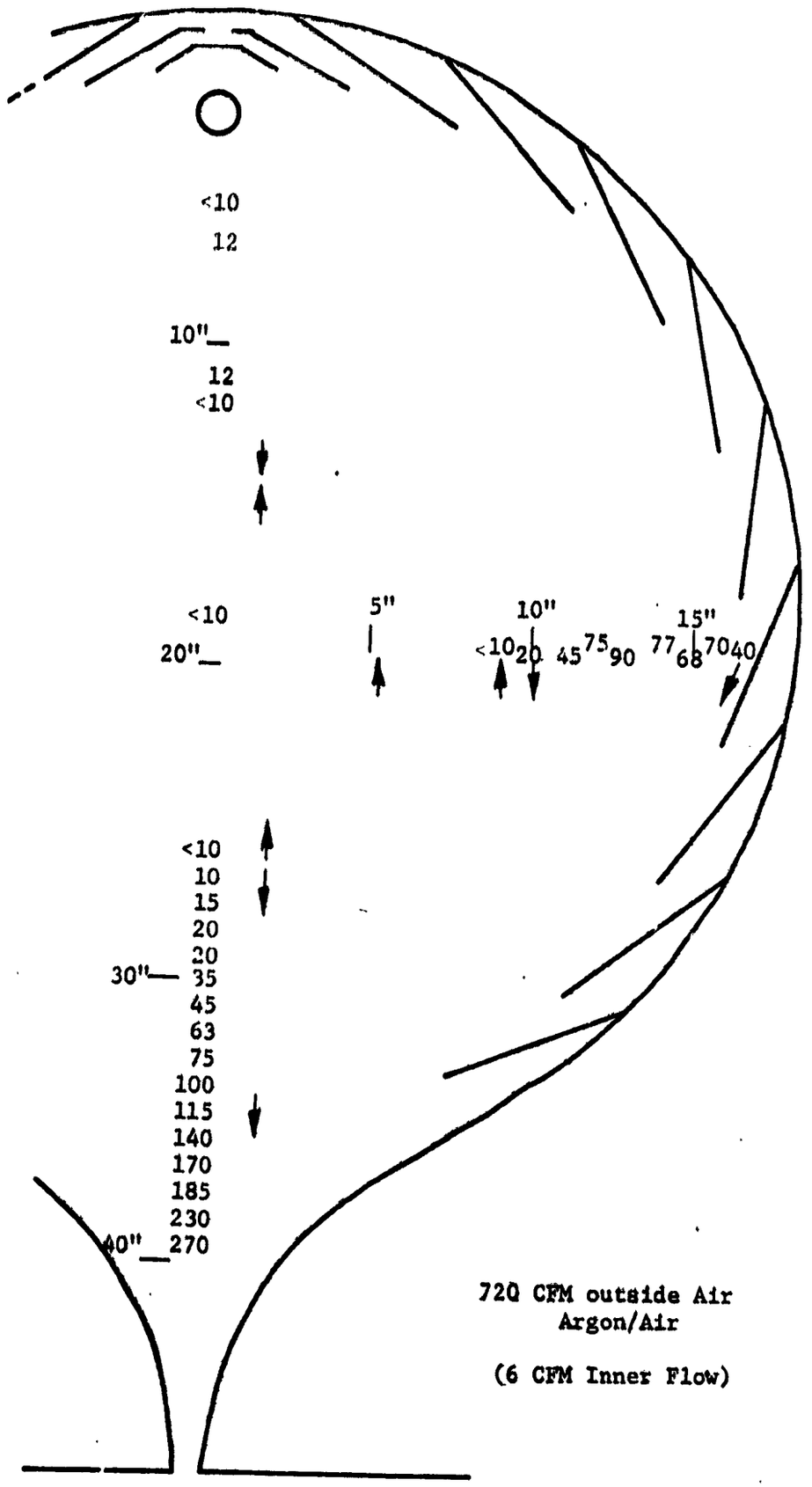

Fig. 5.22 Typical velocity profile map of 36 in. two-dimensional test cavity

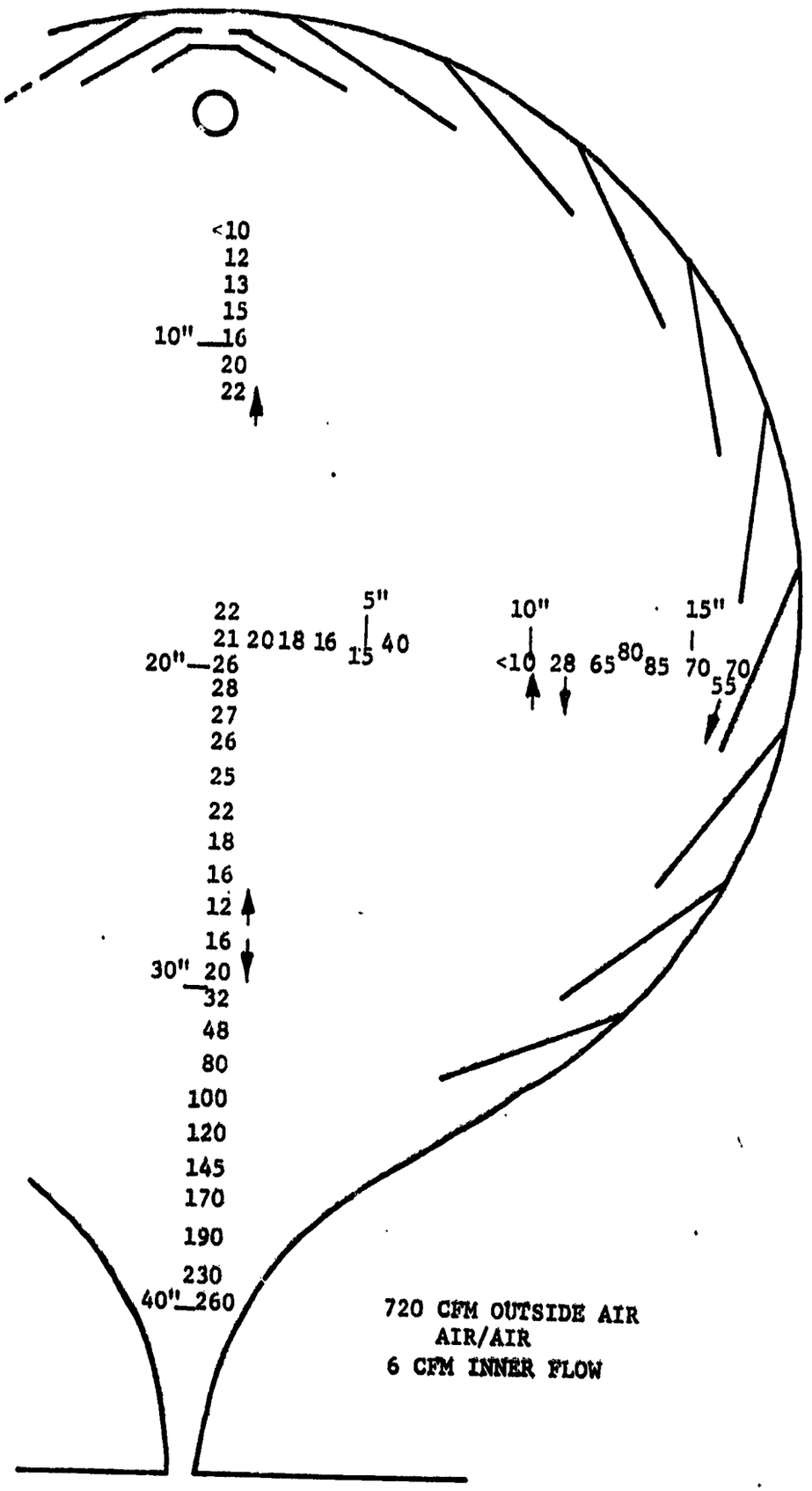

Fig. 5.23 Typical velocity profile map of 36 in. two-dimensional test cavity

For the sweep-out rate tests, air was used for both inner and outer gas, with the injector 10 in. below the top of the 36 in. 2-D cavity. A photograph was taken at steady state operating conditions, and the inner gas was shut-off. A timed sequence of photographs were then taken until no visible smoke remained in the cavity. The negatives were scanned across midplane with the densitometer, and an "eye-ball" estimate of the average smoke density for each picture in the series made. These average densities were plotted vs decay time as shown in Figure 5.24. Average sweep-out rates were determined from these plots and graphed against initial center gas injection rate in Figure 5.25 and against outer gas flow rate in Figure 5.26.

The sketchy and qualitative nature of these results do not appear to be sufficient grounds for making any firm conclusions. The results were not totally self-consistent,* the sweep-out rates were not consistent, let alone constant, during decay time. No minimum effect rate was determined, and if one exists, it is at a higher value than any tested. The last two figures indicate that the sweep-out rate seems to be a rather weak function of initial center gas injection rate, and a stronger function of outer gas flow rate. No noticeable change in the size of the central turbulence region was detected in the course of these tests. More exact information on central gas densities must be obtained before additional conclusions can be drawn from this type of testing.

5.6 Upfiring Tests

The results of running the test cavities upside down, so that the effect of gravity is reversed are shown in Figures 5.27 to 5.29. Good containment of all inner gases was demonstrated. At low outer flow rates, it becomes difficult to prevent the heavier inner gases from settling down very near to the cavity walls, which would create a problem in an operating reactor because of the heat. A configuration of this type could be used in MHD or heat source related applications, while the problems involved in propellant reversal make this configuration impractical for rocket engine applications.

5.7 Dust Injection Tests

The effects involved in solid particle, or dust, injection methods were investigated. Such schemes would be of utility in start-up of an operable gas core reactor. The effect of upward vs downward initial scattering of the dust is shown in Figure 5.30. A small variable speed rotating propeller fan was the scattering method used for the dust. A small amount of experimentation was done on dust composition, that is flour, bicarbonate of soda, Al_2O_3, and talc were all tried. Talc seemed to give the best results.

One problem identified with these dust injection schemes can be identified from the background pictures shown in Figure 5.30. That is the dust tends to settle out onto the walls of the cavity. More effort will be

---

* Pointing out once again the very complex nature of the interactions within the flowing gas cavity.

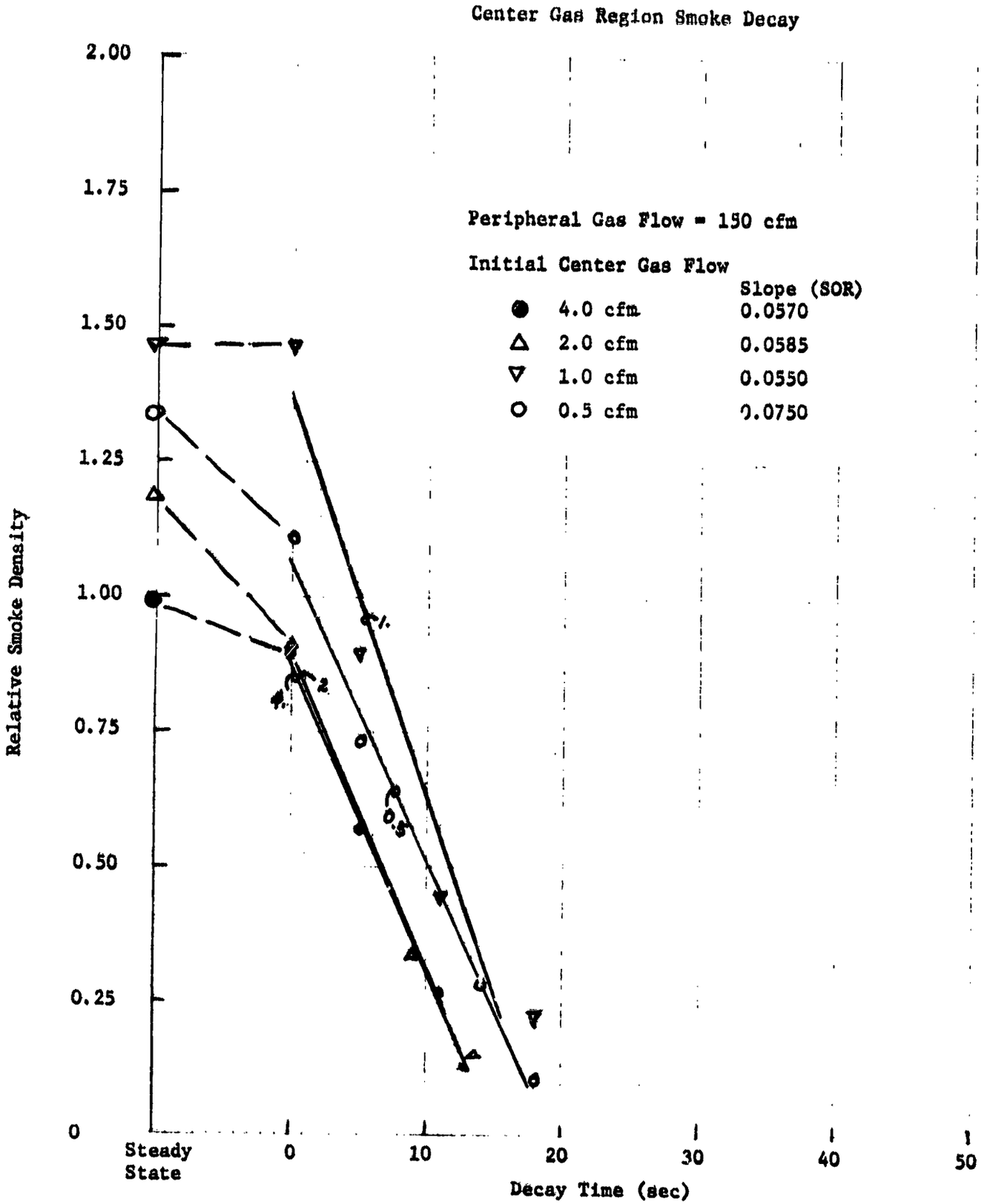

Fig. 5.24 Cavity smoke density vs decay time

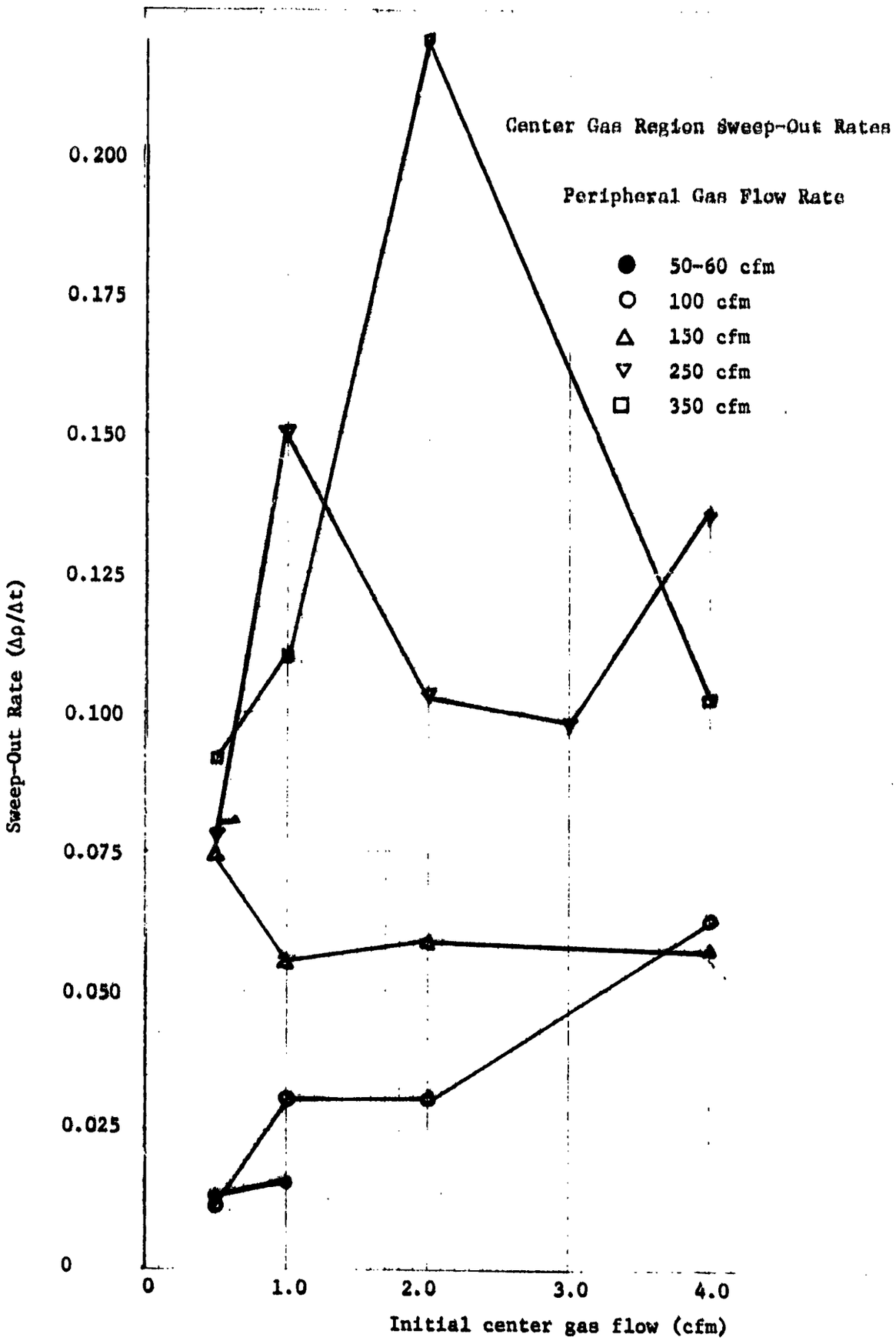

Fig. 5.25 Cavity sweepout rate vs initial center gas flow rate

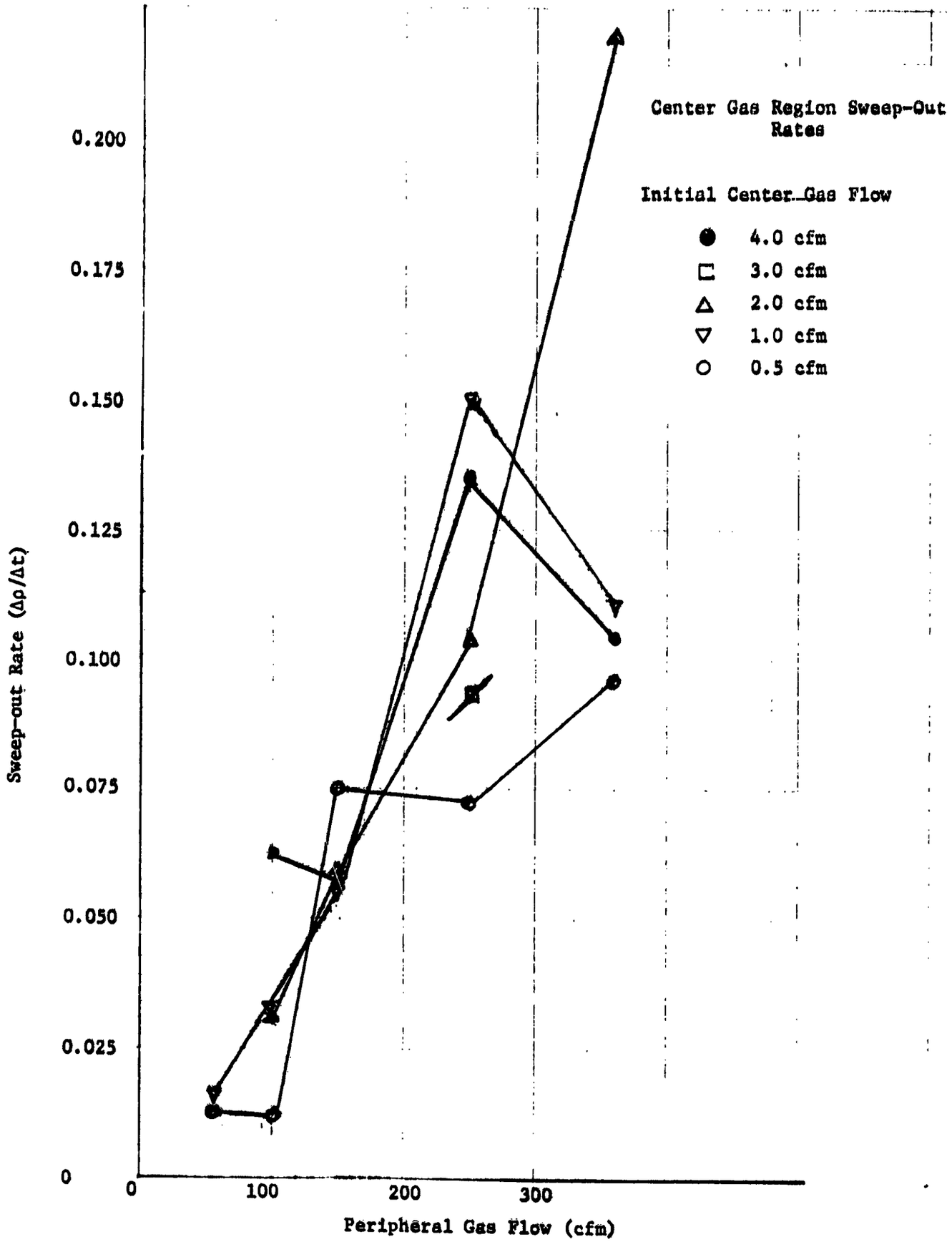

Fig. 5.26 Cavity sweep-out rate vs outer gas flow rate

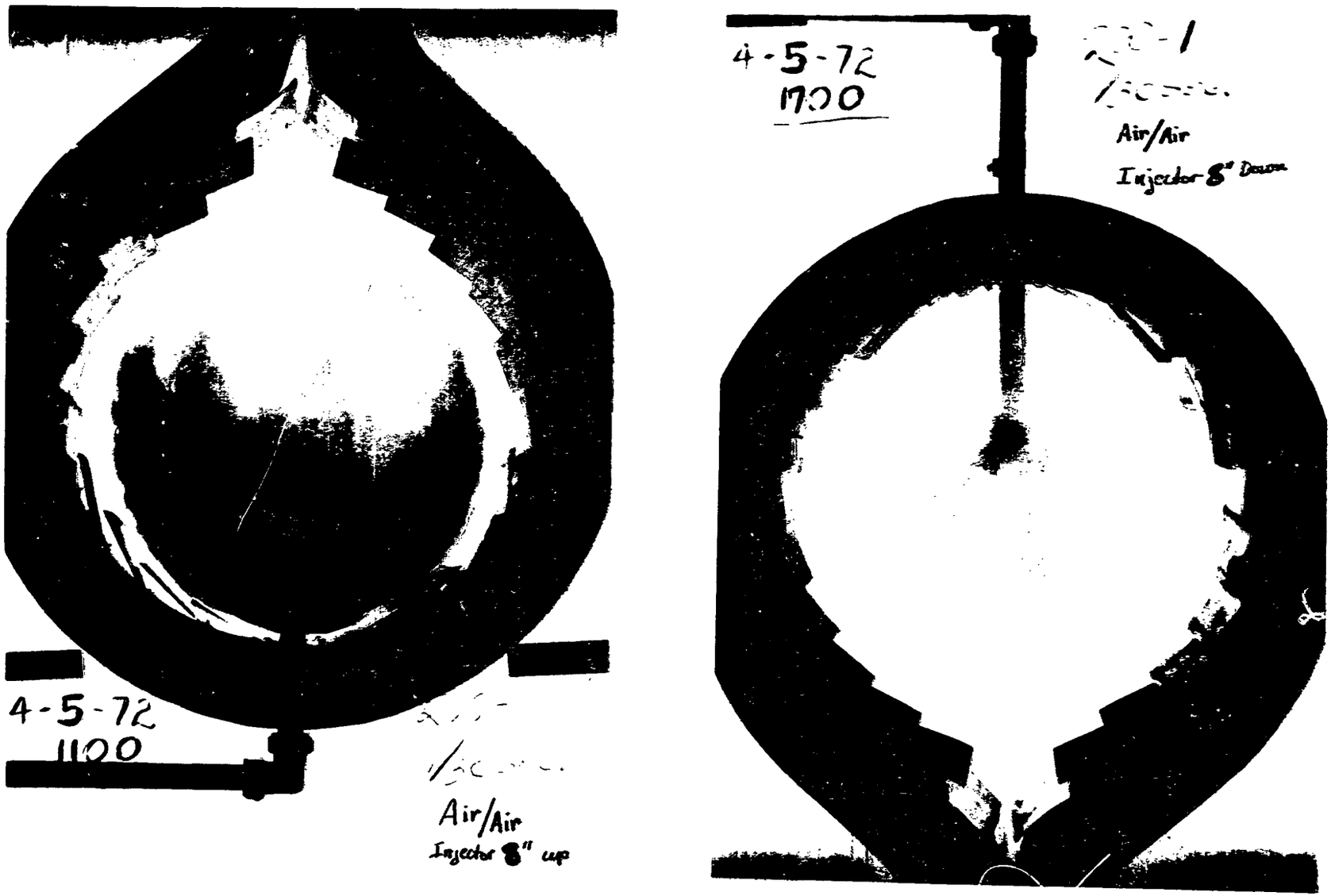

Fig. 5.27 Comparison of upward exhausting cavity case to downward exhausting cavity

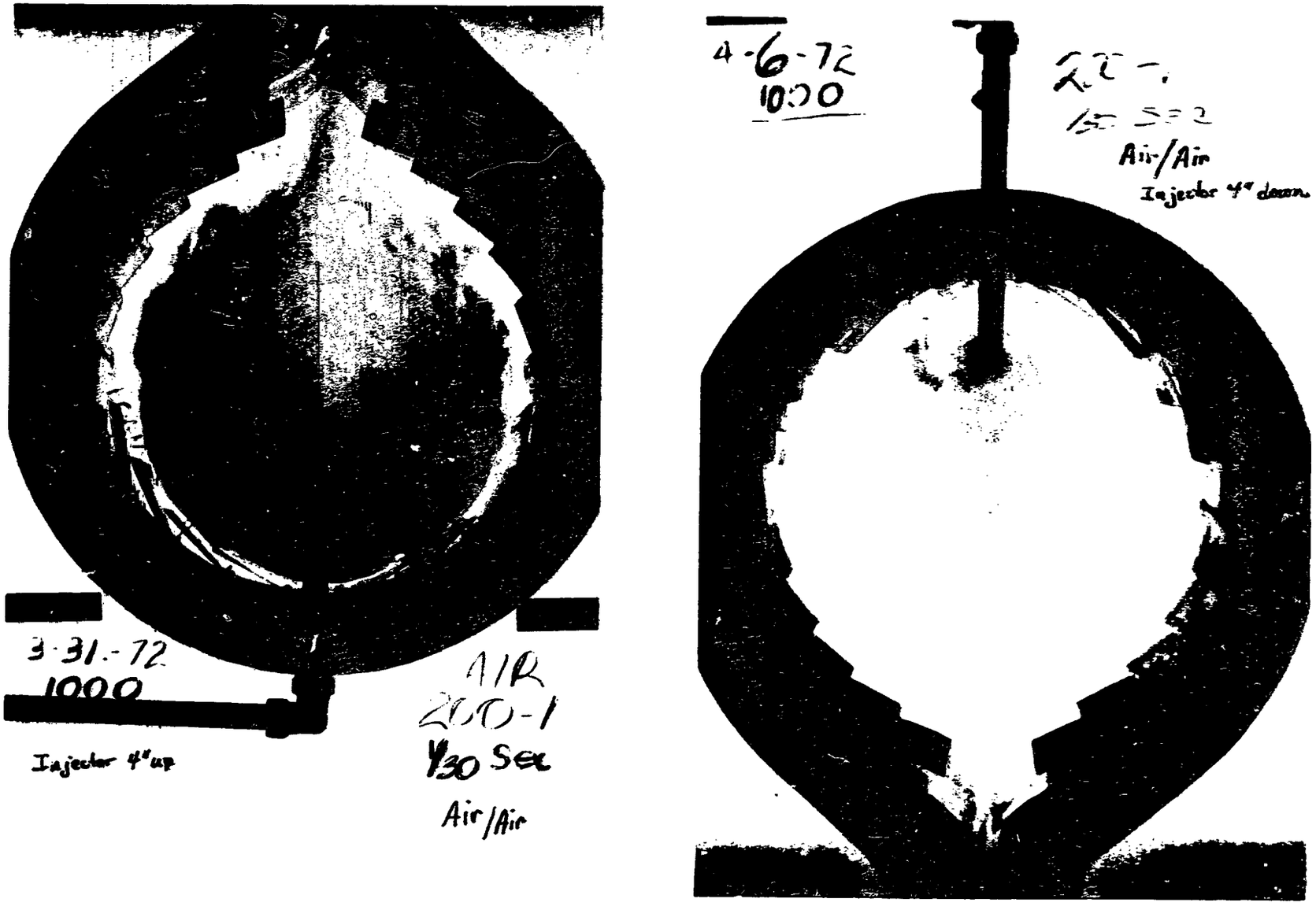

Fig. 5.28 Comparison of upward exhausting cavity case to downward exhausting cavity

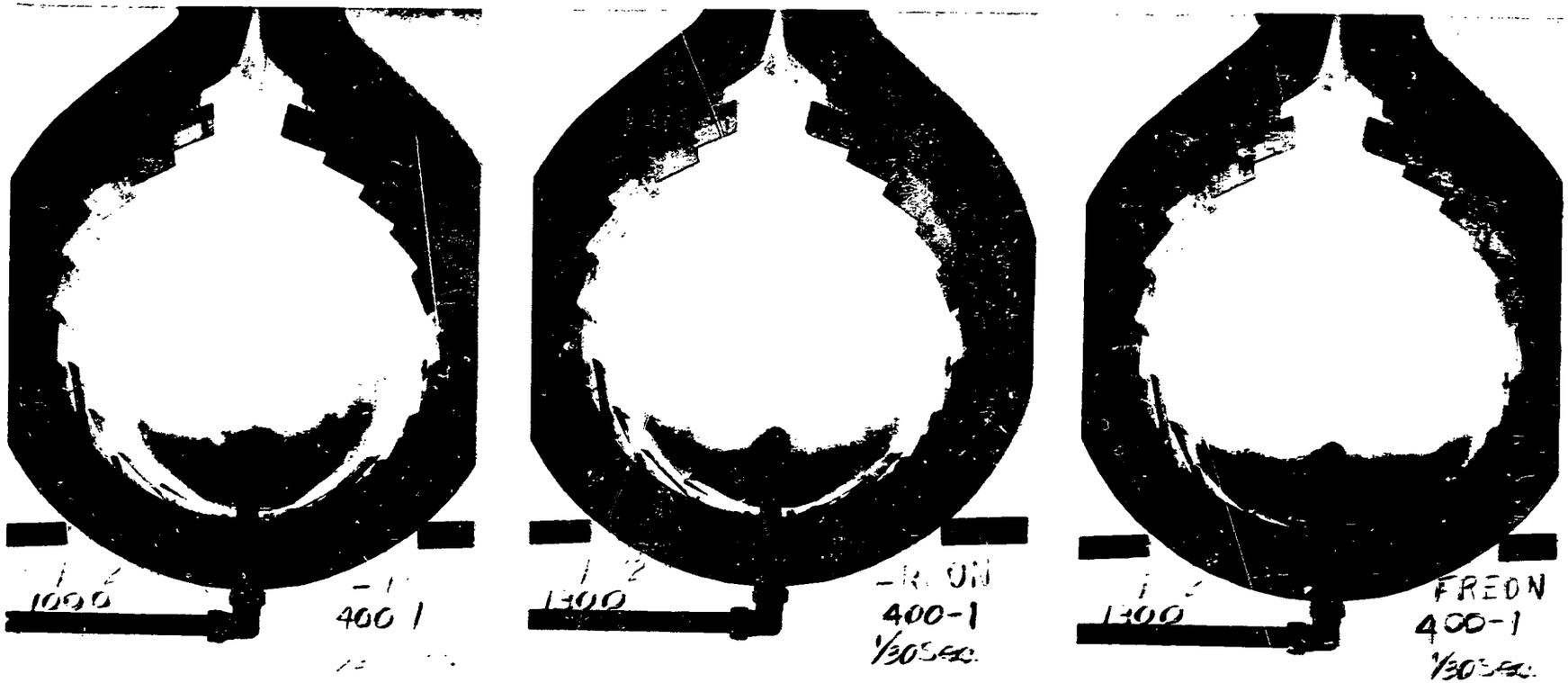

Fig. 5.29 Up-firing cavity cases showing good containment of air, argon, and freon

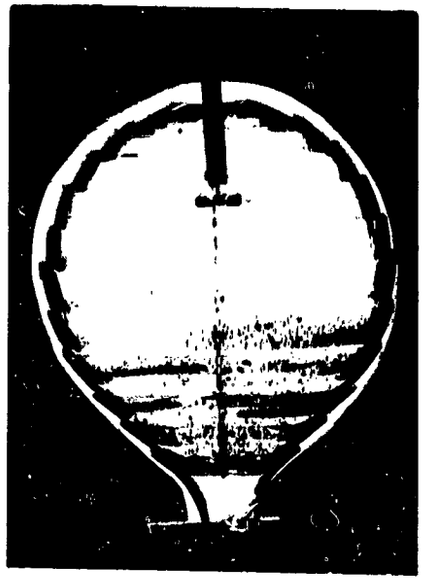

Blank

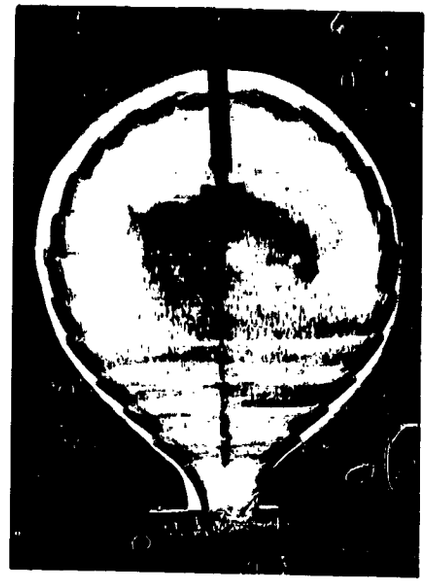

Upward scattering rotor

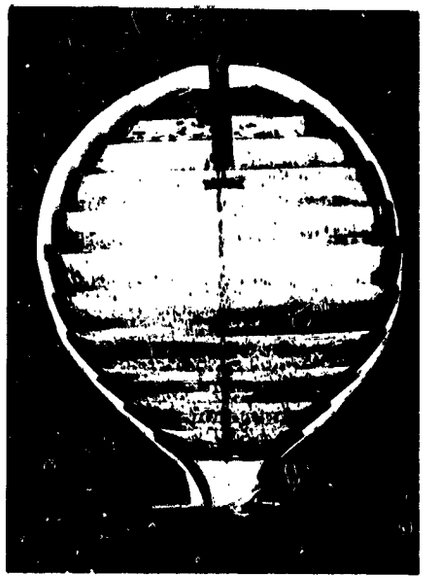

Blank

Downward scattering rotor

Fig. 5.30 Dust injection series showing effect of scattering dust both upward and downward

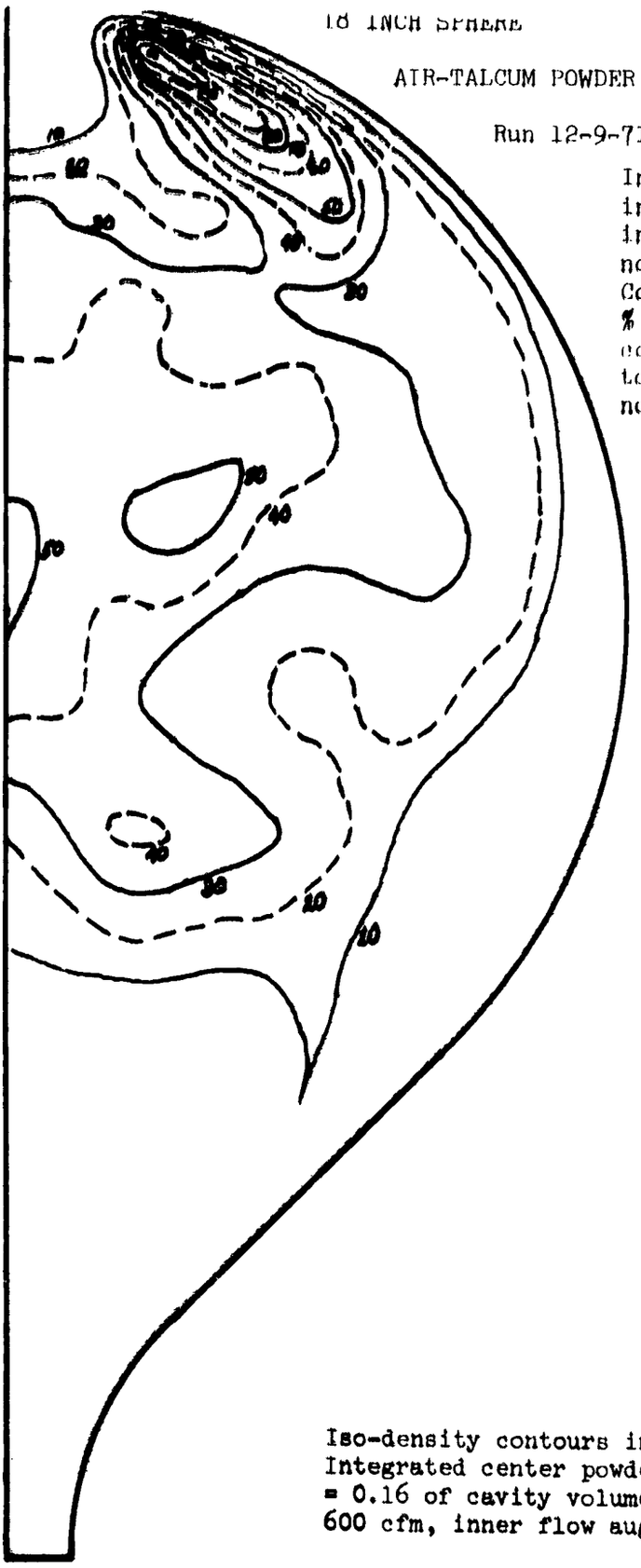

Fig. 5.31 **Isodensity contour map for typical dust (talcum powder) injection test**

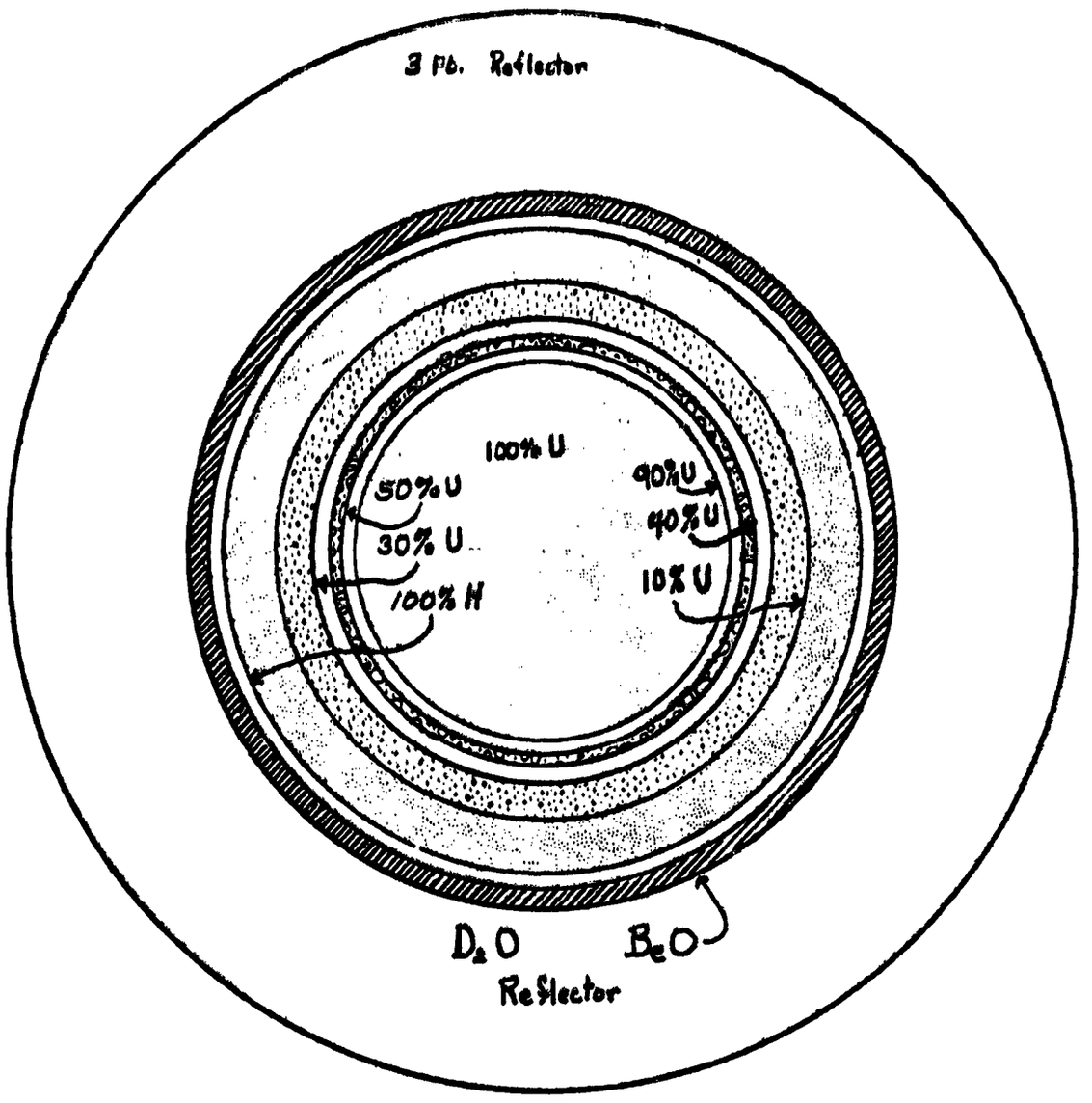

Fig. 5.32 Computer Solution Model I

35% Volume Fraction, 0.93 Radius Ratio
Reff = 82.35 cm. , Total Fuel Mass = 119 kg.

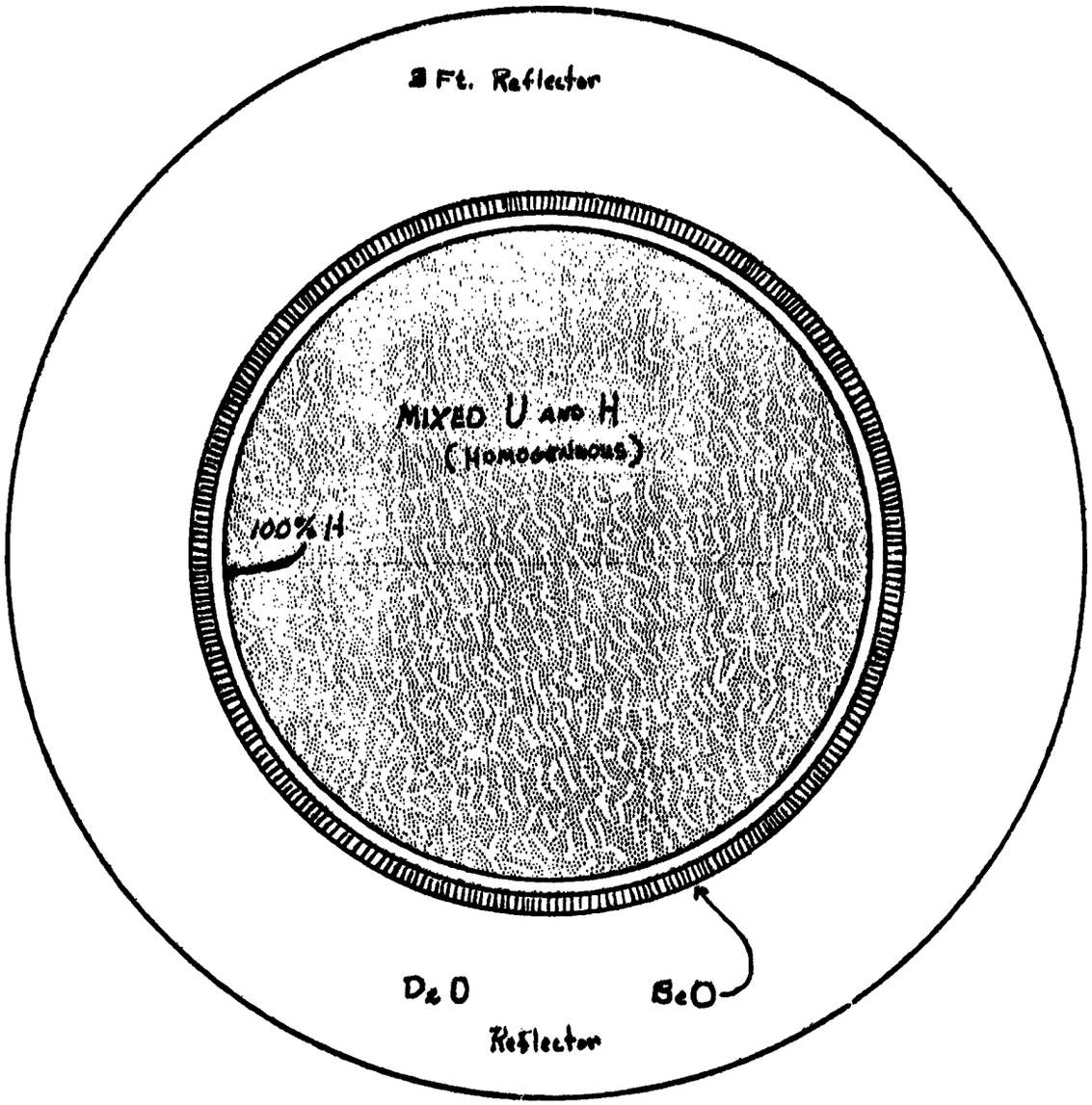

Fig. 5.33 Computer Solution Model IX

35% Volume Fraction, 0.93 Radius Ratio
Reff = 108.78 cm. , Total Fuel Mass = 119 kg.

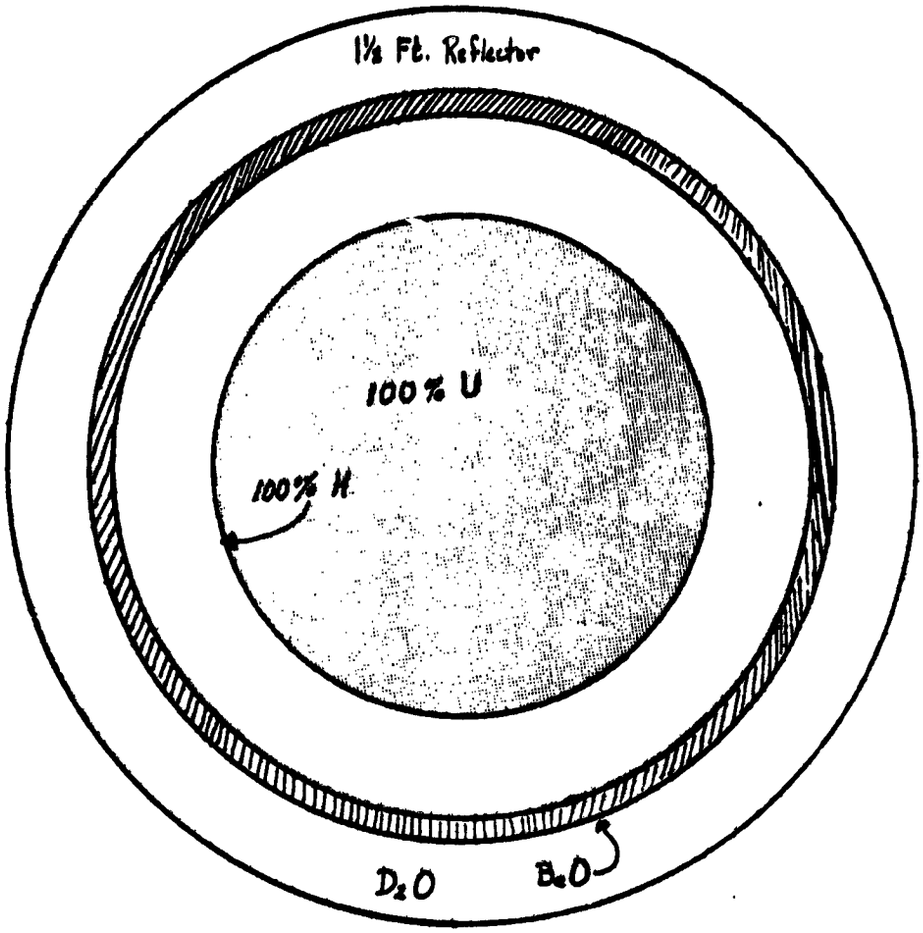

Fig. 5.34 Computer Solution Model X

35% Volume Fraction, 0.70 Radius Ratio
Reff = 80.55 cm. , Total Fuel Mass = 119 kg.

Table 5.3

35% Volume Fraction Model Specifications

Model	Region No.	Material No.	No. of Mesh Points	Outer Radius	Region Thickness	Cavity % Volume Occupied by Region
I	1	1	20	84.75	84.75	17.2
	2	2	5	92.28	7.53	5.0
	3	6	5	96.00	3.72	2.8
	4	7	10	104.02	8.02	6.8
	5	8	15	121.68	17.66	19.1
	6	10	25	145.04	23.36	35.3
	7	100	10	152.4	7.36	13.8
	8	200	10	162.56	10.16	--
	9A	201	20-40	198.12	35.56	--
	9B	201	40	243.84	81.28	--
IV	1	7	11	56.00	56.00	5.0
	2	6	2	60.00	4.00	1.0
	3	2	2	65.00	5.00	1.8
	4	1	7	96.00	31.00	17.2
	5	2	3	100.00	4.00	3.2
	6	6	3	102.00	2.00	1.8
	7	7	3	104.00	2.00	1.8
	8	8	5	110.00	6.00	5.8
	9	10	9	120.00	10.00	11.2
	10	8	10	130.00	10.00	13.3
	11	10	25	145.04	15.04	24.1
	12	100	10	152.40	7.36	13.8
	13	200	10	162.56	10.16	--
	14	201	40	243.84	81.28	--
VI	1	10	30	107.71	107.71	35.3
	2	8	15	124.41	16.70	19.1
	3	7	5	129.39	4.98	6.8
	4	6	5	13.33	1.94	2.8
	5	2	5	134.67	3.34	5.0
	6	1	20	145.04	10.37	17.2
	7	100	10	152.4	7.36	13.8
	8	200	10	162.56	10.16	--
	9	201	40	243.84	81.28	--
IX	1	35	80	145.04	145.04	86.2
	2	100	10	152.40	7.36	13.8
	3	200	10	162.56	10.16	--
	4	201	40	243.83	81.28	--
X	1	1	50	107.40	107.40	35.2
	2	100	40	152.40	45.00	64.8
	3	200	10	162.56	10.16	--
	4	201	40	243.84	81.28	--

Table 5.4

Material Specifications

Material No.	Composition	Atom Densities ($\times 10^{-5}$ atoms/cm)
1	100% U	1.958
2	90% U	1.762
	10% H	0.5905
6	50% U	0.9789
	50% H	2.953
7	40% U	0.7832
	60% H	3.568
8	30% U	0.5874
	70% H	4.134
10	10% U	0.1958
	90% H	5.315
35	40.6% U	0.7950
	59.4% H	3.489
100	100% H	21.090
200	100% BeO	7280.
201	100% D_2O + 0.0022%H	3310.

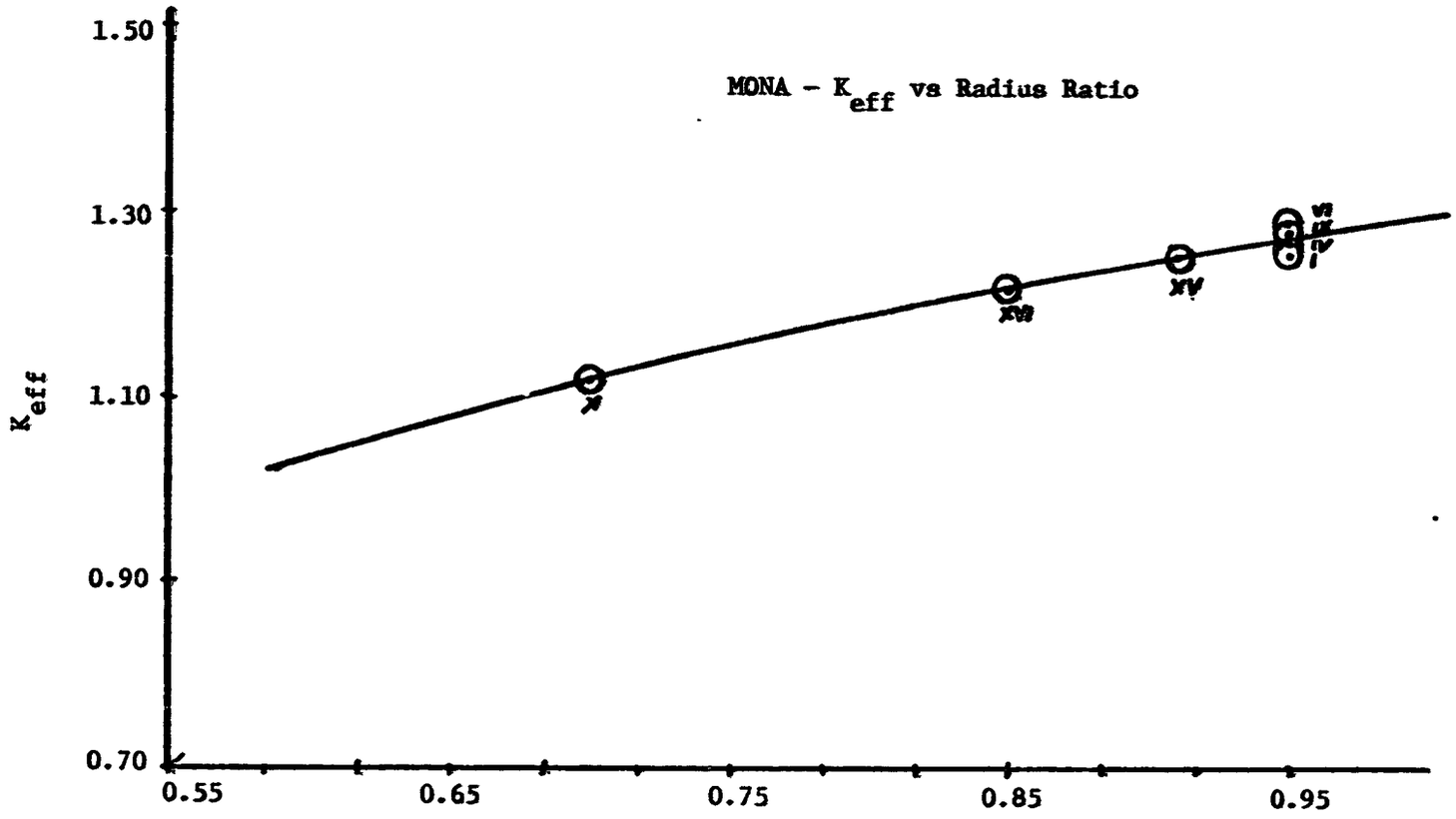

Fig. 5.35 MONA Computer Solutions – K_{eff} vs Radius Ratio

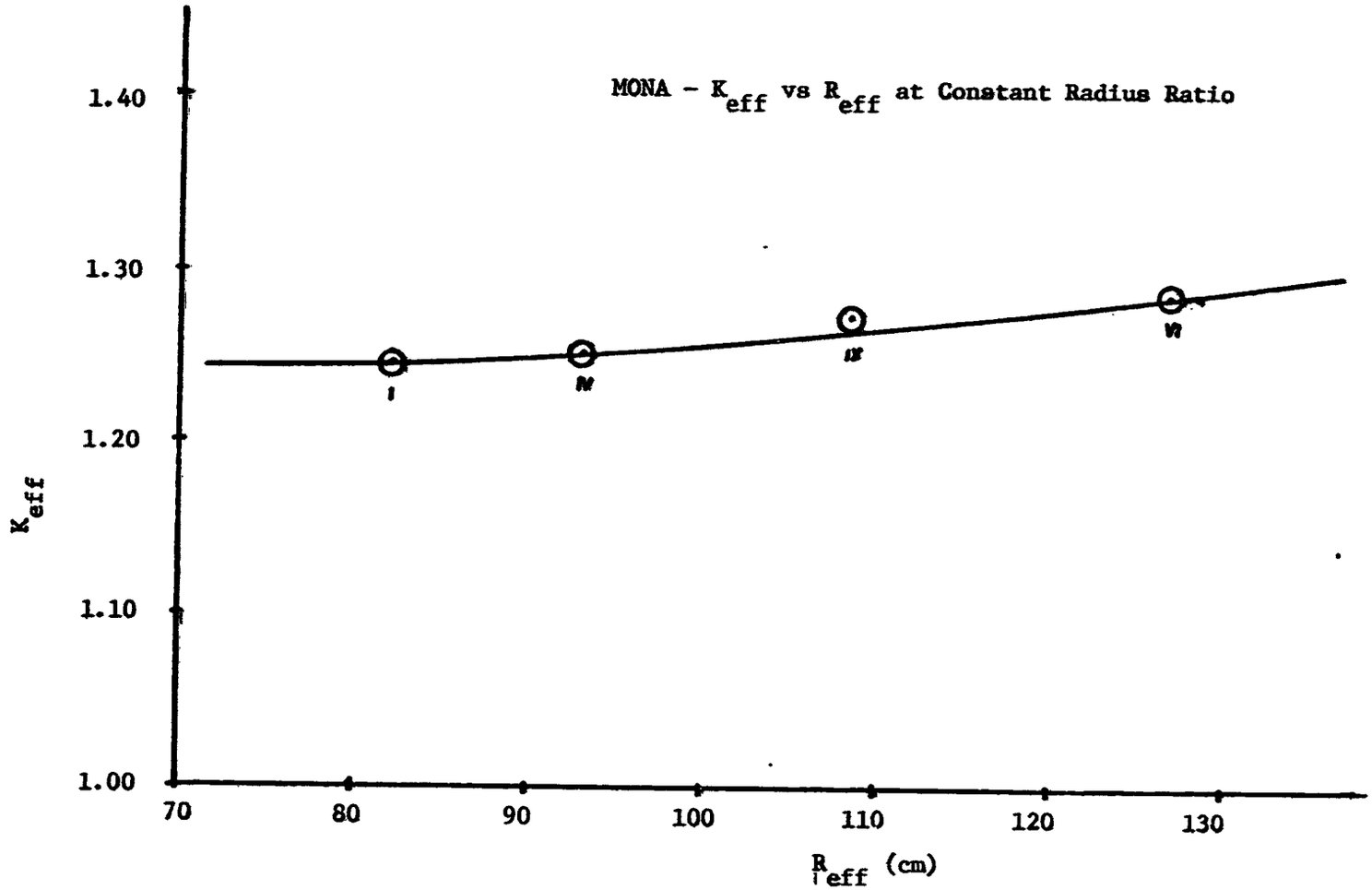

Fig. 5.36 MONA Computer Solutions - K_{eff} vs R_{eff} at Constant Radius Ratio

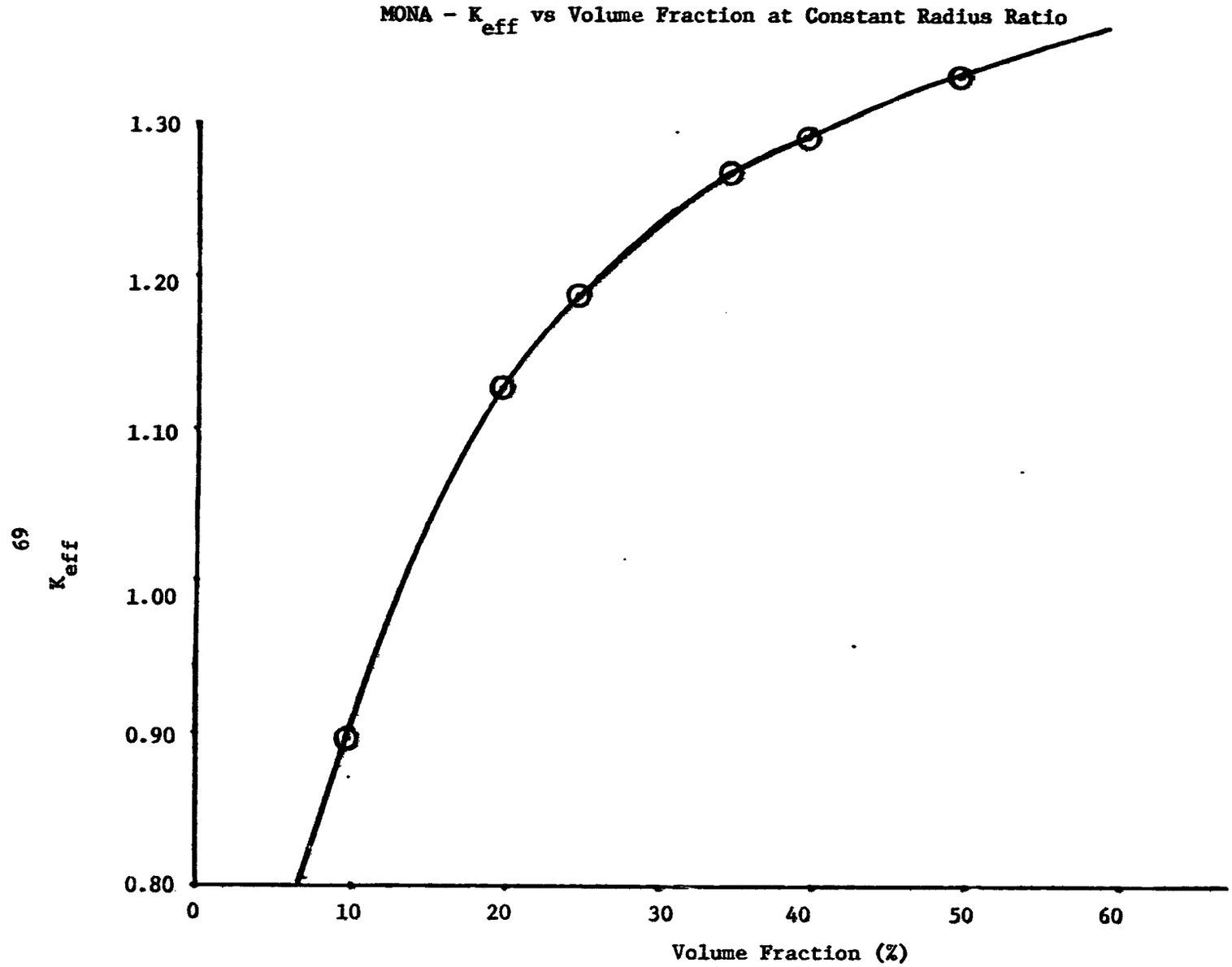

Fig. 5.37 MONA Computer Solutions - K_{eff} vs Volume Fraction at Constant Radius Ratio

necessary to perfect these schemes to protect the cavity walls during operation of the reactor, if solid dust is to be injected during startup. Figure 5.31 is an isodensity contour plot for an air talc test. The background reading was taken to be an average of frames exposed before and after the tests to account for buildup of dust on the cavity walls. Because the talc is such a fine powder, the 16% volume fraction yields only about 1.6 gms of talc per about 10 gms of air in the cavity. High pressures will have to be investigated if this startup scheme is to operate.

5.8 Criticality Calculations and Selected Results

In an effort to relate nuclear criticality to flowing gas parameters, computer modelings for diffusion and transport theory computer calculations were done from the flow cases tested. An idealized base configuration was arrived at by generalizing the isodensity contour plots drawn in the flow testing. Variations on this base were performed to determine qualitatively the magnitude of nuclear criticality changes associated with possible fluctuations in the central fuel plasma. Some of the basic models are shown in Figures 5.32 to 5.34. Some of the pertinent data for the basic cases are listed in Table 5.3. The material specifications are listed in Table 5.4. Hydrogen compositions used were obtained from Patch[9] for 500 atm and the appropriate temperatures. Virtually all the hydrogen is atomic at the high temperatures and pressures of interest in the gaseous core. The uranium atom densities were obtained from the ideal gas laws, and considering the uranium atoms to be doubly ionized. In mixing hydrogen with uranium, three atoms or hydrogen replace one of uranium and its two electrons to keep the pressure constant.

5.8.1 K_{eff} vs Radius Ratio at Constants Volume Fraction

The effect of varying the ratio of the radius to which the fuel expands to the cavity radius at a constant volume fraction, and hence fuel mass, was checked. This effect is shown graphically in Figure 5.35. This is the most important predominant parameter identified.

5.8.2 K_{eff} vs R_{eff} at Constant R.R. and V.F.

To determine the relative effects of varying the regions of different fuel density at constant fuel mass and radius ratio, a density-weighted effective radius, K_{eff} was defined

$$R_{eff} = \frac{\Sigma\ 2\pi r_i^2\ \rho_i\ \Delta r_i \times r_i}{\Sigma\ 2\pi r_i^2\ \rho_i\ \Delta r_i}$$

This effect is shown graphically in Figure 5.36.

5.8.3 K_{eff} vs Volume Fraction at Constant Radius Ratio

The naturally intuitive feeling, that the more fuel the higher the criticality factor, was verified in one calculational series. This result is shown in Figure 5.37.

5.8.4 Other Factors Influencing K_{eff}

The effect of using U-233 for fuel over U-235 was shown to decrease critical mass by about a factor of two. Increasing the reflector thickness increases K_{eff}. A cost-benefit analysis will be necessary to obtain the optimum reflector thickness for an actual rocket engine.

5.8.5 Diffusion vs Transport Theory Codes

The initial calculations were performed with a single thermal group, no upscatter diffusion theory code, DISNEL[10]. Due to the uniform nature of the results of these calculations, showing no sensitivity to fuel arrangement in the cavity. The results were checked with a multi-thermal, full thermal upscatter S4 Transport Code SCAMP[11]. There was a wide divergency of results indicating an inadequacy in DISNEL for hot gas core work. Since transport codes consume so much computer time, a multi-thermal diffusion theory code MONA[12], using an energy format and cross section library identical to SCAMP was used to see if the divergence was due to transport effects or upscatter effects in the thermal groups. MONA and SCAMP agreed to within 1%Δk. Figure 5.38 shows a comparison of the three codes for a few models calculated.

The general trend of the calculations seem to lead to a confirmation of the feasibility of the gas core rocket engine concept. The results further point out the need for further study and optimization of flowing gas cavity parameters for obtaining the best design for a nuclear rocket engine.

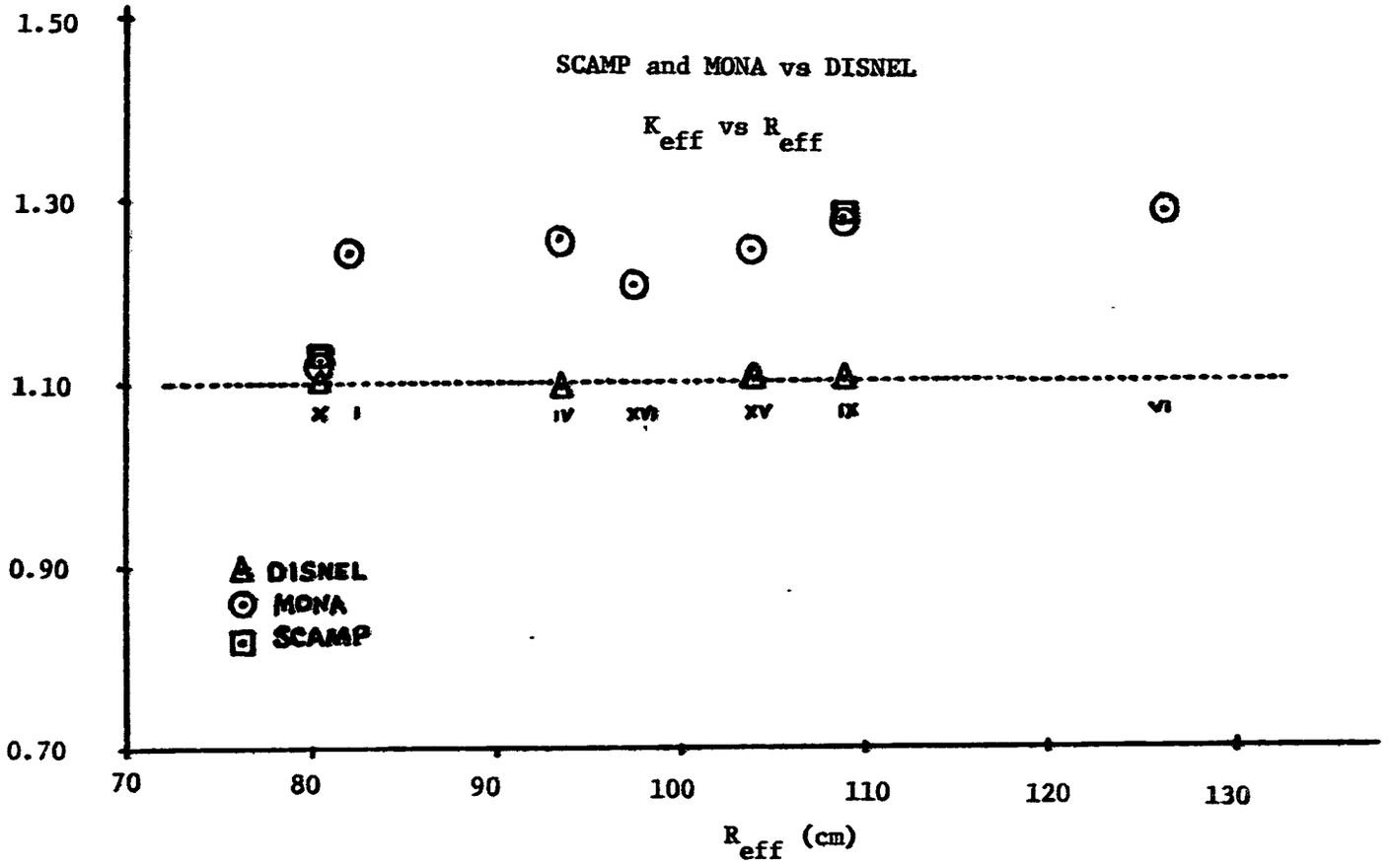

Fig. 5.38 Comparison of Computer Solutions – SCAMP and MONA vs DISNEL
K_{eff} vs R_{eff}

6.0 CONCLUSIONS AND RECOMMENDATIONS

The feasibility of the gas core reactor concept has been strengthened by the experiments reported herein. It cannot be stated that absolute feasibility has been demonstrated, since the interaction effects of thermodynamics (radiant and some convective heat transfer) with the fluid hydraulics have not been experimentally studied except on a small scale (Reference TAFA work). However, the nuclear coupling with the fluid flow patterns reported in the previous sections has been studied, both under room temperature conditions and at high temperature.

General conclusions that can be stated at this time are the following:

1. The gas core continues to appear feasible. However, operation in the upfiring (against acceleration or gravity) direction, as could be done for MHD applications but which would require thrust reversal for a rocket, makes the attaining of a critical configuration much easier. Protection of the cavity walls from burnout is more difficult, however.

2. If operation is to be in the downfiring direction, as with a rocket, then center gas injection in a direction other than downward from the top appears to offer significant enhancement of fuel density and hence of nuclear reactivity.

3. A central "updraft" can be enhanced by shaping of the walls. Such an "updraft" along with alternate injection schemes as mentioned in (2) above also can result in significant enhancement of fuel density. These schemes are found essential when the center gas was much heavier than the outer gas.

4. With standard center injection near the top, the theoretical[8] predictions by Putre of density vs buoyancy number have been essentially verified experimentally. These do show that the large cavity, low thrust, high temperature operating design conditions will not be able to operate nuclearly unless schemes such as outlined in conclusions (2) and (3) above are employed.

5. The hot hydrogen nuclear effect is extremely significant and highly controlling. If anything, it would appear to add a high stability factor to the cavity operation.

As to recommendations for areas of most critical investigative need, the following seem most pertinent at this time:

1. Start-up conditions with dust fuel appeared woefully lacking in the needed density of fuel when run at low pressure. High pressure testing needs to be done to determine if dust is a feasible start-up mechanism.

2. The hot hydrogen effect was studied only somewhat cursorily, and found to be extremely significant. More attention and detail needs to be given to this unusual nuclear problem.

3. The observed strong mixing at the edge of the highly turbulent boundary layer leads to the conclusion that convection in this region may be extremely significant. If indeed convection needs to be added to the radiative transfer model, these studies should be undertaken before further serious design work is done.

REFERENCES

1. J. F. Kunze et al., "Phase I Topical Report, Flowing Gas, Non-Nuclear Experiments on the Gas Core Reactor," NASA CR-120824, ANCR-1032, Aerojet Nuclear Company (February 1972).

2. R. G. Ragsdale, "High-Specific-Impulse Gas-Core Reactors," NASA TM X-2243, NASA, Lewis Research Center, (March 1971).

3. J. C. Bennett and B. V. Johnson, "Experimental Study of One- and Two-Component Low-Turbulence Confined Axial Flows," NASA CR-1851 (June 1971).

4. H. Weinstein et al., "Turbulence in the Mixing Region Between Ducted Coaxial Streams," NASA CR-1335 (July 1969).

5. C. G. Lanzo, "A Flow Experiment on a Curved-Porous-Wall-Gas-Core Reactor Geometry," Nuclear Applications and Technology, 8, p. 6 (1970).

6. J. F. Kunze, G. D. Pincock and R. E. Hyland, "Cavity Reactor Critical Experiments," Nuclear Applications, 6, p. 104 (1969).

7. J. F. Kunze et al., "Benchmark Gas Core Critical Experiment," Nuclear Science and Engineering, 47, p. 59 (1972).

8. H. A. Putre, "Effect of Buoyancy on Fuel Containment in an Open-Cycle Gas-Core Nuclear Rocket Engine," 2nd Symposium on Uranium Plasma: Research and Applications, Atlanta Georgia, (November 1971).